

Article

Discovery of Novel Naphthylphenylketone and Naphthylphenylamine Derivatives as Cell Division Cycle 25B (CDC25B) Phosphatase Inhibitors: Design, Synthesis, Inhibition Mechanism and in Vitro Efficacy against Melanoma Cell Lines

Carmen Cerchia, Rosarita Nasso, Matteo Mori, Stefania Villa, Arianna Gelain, Alessandra Capasso, Federica Aliotta, Martina Simonetti, Rosario Rullo, Mariorosario Masullo, Emmanuele De Vendittis, Maria Rosaria Ruocco, and Antonio Lavecchia

J. Med. Chem., **Just Accepted Manuscript** • DOI: 10.1021/acs.jmedchem.9b00632 • Publication Date (Web): 11 Jul 2019

Downloaded from pubs.acs.org on July 16, 2019

Just Accepted

“Just Accepted” manuscripts have been peer-reviewed and accepted for publication. They are posted online prior to technical editing, formatting for publication and author proofing. The American Chemical Society provides “Just Accepted” as a service to the research community to expedite the dissemination of scientific material as soon as possible after acceptance. “Just Accepted” manuscripts appear in full in PDF format accompanied by an HTML abstract. “Just Accepted” manuscripts have been fully peer reviewed, but should not be considered the official version of record. They are citable by the Digital Object Identifier (DOI®). “Just Accepted” is an optional service offered to authors. Therefore, the “Just Accepted” Web site may not include all articles that will be published in the journal. After a manuscript is technically edited and formatted, it will be removed from the “Just Accepted” Web site and published as an ASAP article. Note that technical editing may introduce minor changes to the manuscript text and/or graphics which could affect content, and all legal disclaimers and ethical guidelines that apply to the journal pertain. ACS cannot be held responsible for errors or consequences arising from the use of information contained in these “Just Accepted” manuscripts.

1
2
3 **Discovery of Novel Naphthylphenylketone and Naphthylphenylamine**
4
5
6 **Derivatives as Cell Division Cycle 25B (CDC25B) Phosphatase Inhibitors:**
7
8
9 **Design, Synthesis, Inhibition Mechanism and *in Vitro* Efficacy against**
10
11 **Melanoma Cell Lines**
12
13
14
15

16 Carmen Cerchia,^{1,+} Rosarita Nasso,^{2,4,+} Matteo Mori,^{3,+} Stefania Villa,³ Arianna Gelain³,
17
18 Alessandra Capasso,² Federica Aliotta,² Martina Simonetti,² Rosario Rullo,^{2,5} Mariorosario
19
20 Masullo,⁴ Emmanuele De Vendittis,² Maria Rosaria Ruocco,^{2,*} Antonio Lavecchia^{1,*}
21
22
23
24
25

26 ¹ *Department of Pharmacy, "Drug Discovery" Laboratory, University of Naples Federico II,*
27
28 *Via D. Montesano, 49, 80131 Naples, Italy*
29
30

31 ² *Department of Molecular Medicine and Medical Biotechnology, University of Naples*
32
33 *Federico II, Via S. Pansini 5, 80131 Naples, Italy*
34
35

36 ³ *Department of Pharmaceutical Sciences, University of Milan, Via Mangiagalli, 25, 20133*
37
38 *Milan, Italy*
39
40

41 ⁴ *Department of Movement Sciences and Wellness, University of Naples "Parthenope", 80133*
42
43 *Naples, Italy*
44
45

46 ⁵ *Institute for the Animal Production Systems in the Mediterranean Environment, Via Argine*
47
48 *1085, 80147 Naples, Italy*
49
50
51
52
53
54
55
56
57
58
59
60

ABSTRACT

CDC25 phosphatases play a critical role in the regulation of the cell cycle and thus represent attractive cancer therapeutic targets. We previously discovered the 4-(2-carboxybenzoyl)phthalic acid (NSC28620) as a new CDC25 inhibitor endowed with promising anticancer activity in breast, prostate and leukemia cells. Herein, we report a structure-based optimization of NSC28620, leading to the identification of a series of novel naphthylphenylketone (NPK) and naphthylphenylamine (NPA) derivatives as CDC25B inhibitors. Compounds **7j**, **7i**, **6e**, **7f** and **3** showed higher inhibitory activity than the initial lead, with K_i values in the low micromolar range. Kinetic analysis, intrinsic fluorescence studies and induced fit docking simulations provided a mechanistic understanding of the activity of these derivatives. All compounds were tested in the highly aggressive human melanoma cell lines A2058 and A375. Compound **4a** potently inhibited cell proliferation and colony formation, causing an increase of the G2/M phase and a reduction of G0/G1 phase of the cell cycle in both cell lines.

INTRODUCTION

The cell division cycle 25 phosphatases (CDC25s) are members of the family of dual-specificity phosphatases (DSPs) and regulate cyclin-dependent kinase (Cdk) complexes, which are key participants in the cell cycle.^{1, 2} CDC25s are also critical components of the cell cycle checkpoints for handling DNA damage and are inactivated or degraded to induce cell cycle arrest. Misregulation of these processes can cause genomic instability^{3, 4} and ultimately lead to cancer. In mammalian cells three variants of CDC25 were identified: CDC25A, -B and -C.⁵ CDC25A dephosphorylates Cdk4-Cyclin D⁶ and Cdk6-Cyclin D complexes,⁷ as well as Cdk1-CyclinB, Cdk2-Cyclin A and Cdk2-Cyclin E complexes,^{8, 9} controlling both G1/S and G2/M progression. CDC25B regulates the G2/M transition by activating Cdk1-Cyclin B complex at the centrosome which is subsequently completely activated by CDC25C in the nucleus at the onset of mitosis.¹⁰ Furthermore, CDC25B was reported to dephosphorylate and activate also Cdk2-Cyclin A and Cdk2-Cyclin E complexes.^{11, 12} CDC25C regulates the G2/M transition by targeting Cdk1-Cyclin B complex.^{13, 14} However, it is believed that all three variants of CDC25 are involved in the regulation of both G1/S and G2/M transitions.¹⁵ CDC25A and CDC25B overexpression is frequently observed in various human cancers, and often associated with more aggressive tumors and poor clinical outcome.^{10, 16} Concerning CDC25C, only a few studies showed an overexpression of this form in cancers.^{17, 18} However, growing evidence suggests that the overexpression of CDC25C could be underrated because of the non-consideration of its alternative splicing.^{19, 20} The overexpression of CDC25s in many human cancers supports their clinical significance and has encouraged the pursuit of specific small molecule inhibitors.

The crystal structures of the catalytic domain of CDC25A (PDB: 1C25)²¹ and CDC25B (PDB:1QB0)²² have been solved at 2.3 Å and 1.9 Å resolution, respectively. Despite the close

1
2
3 structural similarity between the two proteins with regard to the catalytic domain, CDC25A
4 fails to bind oxyanions in its catalytic site, whereas CDC25B readily binds tungstate and
5 sulfate. Moreover, the C-terminal region is well ordered in the crystal structure of CDC25B
6 (residues 531–547), and folded into a well-defined α -helix, while in the CDC25A crystal
7 structure this region is undefined. The active-site region of CDC25A appears in a flat
8 conformation and exposed to bulk solvent, whereas the structure of the catalytic domain of
9 CDC25B reveals a shallow active site cleft, positioned near a large cavity formed by highly
10 hydrophilic moieties in the C-terminal residues of CDC25B, which was referred to as the
11 “swimming pool” due to the abundant presence of many well organized water molecules.²³
12
13 Therefore, the structure-based design of inhibitors and the derivation of significant structure-
14 activity relationships (SAR) are really challenging. Nevertheless, several CDC25s inhibitors
15 with different structural features were discovered over the past years, the most potent of
16 which are quinonoid-based derivatives.²⁴⁻²⁷ These latter mainly act via irreversible inhibition
17 of CDC25s by electrophilic modification^{28, 29} or oxidation of the critical cysteine residue in
18 the catalytic domain by reactive oxygen species (ROS).^{30, 31} Furthermore, quinone-containing
19 agents could potentially trigger a range of unrelated events in cells because ROS may oxidize
20 other phosphatases, as well as unrelated cysteine-based enzymes,²⁶ raising questions about
21 their potential toxicity and limiting their therapeutic applications.³²
22
23

24
25
26 Among the CDC25 inhibitors reported to date, very few display reversible inhibition
27 kinetics. The indolyhydroxyquinone **8L**,³³ the naphthofurandione 5169131,³⁴ the pyrazolone
28 derivative EK-6136,³⁵ the thiazolepyrimidine **44**³⁶ and the aminoisoquinolinone **13**³⁷ in
29 Figure 1 are some representatives. However, most of the reversible inhibitors have potency
30 within the micromolar range with no currently defined clinical utility. Thus, the identification
31 of non-quinoid reversible inhibitors that do not oxidize cysteine residues or generate ROS
32
33
34
35
36
37
38
39
40
41
42
43
44
45
46
47
48
49
50
51
52
53
54
55
56
57
58
59
60

1
2
3 would have great potential for the development of pharmaceutical agents and useful
4
5 biological tools.
6

7
8 Insert Figure 1
9

10 We have previously reported the discovery of a new CDC25 inhibitor with cytotoxic
11 activity, the 4-(2-carboxybenzoyl)phthalic acid (NSC28620) by means of a structure-based
12 high-throughput virtual screening.³⁸ This compound displayed reversible, competitive
13 inhibition kinetics with K_i values of 2.3 and 5.3 μM for CDC25A and -B, respectively,
14 arrested cells at the G0/G1 and G2/M phases of the cell cycle, increased Cdk1
15 hyperphosphorylation in K562 leukemia cells and significantly inhibited the growth of
16 human MCF-7 breast, PC-3 prostate and K562 leukemia cancer cell lines.
17
18
19
20
21
22
23
24
25

26 Metastatic melanoma is one of the most aggressive and therapy-resistant human cancers.
27 So, much effort is being directed at discovering new, effective agents for the treatment of this
28 cancer, by targeting various signaling pathways and attacking elements that underlie the
29 tumor's propensity for growth and chemoresistance.³⁹ Previous studies have reported that
30 Cdk2, Cdk4, Cdk6, cyclins D1, E, and D3 and CDC25A were significantly overexpressed in
31 metastatic melanomas as compared to nevus tissue.⁴⁰⁻⁴² Moreover, other literature data have
32 indicated that phosphorylation and inhibition of CDC25B cause delayed progression from G2
33 into mitosis in melanoma cells.⁴³ Finally, we have recently demonstrated that a small
34 molecule CDC25 inhibitor was able to arrest melanoma cells in G2/M phase through an
35 intrinsic apoptotic pathway.²⁷ Taken together, these evidences emphasize that CDC25 could
36 be considered as a possible target in treating melanoma.
37
38
39
40
41
42
43
44
45
46
47
48
49

50
51 Herein we present the results of our lead optimization program, pursued on the CDC25
52 inhibitor lead NSC28620. Guided by preliminary docking studies, we rationally explored
53 different substitution patterns with the purpose of improving the inhibitory profile of the
54 starting lead and optimizing its potential as antitumor drug. A total of 31
55
56
57
58
59
60

1
2
3 naphthylphenylketone (NPK) and naphthylphenylamine (NPA) derivatives were synthesized
4 (Table 1) and tested according to a SAR investigation by a step-by-step modification strategy.
5
6 Among them, twelve compounds (**3**, **3b**, **6b,d,e**, **7d,f,i,j**, **8**, **9** and **12**) displayed an inhibition
7
8 potency similar or even higher compared to that exerted by the lead compound NSC28620
9
10 (Table 1), **7j** being 7-fold more active than NSC28620; the remaining nineteen derivatives
11
12 conserved a lower but measurable inhibition. The biological effect of these compounds was
13
14 evaluated in a cellular context, using the highly aggressive human melanoma cell lines A2058
15
16 and A375. The data showed that, when tested at a very low concentration, only compound **4a**
17
18 was by far the most effective one in the inhibition of cell proliferation and colony formation,
19
20 as emerging from the cytotoxicity tests. Furthermore, compound **4a** affected the cell cycle
21
22 progression of either A2058 and A375 cells with a significant increase of the G2/M phase
23
24 and a reduction of G0/G1 phase.
25
26
27
28
29
30
31
32
33

34 RESULTS AND DISCUSSION

35 Structure-Guided Optimization of Lead NSC28620 to Target the CDC25B Phosphatase.

36 We used the binding mode of the lead compound NSC28620 into the CDC25B catalytic
37
38 domain as predicted by docking experiments³⁸ (Figure 2A) for the rational design of new
39
40 analogues to study the SAR and to achieve further increases in potency. Four regions in
41
42 NSC28620 were explored for modifications (Figure 2B) to design new compounds based
43
44 upon structural data. First, we explored additional optimization of the phthalic moiety that
45
46 binds to the swimming pool pocket of CDC25B, a protein region near to the catalytic site and
47
48 composed by both hydrophobic (F543, L445, M483, W550, P444 and L545) and polar
49
50 residues (Y428, R479, R482, E446, R544, T547 and S549).
51
52
53
54
55
56

57 Insert Figure 2
58
59
60

1
2
3 As depicted in Figure 2A, the two carboxylate groups of the phthalic moiety (positions 1
4 and 2) of NSC28620 protrude into the swimming pool region and form salt-bridges with both
5 R482 and R544 side chains. In order to explore new potential interactions (hydrophobic
6 and/or hydrophilic) within the swimming pool aimed at improving the inhibition power, we
7 thoroughly replaced the phthalic system of NSC28620 with a bulkier naphthalene ring
8 system; this moiety was undecorated (compounds **1-7**) or decorated with hydroxy, methoxy
9 or amino groups linked to one out of the positions 3, 4 and 5, corresponding to substituents
10 R¹, R² and R³, respectively (compounds **1a-c**, **3a,b**, **4a,b**, **6a,b,d,e,f**, **7a,b,d,e,f,i,j**, **8**, **9**, **10**,
11 **11**, **12**) (Table 1). In the next step, we performed the optimization of the benzoyl substituent
12 interacting with the catalytic site of CDC25B. In the complex of CDC25B with NSC28620,
13 the carboxylate group of the benzoyl moiety binds deep in the catalytic site, making a salt-
14 bridge with the R479 guanidinium group and a H-bond with the catalytic backbone NHs of
15 R479 and E478. This moiety occupies the same location as the sulfate ion bound to the
16 catalytic site of the CDC25B crystal structure.²² Therefore, we sought to explore the role of
17 the carboxylic acid function at position 2 or 3 of the benzoyl moiety (substituents R⁴ and R⁵,
18 respectively) in order to establish more favorable interactions within the catalytic domain
19 (compounds **1**, **1a-c**, **6**, **6a,b,d,e,f**, **7**, **7a,b,d,e,f,i,j** and **12**). Moreover, according to the well-
20 known Caco-2 uptake studies⁴⁴, demonstrating the enhanced permeability of esters compared
21 to their corresponding acids, the carboxylic acidic moiety was modified via esterification
22 with the aim of increasing the lipophilicity and enhancing the cellular uptake (compounds **2**,
23 **3**, **3a,b**, **4**, **4a,b**, **8**, **9**, **10**, **11**). Finally, the NSC28620•CDC25B complex revealed that the
24 carbonyl group of the inhibitor accepts a H-bond from the Y428 OH group (Figure 2A). On
25 the basis of the structural model, we replaced the carbonyl group (position X) with an amino
26 group with the overall goal to explore the H-bond acceptor or donor capability at this position
27 (compounds **3**, **3a,b**, **4**, **4a,b**, **5**, **6**, **6a,b,d,e,f**, **7**, **7a,b,d,e,f,i,j**, **8**, **9**, **10**, **11**, and **12**).
28
29
30
31
32
33
34
35
36
37
38
39
40
41
42
43
44
45
46
47
48
49
50
51
52
53
54
55
56
57
58
59
60

1
2
3
4
5
6 **Synthesis of Rationally Designed NPK and NPA Derivatives.** The general synthetic
7 strategy followed for the preparation of NPK derivatives is outlined in Scheme 1 and Scheme
8
9
10 2. Grignard's reagent was prepared *in situ* starting from the commercially available 1-
11 bromonaphthalene in presence of magnesium turnings. The organomagnesium halide was
12 added to a solution of phthalic anhydride in dry tetrahydrofuran to afford compound **1**.⁴⁵ The
13
14
15 subsequent Fischer esterification of the carboxylic group in ethanol with sulfuric acid as
16
17
18 catalyst provided the final ester **2** (Scheme 1).⁴⁶
19
20

21
22 Insert Scheme 1
23

24
25 Otherwise, in order to obtain the same class of compounds previously described but
26 bearing a hydroxyl group on the naphthalene ring, a second synthetic approach was
27 developed (Scheme 2).
28
29

30
31 The 1-aminonaphthalene (**24**), by halogenation with bromine in acetic acid, provided the
32 intermediate **13** whose treatment with sodium nitrite led to the formation of the diazonium
33 salt **14**,⁴⁷ which was isolated and characterized. The conversion of **14** into the 4-bromo-2-
34
35 hydroxynaphthalene **15a** was performed with sodium borohydride. This latter or the
36
37 commercially available 4-bromo-1-hydroxynaphthalene (**15b**) were subsequently protected as
38
39 methyl ether in the presence of iodomethane to provide the intermediates **16a,b**. Finally, the
40
41 exchange of the halogen atom with lithium by treatment with a solution of *n*-butyllithium (*n*-
42
43 BuLi) dry THF at -78°C, followed by the formylation with *N,N*-dimethylformamide, led to
44
45 the naphthaldehydes **17a,b** (Scheme 2).
46
47
48
49

50
51 On the other hand, the key intermediate **20**⁴⁸ was obtained by condensation of the
52
53 commercially available 2-bromobenzoic acid with 2-amino-2-methyl-1-propanol to afford the
54
55 intermediate **18**. This latter was reacted with thionyl chloride in diethyl ether to give the
56
57
58
59
60

1
2
3 oxazoline **19**, which underwent a metal-halogen exchange in the presence of the
4 organolithium species *n*-BuLi to afford **20**.
5

6
7
8 Compound **20** reacted with the appropriate substituted naphthaldehydes **17a,b** and the acid-
9 catalyzed deprotection of the carboxylic moiety led to the desired lactones **21a,b** in alkaline
10 condition. The oxidation of these latter with potassium permanganate and 25% aqueous
11 solution of KOH in pyridine afforded the 2-(methoxy-1-naphthyl)benzoic acids **1a** and **1b**.
12
13 Finally, the cleavage of the methyl ether of **1a** with a 1M solution of boron tribromide in
14 dichloromethane provided the final product **1c** (Scheme 2).
15
16
17
18
19
20

21
22
23
24
25
26
27
28
29
30
31
32
33
34
35
36
37
38
39
40
41
42
43
44
45
46
47
48
49
50
51
52
53
54
55
56
57
58
59
60

Insert Scheme 2

In parallel, the synthesis of NPA derivatives was carried out (Schemes 3 and 4). The appropriate substituted aryl halide and aryl amine underwent a palladium-catalyzed Buchwald amination reaction⁴⁹ (compounds **3**, **3a-c**, **3h**, **4**, **4a-c**, **4g,h** and **5**) using a mixture of palladium acetate (Pd(OAc)₂) and racemic 2,2'-bis(diphenylphosphino)-1,1'-binaphthalene (BINAP) as catalysts, in the presence of Cs₂CO₃. Since the yield of the aryl amination reaction was critically hindered by the electron deficiency of the amine, the combination of the more nucleophilic amine and more electrophilic aryl bromo derivatives was used (procedures C1 and C2, Scheme 3).

The appropriate bromo naphthylamines for the synthesis of **4g,h** were *N*-protected with di-*tert*-butyl dicarbonate.⁵⁰ The protection of the substituted benzoic acids to obtain ethyl-2(3)-bromobenzoate (**22**, **23**) was performed by Fischer esterification.⁵¹

Insert Scheme 3

A basic hydrolysis of the ester group was then performed, leading to the formation of the corresponding acids **6**, **6a-c**, **7**, **7a-c**, **7g,h** and **12** (Scheme 4)⁵². The cleavage of methoxy protection was performed with a 1M solution of boron tribromide in dichloromethane to afford compounds **6d-f** and **7d-f** (Scheme 4). The *N*-Boc protecting group of compounds **7g**

1
2
3 and **7h**, was hydrolyzed with HCl (4M in 1,4-dioxane) to give compounds **7i,j** while by using
4 trifluoroacetic acid products **10** and **11** were obtained (Scheme 4). From the deprotected
5 intermediate **10**, using the same conditions, product **12** was obtained (Scheme 4). The esters **8**
6 and **9** were achieved by esterification of compounds **6f** and **7f** respectively, in acid conditions
7 by microwave irradiation (Scheme 4).
8
9

10
11
12
13
14
15
16
17
18
19
20
21
22
23
24
25
26
27
28
29
30
31
32
33
34
35
36
37
38
39
40
41
42
43
44
45
46
47
48
49
50
51
52
53
54
55
56
57
58
59
60
Insert Scheme 4

Effect of NPK and NPA Derivatives on the Phosphatase Activity of Purified Recombinant Form of CDC25B. The evaluation of the inhibition properties exhibited by the NPK and NPA derivatives was carried out through kinetic measurements of the phosphatase activity sustained by the recombinant form of CDC25B. In particular, the hydrolysis rate of the synthetic substrate 3-O-methylfluorescein phosphate (OMFP) triggered by CDC25B was measured at different substrate concentrations, in the absence or in the presence of various inhibitor concentrations. The resulting data of initial velocity (v_i) were analyzed in Lineweaver-Burk plots, thus allowing an inspection on the inhibition mechanism possessed by the novel compounds. As reported in Table S1 (Supporting information), the affinity for the substrate OMFP measured in the absence of inhibitor ($K_M = 2.7 \pm 0.2 \mu\text{M}$), remained essentially unvaried in the presence of some inhibitors, decreased with other inhibitors or slightly increased with the remaining ones. On the other hand, the maximum velocity of OMFP hydrolysis measured in the absence of inhibitor ($V_{\text{max}} = 323 \pm 10 \text{ AU/min}$) significantly decreased in the presence of the indicated concentrations of all synthesized compounds. These findings differ from the data already reported for NSC28620, because this compound caused an increase of the K_M without any variation of the V_{max} , a typical behavior for a competitive inhibition of CDC25B.³⁸ Therefore, none of the analyzed compounds may be ranked as a competitive inhibitor of CDC25B; probably, the addition of a bulky benzene

ring in all derivatives causes a variation in the binding mode of the inhibitors to CDC25B. However, this different interaction drives in some cases to a stronger inhibition of CDC25B (Table 1). An inspection of the kinetic data allowed a putative assignment of the compounds to different categories of inhibition mechanism. Hence, inhibitors were classified as non-competitive (Figure S1 of Supporting Information), un-competitive (Figure S2 of Supporting Information) or mixed (Figure S3 of Supporting Information) on the basis of the comparison of the Lineweaver-Burk plots obtained in the presence of different inhibitor concentrations with that obtained in the absence of inhibitor. For instance, as depicted in Figure 3A, **7j** appears as a typical non-competitive inhibitor, because the progressive decrease of the V_{\max} at increasing inhibitor concentration occurs without a significant change of the K_M for OMFP (see also Table S1). On the other hand, **3** exhibits a kinetic behaviour approaching that of an un-competitive inhibitor, because the progressive decrease of V_{\max} appears to be concomitant to a roughly similar decrease of the K_M (Figure 3B and Table S1).

Insert Figure 3

This kinetic approach allowed the calculation of the inhibition constant (K_i) for each derivative on the basis of the varied kinetic parameters resulting from the inhibition. The K_i values (Table 1) are comprised in a large interval ranging from 0.8 μM to 69 μM , thus indicating that the inhibition properties of this series of compounds are dependent on the modifications realized through the optimization program. In particular, some derivatives (such as **7j**, **7i**, **6e**, **7f** or **3**) are endowed with a significantly stronger inhibition potency compared to that of the initial lead NSC28620 ($K_i = 5.3 \mu\text{M}$), whereas the remaining compounds display a comparable or lower inhibition.

Insert Table 1

Most of the CDC25B inhibitors, including the lead compound NSC28620, are also active against CDC25A and CDC25C.^{27, 38} Hence, an evaluation of the inhibition properties of some

1
2
3 NPA derivatives towards the recombinant forms of both CDC25A and -C was considered. In
4 particular, we have checked the inhibition potency of the most potent non-competitive and
5 un-competitive inhibitor, i.e. **7j** and **3**, respectively. Using the same approach and
6 experimental conditions adopted for CDC25B, the kinetic parameters K_M and V_{max} measured
7 for CDC25A in the absence of inhibitors were 2.0 μM and 217 AU/min, respectively; these
8 values were quite similar to those obtained for CDC25B. On the other hand, the
9 corresponding K_M and V_{max} measured for CDC25C were 16 μM and 182 AU/min, thus
10 indicating that this CDC25 form exhibits a lower catalytic efficiency, essentially due to a
11 lower affinity for the synthetic substrate OMFP. The kinetic measurements obtained in the
12 presence of the inhibitors **7j** and **3** indicated that both compounds were active also on
13 CDC25A and -C. In particular, the K_i of **7j** towards CDC25A and -C was 0.6 μM and 4.0
14 μM , respectively, whereas the corresponding K_i of **3** was 0.6 μM and 0.4 μM , respectively. In
15 the complex, the analysis of the inhibition parameters related to the three CDC25 forms could
16 reflect slight differences in the binding mode of substrate and/or inhibitor, as already reported
17 for other CDC25 inhibitors.^{27, 38}

18
19
20
21
22
23
24
25
26
27
28
29
30
31
32
33
34
35
36
37
38
39
40 **SAR Investigation.** The biochemical evaluation of the inhibitory effects of the thirty-one
41 compounds against CDC25B allowed a comprehensive description of the SAR for both NPK
42 and NPA scaffolds. Derivatives bearing a carbonyl group as linker were all less active than
43 the lead compound NSC28620 (**1**, **1a**, **1c** and **2**), with only compound **1b** showing a nearly
44 comparable activity. Indeed, the replacement of the carbonyl group with a secondary amino
45 group in the X position caused an overall improvement of the inhibition power of this series
46 of derivatives, as emerging from the comparison of the K_i values of **1** vs **6** (69 vs 22 μM), **1a**
47 vs **6a** (36 vs 16.9 μM), **1c** vs **6d** (34 vs 5.1 μM), or **2** vs **3** (54 vs 2.8 μM).

1
2
3 Then, we analyzed the effects observed for the compounds bearing the carboxylic acid
4 moiety at R⁵ (derivatives **7** and **7a,b,d-f,i,j**). The unsubstituted derivative **7**, as well as
5 compounds bearing the methoxy group at R¹ (**7a**) or R² (**7b**) showed poor inhibitory activity
6 (K_i 30, 55 or 45 μ M in **7**, **7a** or **7b**, respectively). Instead, the introduction of polar
7 substituents caused an interesting increase in inhibition potency. Indeed, the presence of the
8 hydroxyl group at R¹ (**7d**), R² (**7e**), and even more at R³ position (**7f**) significantly enhanced
9 the inhibition power, as reflected by the decrease of the K_i value in the order: 30 μ M in **7** >>
10 5.8 μ M in **7d** ~ 6.4 μ M in **7e** > 2.9 μ M in **7f**. Furthermore, the introduction of the amino
11 group at R² in **7i** and even more at R³ in **7j** provoked a further increase of the inhibition
12 power (1.4 μ M in **7i** and 0.8 μ M in **7j**), leading to the most potent compound of the whole
13 series of inhibitors. Moreover, **7j** was 7-fold more active than the initial lead NSC28620.
14 Therefore, the presence of one polar group (hydroxyl or amino) on the naphthalene system of
15 inhibitors carrying a carboxylic group at R⁵ significantly increased their capability of
16 inhibiting the CDC25B phosphatase activity.
17
18
19
20
21
22
23
24
25
26
27
28
29
30
31
32
33
34
35

36 A somehow similar trend was observed when the free carboxylic moiety was moved at
37 position R⁴ (derivatives **6**, **6a,b,d-f**, **12**). The unsubstituted derivative **6** had a low inhibition
38 activity (K_i 22 μ M), similar to that obtained after the introduction of the methoxy group at
39 position R¹ in **6a** (K_i 16.9 μ M); however, when this group was moved at R² in **6b**, a
40 remarkable increase of the inhibition potency was observed (K_i 6.1 μ M). Instead, the
41 presence of the hydroxy group at R² in **6e** conferred the highest potency in this series (K_i 2.7
42 μ M), but shifting this group at R¹ in **6d** or even more at R³ in **6f** caused a decrease in potency
43 (K_i 5.1 μ M in **6d** and 13.4 μ M in **6f**). Instead, derivative **12**, where position R³ was occupied
44 by an amino group, showed an improved inhibition (K_i 6.5 μ M) compared to **6d**.
45
46
47
48
49
50
51
52
53
54
55

56 In some derivatives the esterification of the carboxylic group at R⁴ (**3**, **3a-b**, **8**, **10**) or R⁵
57 (**4**, **4a-b**, **9**, **11**) position was performed in order to increase the lipophilicity of the compound.
58
59
60

1
2
3 Among the ester series at R⁴, the unsubstituted derivative **3** showed the highest potency (K_i
4 2.8 μM). No improvement of the inhibition power was obtained with the introduction of a
5 methoxy group at position R¹ in **3a** or R² in **3b**, or with the presence of a polar substituent,
6
7 such as hydroxyl or amino group at position R³ in **8** or **10**, respectively. Instead, the K_i value
8 of the substituted derivatives raised to 12.5 μM in **3a**, or slightly increased to 6.9 μM in **3b**,
9
10 7.4 μM in **8** or 9.9 μM in **10**. Therefore, the activity of these compounds is not improved by
11
12 the presence of different substituents on the naphthalene moiety.
13
14
15
16
17
18

19 Moving to the ester function at R⁵, in four out of five derivatives the inhibition power
20 was essentially similar to that exhibited by the corresponding ester analogues at R⁴. In
21 particular, the unsubstituted derivative **4** displayed a slightly lower potency (K_i 7.3 μM) than
22 the analogue **3**. Derivatives bearing the methoxy group at R¹ (**4a**) or R² (**4b**) showed potency
23 in the same range (8.5 and 11.9 μM , respectively) of the analogues **3a** and **3b**. A slight
24 improvement of the potency (K_i 4.9 μM) was obtained upon the introduction of the hydroxyl
25 group at R³ in **9**; in contrast, the presence of the amino group at this position was,
26 surprisingly, detrimental (K_i 36 μM in **11**).
27
28
29
30
31
32
33
34
35
36

37 In conclusion, the presence of the NPA scaffold appears to be sufficient to attain the best
38 inhibition, when the carboxylic group at R⁴ or R⁵ was esterified.
39
40
41
42
43

44 **Intrinsic Fluorescence of the CDC25B Catalytic Domain Upon the Addition of Typical**
45 **NPA Derivatives.** The amino acid sequence of the catalytic domain of CDC25B includes one
46 tryptophan (W550) and eleven tyrosine residues (Y382, Y400, Y428, Y430, Y432, Y497,
47 Y501, Y502, Y506, Y512 and Y528).²² In particular, W550 is located in the protein region
48 known as “swimming pool” for the great number of water molecules found in the crystal
49 structure.²² These findings prompted an investigation on the intrinsic fluorescence of the
50 purified recombinant CDC25B; Figure 4 shows the emission spectrum obtained at the
51
52
53
54
55
56
57
58
59
60

1
2
3 excitation wavelength of 280 nm (black line). The emission maximum at 357 nm is likely due
4
5 to the intrinsic fluorescence of W550, whereas the shoulder around 310 nm is probably due to
6
7 the emission of the eleven tyrosine residues. This hypothesis was confirmed by the emission
8
9 spectrum recorded at 295-nm excitation wavelength. Under this condition, a drastic reduction
10
11 of the tyrosine emission was obtained and, as predicted, the shoulder at 310 nm essentially
12
13 disappeared, whereas the emission maximum at 357 nm was still present, although reduced in
14
15 quantum yield (not shown). These findings indicate a clear distinction between tryptophan
16
17 and tyrosine emission; furthermore, the position of the emission peak at 357 nm is typical of
18
19 the great exposure of W550 to the water environment, thus suggesting that this residue lays
20
21 on the edge of the swimming pool.
22
23
24
25

26
27 The effect of the inhibitors on the intrinsic fluorescence of CDC25B was investigated
28
29 by adding some NPA derivatives causing a measurable inhibition of the CDC25B
30
31 phosphatase activity. In particular, compounds **7j** and **7i**, typical non-competitive inhibitors,
32
33 were added at 1.5 μM and 3 μM respectively, whereas the un-competitive inhibitors **3** and **4a**
34
35 were added at 4 μM and 10 μM , respectively. The chosen concentrations reflected the
36
37 different inhibition potency of the various inhibitors. As shown in Figure 4, **7j** (purple line)
38
39 and **7i** (green line) caused an evident quenching of the fluorescence yield, without shifting the
40
41 emission maximum at 357 nm. On the other hand, the addition of **3** (red line) or **4a** (blue line)
42
43 was ineffective in altering the CDC25B emission maximum. A possible explanation for the
44
45 different behavior of the inhibitors is hereafter reported. Indeed, the non-competitive
46
47 inhibitors **7j** and **7i** could directly bind to CDC25B and this interaction caused a
48
49 conformational change in the region containing W550. On the other hand, the un-competitive
50
51 inhibitors **3** and **4a** could be unable to directly bind to the enzyme, because binding of these
52
53 compounds should require the preformed enzyme•substrate complex. Obviously, the
54
55 substrate OMFP was omitted in fluorescence experiments, owing to its fast hydrolysis.
56
57
58
59
60

1
2
3
4
5
6
7
8
9
10
11
12
13
14
15
16
17
18
19
20
21
22
23
24
25
26
27
28
29
30
31
32
33
34
35
36
37
38
39
40
41
42
43
44
45
46
47
48
49
50
51
52
53
54
55
56
57
58
59
60

Insert Figure 4

Docking Studies. Among the thirty-one synthesized derivatives, compounds **7j** and **3** are representative members of a different binding interaction with CDC25B, as emerging from the kinetic and fluorescence studies. Extensive efforts trying to co-crystallize CDC25B with **7j** and **3** or to soak **7j** and **3** into crystals of CDC25B were unsuccessful. We next carried out docking experiments into the CDC25B crystal structure (PDB ID: 1QB0)²² in an attempt to determine the binding mode of these two NPA derivatives and to rationalize the observed SAR data. Under this concern, we have the information of the kinetic data, indicating that **7j** and **3** are non-competitive and un-competitive inhibitor, respectively. This means that **7j** and **3** must, by definition, be able to bind in a site distinct from the substrate active site and leave the active site unblocked. However, **7j** should equally react with free enzyme or the enzyme•substrate complex, whereas **3** should react only with the complex. In addition, several CDC25B inhibitors identified by other groups have been proposed to bind into the swimming pool,^{23, 34, 53-55} that is a deep and concave pocket between the C-terminal helix A and the P-loop and does not face the catalytic site directly. Another useful information for docking experiments comes from the fluorescence studies, suggesting that **7j** directly binds to CDC25B in a region affecting the emission of W550, the residue located in the C-terminal helix lining the swimming pool. Vice versa, **3** seems to be unable to directly bind to the free enzyme. Hence, our docking studies were focused on the swimming pool site.

Analysis of the available crystal structures of the native catalytic domain of CDC25B (Figure S4 of Supporting Information) showed that several residues of the swimming pool (W550, R548, R544, F543, L540, N532, Y428, E446, R482), as well as residues that surround the active site cleft exhibit much higher B-factors, which is indicative of their higher flexibility. In particular, R482, which plays an important role in the catalytic activity of the enzyme,⁵⁶ showed the highest degree of mobility. Thus, **7j** and **3** were docked to the

1
2
3 structure of CDC25B using the Induced Fit Docking (IFD) protocol of the Schrödinger
4 suite,^{57, 58} that is intended to circumvent the inflexible binding site and accounts for the side
5 chain (Figure S4 of Supporting information) or backbone movements or both upon ligand
6 binding. Docking results were validated with the metadynamics method described by Clark et
7 al., which allows accurate and reliable predictions of protein•ligand binding poses at a
8 feasible computational cost.⁵⁹

9
10 As illustrated in Figure 5A, the top-ranked solution for the most potent non-competitive
11 inhibitor **7j** was deeply inserted into the swimming pool, with the carboxylic acid moiety
12 forming two strong salt-bridges with R482 and R544. This latter formed an additional cation-
13 π interaction with the naphthalene moiety of the ligand. Notably, both arginine residues are
14 involved in the recognition of the Cdk phosphate group and were previously described to be
15 critical for the binding of CDC25 inhibitors by both site-directed mutagenesis⁶⁰ and
16 computational studies.^{55, 61} In addition, the participation of R482 and R544 in the binding of
17 CDC25B inhibitors was also revealed by the crystal structure of CDC25B in complex with a
18 modified peptide.⁶² The secondary amino group at position X of the NPA derivative engaged
19 a H-bond with the side chain of E446, whereas the amino group at position R³ formed
20 contacts with C426 (the “back-door cysteine”)²² through a H-bond with the CO backbone.
21 The inhibitor established further hydrophobic interactions with the side chains of M483,
22 Y428 and W550, as also confirmed through the fluorescence studies. In summary, **7j** lies
23 within the swimming pool pocket and does not interfere with the substrate binding in the
24 active site, thus explaining the non-competitive nature of the inhibition, as determined
25 through kinetic analyses. Therefore, the interaction of the carboxylic acid moiety in **7j** and its
26 congeners with R482 and R544 may explain the increased inhibitory potency towards
27 CDC25B. This model also suggests that the differences in potencies observed when the polar
28 amino group was moved to another position on the naphthalene moiety (**7i**), or replaced by
29
30
31
32
33
34
35
36
37
38
39
40
41
42
43
44
45
46
47
48
49
50
51
52
53
54
55
56
57
58
59
60

1
2
3 the hydroxyl group in various positions (**7d,e,f**), could be due to a less efficient interaction
4
5 with residue C426.
6

7
8 Insert Figure 5
9

10 Next, we went on to characterize the binding mode of the most potent un-competitive
11 inhibitor **3**. Taking into account that such inhibition mechanism implies the binding of the
12 inhibitor to the enzyme•substrate complex, a model of the artificial substrate OMFP bound to
13 CDC25B was first generated. Therefore, OMFP was docked to the structure of CDC25B
14 using the IFD protocol and the binding pose metadynamics was employed to select the most
15 stable pose consistent with the catalytic mechanism. As depicted in Figure 5B, the
16 phosphoryl group of the artificial substrate was found to bind within the active site pocket of
17 CDC25B, where it formed interactions with the residues of the P-loop containing the catalytic
18 cysteine (C473). The orientation of the phosphoryl group mimicked exactly the structure of
19 the bound sulfate, mimicking a bound phosphorylated substrate, in the CDC25B crystal
20 structure.²² The xanthene moiety of OMFP protruded into the swimming pool and formed H-
21 bonds with Y428 and T547 residues as well as a π -cation interaction with R544, whereas the
22 spirobenzofuranone system was engaged in H-bonds with the side chain of R544. The
23 interaction between aromatic rings of OMFP and the M531, Y428, F543 and W550 side
24 chains further contributed to the binding through hydrophobic stabilization.
25
26
27
28
29
30
31
32
33
34
35
36
37
38
39
40
41
42
43
44

45 The newly generated CDC25B•OMFP complex was employed for further docking of **3**.
46 The resulting top-ranked binding mode, which places **3** directly in the swimming pool near
47 the bound substrate OMFP, is consistent with its un-competitive mode of inhibition. In
48 particular, the naphthalene ring of **3** was sandwiched between R482 and the xanthene moiety
49 of OMFP, with this latter forming a π -stacking interaction. In addition, **3** engaged further
50 hydrophobic interactions with M483 and L445, whereas the phenyl ring holding the ester
51 function at position 2 also stacked against the spirobenzofuranone ring of OMFP. The linker
52
53
54
55
56
57
58
59
60

1
2
3 amino group and the carbonyl ester of the inhibitor was engaged in H-bonds with the CO
4 backbone and the side chain of S549, respectively, while the ethyl-ester group interacted with
5
6 the non-polar side chain carbons of R548.
7
8
9

10 Therefore, the upper wall of the swimming pool together with the substrate OMFP
11 provide a hydrophobic environment critical for binding of the bulky NPA scaffold of **3**.
12 Indeed, the inhibition of CDC25B by **3** seems to occur when the binary enzyme•OMFP
13 complex is formed. Moreover, as evidenced by SAR data, the binding affinity of this series of
14 compounds is less influenced by the nature and position of substituents on the naphthalene
15 ring. Indeed, the unsubstituted **3** tightly fits in the hydrophobic cleft lined by the swimming
16 pool and OMFP, whereas the introduction of a methoxy group at R¹ (**3a**) is disfavored due to
17 steric clashes with E478 and R479.
18
19
20
21
22
23
24
25
26
27

28 The lower affinity of **3** and its congeners compared to **7j** seems to be due to the presence
29 of the ester function in place of the acidic one: in the first case the ester function forms only
30 weak hydrophobic interactions with the enzyme, while in the second case the free acidic
31 group is involved in strong salt-bridges with the key arginine residues within the swimming
32 pool. For these reasons, **3** adopts a different binding mode that generates a side-chain
33 reorientation into the swimming pool pocket, likely disrupting the network of interactions
34 critical for the catalytic activity of the enzyme.
35
36
37
38
39
40
41
42
43
44
45
46

47 **Effects of the NPK and NPA Derivatives on Cell Growth Rate of Melanoma Cells.** We
48 previously documented that the lead NSC28620 affected the cell cycle, increased the levels of
49 the inactive p-Cdk1, as well as reduced the cell viability of some cancer cell lines.³⁸ We next
50 evaluated the effects of the novel NPK and NPA derivatives in the metastatic human
51 melanoma cell line A2058, a highly resistant and aggressive cancer type. In a preliminary
52 screening, the effect of these compounds, added at 50 μ M, was assessed after different times
53
54
55
56
57
58
59
60

1
2
3 of treatment, using the MTT assay. After 24 h, only **4a** caused an evident cytotoxic activity,
4
5 but when the analysis was prolonged, also another compound, *i.e.* **4**, resulted cytotoxic after
6
7 48-h treatment (not shown).
8
9

10 To check the minimum concentration of **4** and **4a** leading to a reduction of the cell
11
12 growth rate, the time-dependent effect of these compounds on A2058 melanoma cells was
13
14 tested at lower concentrations, *i.e.* 2.5 and 5 μM (Figure 6, panels A and B). The data indicate
15
16 that only **4a** exerted a progressive reduction of cell viability. Indeed, after 48-h incubation,
17
18 the cell growth was significantly reduced in the presence of 5 μM **4a** and, after 72-h
19
20 treatment, the reduction of cell viability was significant even at 2.5 μM (Figure 6B). We have
21
22 then evaluated if compound **4a** exerted a cytotoxic effect even in normal cells, such as the
23
24 non-malignant human fibroblast cell line BJ-5ta (Figure 6C). The MTT assay, performed at
25
26 different concentrations and prolonged up to 72 h, clearly indicates that compound **4a** was
27
28 not cytotoxic for this non-tumor cell line, even when present at 10 μM . It is known that
29
30 fibroblasts are consistently and ubiquitously present in any body tissue; interestingly, the lack
31
32 of cytotoxicity of **4a** in BJ-5ta suggests that this compound could not cause unspecific side-
33
34 toxic effects in a normal cellular context.
35
36
37
38
39

40 Insert Figure 6
41

42 The cytotoxic effect of **4a** in melanoma cells prompted us to extend the evaluation of its
43
44 inhibition power towards the recombinant forms of CDC25A and -C, besides that of -B.
45
46 Under this concern, the values of K_i determined for CDC25A and -C were 3.0 μM and 1.9
47
48 μM , respectively. These data indicate that **4a** is active towards the three different forms of
49
50 CDC25. In the light of all these observations, compound **4a** was chosen for further biological
51
52 studies to better investigate its cytotoxicity in melanoma cell lines. Notably, the melanoma, in
53
54 its late stage, represents one of the most aggressive tumors, characterized by a low
55
56 responsiveness to conventional anti-tumoral therapies.⁶³ Therefore, **4a** is particularly
57
58
59
60

1
2
3 attractive as it is active at low concentrations in melanoma cells. Under this concern, we
4
5 should point out that the biological activity of the initial lead NSC28620 was observed only
6
7 at much higher doses, *i.e.* 200 μM , and in more responsive tumor cell lines.³⁸
8
9

10
11 Insert Figure 6

12 To evaluate the long-term cell growth inhibitory effect, we determined if **4a** could
13
14 suppress colony formation of melanoma cells. To this aim, A2058 and A375 melanoma cell
15
16 lines were exposed to increasing concentrations of **4a** (0-10 μM) and colony formation was
17
18 monitored. As shown in Figure 7, **4a** affected colony formation in a progressive and
19
20 remarkable manner. Indeed, the number of cell clones progressively decreased with 0.625,
21
22 1.25 and 2.5 μM **4a** and was almost absent in the presence of 5 or 10 μM inhibitor in both
23
24 cell lines. Hence, the capability to form cell clones, an intrinsic characteristic of tumors
25
26 cells,⁶⁴ was reduced when melanoma cells were treated with very low concentration of **4a**.
27
28
29

30
31 Insert Figure 7

32
33
34
35 **Effect of 4a on Cell Cycle Progression and p-Cdk1.** A further investigation on the
36
37 mechanisms mediating the toxic action of **4a** in melanoma cells was carried out. It is
38
39 noteworthy that CDC25 enzymes play a pivotal role in the regulation of cell cycle, as well as
40
41 in the control of DNA damage.¹⁵ Hence, the inhibitory potential of **4a** towards the CDC25B
42
43 phosphatase activity suggests that this compound could lead to a cell cycle arrest in cultured
44
45 cells. To evaluate the effect of **4a** on cell cycle progression, melanoma cells were exposed to
46
47 10 μM **4a** for 8- and 16-h and the cell cycle phase distribution was cytofluorimetrically
48
49 monitored after PI staining for either A2058 (Figure 8) or A375 (Figure 9) cells. Compared to
50
51 untreated cells, a significant increase of the G2/M phase associated to a reduction of G0/G1
52
53 phase was detected after 8-h treatment with **4a** in both A2058 (Figure 8A) and A375 (Figure
54
55 9A) cells. When the incubation was prolonged up to 16-h, a somehow different response
56
57
58
59
60

1
2
3 emerged from the two cell lines. In A2058 cells, a further increase of cell percentage arrested
4 in G2/M was evident, as well as an ulterior decrease of cells in G0/G1 phase, together with a
5 small not-significant increase of the sub G1 phase (Figure 8B). On the other hand, in A375
6 cell lines the number of cells arrested in G2/M phase was similar between treated and
7 untreated cells, the reduction of cell in G0/G1 phase was still evident but less pronounced
8 compared to 8 h treatment, but interestingly, the increase of sub G1 phase became greatly
9 significant, compared to untreated cells (Figure 9B). These results could indicate that the
10 arrest in G2/M represents a cellular response to the toxic effect of **4a**, perhaps mediated by
11 the CDC25 inhibition; however, this effect could evolve in cell death after a prolonged
12 treatment, as suggested by the behavior of A375 cells. The significant increase of a sub G1
13 phase observed in A375 melanoma cells after 16-h treatment is probably due to the derivation
14 of this cell line from a primary tumor, whereas A2058 is a metastatic tumor cell line; this
15 different histological origin could explain the greater responsiveness of A375 cells to the
16 drug treatment.

34
35
36
37
38
39
40
41
42
43
44
45
46
47
48
49
50
51
52
53
54
55
56
57
58
59
60
Insert Figures 8 and 9

The arrest in G2/M of both melanoma cell lines during treatment with **4a** could be related to the inhibitory capacity of this molecule toward CDC25 phosphatase activity also in a cellular system. It is known that CDC25 enzymes regulate cell cycle progression by modulating the activity of Cdks, which represent their main targets.^{65, 66} In particular, the phosphorylation of different substrates by Cdk1 is responsible for the modulation of many biochemical events involved in the entry to mitosis. Under this concern, a critical event for the activation of Cdk1 is the dephosphorylation of its inactive form, p-Cdk1, mediated by CDC25.⁶⁷⁻⁶⁹ Therefore, we verified if the treatment of melanoma cells with **4a** could affect the protein levels of p-Cdk1. Indeed, as shown in Figure 10, an increase of p-Cdk1 became evident in both melanoma cell lines after a short incubation time (8 h) with **4a**. Hence, the

1
2
3 higher protein levels of p-Cdk1 found in melanoma with respect to untreated cells could
4 represent a further evidence of the inhibitory effect exerted by **4a** on CDC25 enzymatic
5 activity in these cellular systems.
6
7
8

9
10 Insert Figure 10
11

12 CONCLUSIONS

13
14 Over the last years, many efforts have been devoted to the discovery of CDC25 inhibitors
15 featuring novel chemotypes; however, only a limited number of literature reports have
16 described the identification of inhibitors based on non-quinoid structures, although these
17 compounds could be more attracting because intrinsically endowed with lower side-toxic
18 effects.
19
20
21
22
23
24

25
26 In the present study we described the design, the synthesis, the inhibition mechanism, as well
27 as the biological effects of novel NPK and NPA derivatives as inhibitors of CDC25B, that
28 were designed starting from the lead compound NSC28620, recently reported by us. Different
29 synthetic pathways allowed the exploration of the effects of various substituents on the
30 naphthalene moiety, as well as the role of the carboxylic function, leading to the
31 identification of the main structural requirements for the inhibitory activity. Interestingly, the
32 structural modifications had a profound impact on the inhibition mechanism: indeed, while
33 the lead compound NSC28620 showed a competitive inhibition, the newly designed
34 inhibitors displayed a non-competitive, or un-competitive, or mixed behavior. Some
35 derivatives (**7j**, **7i**, **6e**, **7f** and **3**) showed higher inhibitory activity than the initial lead
36 NSC28620, with the most potent inhibitor **7j** being 7-fold more active (K_i of 0.8 μ M). IFD
37 simulations helped to rationalize the molecular basis of the activity of this series of
38 derivatives, which bind within the swimming pool pocket, as also demonstrated by kinetic
39 analysis and intrinsic fluorescence studies. Moreover, the interaction of the carboxylic acid
40 moiety of **7j** and its congeners with the key residues R482 and R544 accounts for the
41
42
43
44
45
46
47
48
49
50
51
52
53
54
55
56
57
58
59
60

1
2
3 increased inhibitory potency towards CDC25B. On the other hand, the un-competitive
4 derivatives, such as **3**, tightly fit in the hydrophobic cleft formed by the substrate OMFP and
5 the swimming pool. These compounds were characterized for their cellular activity in the
6 highly aggressive human melanoma cell lines A2058 and A375. In particular, compound **4a**
7 was the most effective one in the inhibition of cell proliferation and colony formation, also
8 causing an increase of the G2/M phase and a reduction of G0/G1 phase of the cell cycle in
9 both cell lines. Importantly, **4a** induced an increase of p-Cdk1, providing a further evidence
10 of the inhibitory effect on CDC25B. Furthermore, it is important to note that this compound
11 exhibits a cytotoxic effect at low concentration in melanoma cells, an important issue for the
12 possible reduction of undesired side effects. Our findings not only demonstrate the feasibility
13 of exploiting CDC25s as a therapeutic target for melanoma, but also suggest that the NPA
14 scaffold represents an attractive starting point for further structural elaboration to achieve
15 higher affinity, and more specific inhibition.
16
17
18
19
20
21
22
23
24
25
26
27
28
29
30
31
32
33
34
35
36
37
38
39
40
41
42
43
44
45
46
47
48
49
50
51
52
53
54
55
56
57
58
59
60

EXPERIMENTAL SECTION

Reagents and Chemicals. Reagents and solvents were purchased from Sigma-Aldrich and used without further purification. Some reactions involving air-sensitive reagents were performed under nitrogen atmosphere and anhydrous solvents were used when necessary. The Biotage Initiator 2.0 microwave synthesizer was used. Reactions were monitored by thin layer chromatography analysis on aluminum-backed Silica Gel 60 plates (70-230 mesh, Merck), using an ultraviolet fluorescent lamp at 254 nm and 365 nm. Visualization was aided by opportune staining reagents. Purification of intermediates and the final compounds was performed by flash chromatography using Geduran® Si 60 (40-63 μm , Merck). ^1H - and ^{13}C -NMR spectra were recorded at room temperature on a Varian Oxford 300 MHz instrument using TMS as internal standard. CDCl_3 , CD_3OD , acetone- d_6 and $\text{DMSO-}d_6$ were used as deuterated solvents for all the spectra run. Chemical shift are expressed as δ (ppm). Multiplicity is reported as *s* (singlet), *br s* (broadened singlet), *d* (doublet), *t* (triplet), *q* (quartet), *m* (multiplet), *dd* (doublet of doublets), *dt* (doublet of triplets). The coupling constants (*J*-values) are given in Hertz (Hz). All spectroscopic data match the assigned structures. The melting points were determined on a Buchi Melting Point B540 instrument. MS analyses were carried out with a Thermo Finnigan LCQ Advantage system, equipped with a quaternary pump, a Diode Array Detector (working wavelength: 254 nm) and a MS spectrometer, with an Electrospray ionization source and an Ion Trap mass analyzer (ionization: ESI positive or ESI negative; capillary temperature: 250°C; source voltage: 5.50 kV; source current: 4.00 μA ; multipole 1 and 2 offset: -5.50 V and -7.50 V, respectively; intermultipole lens voltage: -16.00 V; trap DC offset voltage: -10.00 V). Elemental analyses (CHN) are within $\pm 0.40\%$ of theoretical values. The results of elemental analyses, carried out with a EurovectorEuro EA 3000 model analyzer, indicated that the purity of all tested compounds was higher than 95%.

1
2
3 **General Procedure A.** To a stirred mixture of the proper lactone (0.172 mmol) in 25%
4 KOH (1 mL) and pyridine (0.5 mL), powdered KMnO_4 (43.5 mg, 0.275 mmol) was added,
5
6 and the mixture was heated at reflux for 5 hours. The hot mixture was filtered and the residue
7
8 was washed with water. Then, the filtrate was extracted with diethyl ether (2×2 mL) to
9
10 remove the unreacted lactone. The aqueous phase was acidified with 3N HCl (2 mL),
11
12 extracted with ethyl acetate (3×2 mL), washed with water and the organic layer was dried
13
14 over anhydrous sodium sulfate. The organic solvent was evaporated under *vacuum* to give a
15
16 crude oil, which was purified by flash chromatography eluting firstly with cyclohexane/ethyl
17
18 acetate (80:20) and then (10:90) to afford the desired compounds.
19
20
21
22
23

24 **General Procedure B.** To a solution of the suitable bromobenzoic acid (2.487 mmol) in
25 ethanol (1 mL), a catalytic amount of concentrated sulfuric acid was added dropwise. The
26
27 resulting mixture was kept under stirring at reflux overnight and, after cooling, the solvent
28
29 was evaporated under *vacuum*. Ethyl acetate (3 mL) was added, and the organic layer was
30
31 firstly washed with a saturated solution of sodium bicarbonate (1×2 mL) and then with water
32
33 (2×2 mL). The organic solvent was dried over anhydrous sodium sulfate and evaporated.
34
35 Purification with flash chromatography (eluent: cyclohexane/ethyl acetate 90:10) was
36
37 performed.⁵²
38
39
40
41

42 **General Procedure C.** *Procedure C1.* A dried flask was purged with argon, charged
43
44 with (±)-BINAP (3% mmol), and then toluene (2.7 mL) was added. The mixture was heated
45
46 to 80°C under stirring until the BINAP was dissolved. The solution was cooled to room
47
48 temperature, and $\text{Pd}(\text{OAc})_2$ (2% mmol) was added. The mixture was stirred at room
49
50 temperature for 1 minute, then a solution of the proper 1-bromonaphthalene (1.0 mmol) and
51
52 the corresponding ethyl aminobenzoate (0.8 mmol) in toluene (0.5 mL) was added. Finally,
53
54 Cs_2CO_3 (1.14 mmol) and other toluene (2 mL) were added to the reaction mixture. The
55
56 solution was heated at 80°C under stirring; then, it was cooled to room temperature, diluted
57
58
59
60

1
2
3 with diethyl ether, filtered and concentrated. The obtained crude product was purified by
4
5 column chromatography to provide the desired adduct.⁴⁹
6

7
8 *Procedure C2.* A dried flask was purged with argon, charged with (±)-BINAP (3%
9
10 mmol), and then toluene (2.7 mL) was added. The mixture was heated to 80°C under stirring
11
12 until the BINAP was dissolved. The solution was cooled to room temperature, and Pd(OAc)₂
13
14 (2% mmol) was added. After stirring the mixture at room temperature for 1 minute, a solution
15
16 of the suitable ethyl bromobenzoate (1.0 mmol) with the appropriate naphthylamine (0.8
17
18 mmol) in toluene (0.5 mL) was added. Cs₂CO₃ (1.14 mmol) was introduced within the
19
20 mixture and toluene (2 mL) was added. The mixture was heated to 80°C under stirring; then,
21
22 it was cooled to room temperature, diluted with diethyl ether, filtered, and concentrated. The
23
24 crude product was purified by column chromatography to obtain the desired adduct.⁴⁹
25
26
27

28
29 **General Procedure D.** To a solution of the suitable ethyl-(naphthylamino)-benzoate
30
31 (0.15 mmol) in 2 mL of THF/EtOH (1:1), 1M NaOH (0.375 mmol) was added. The resulting
32
33 mixture was refluxed for a different period of time, depending on the substrate. The solvent
34
35 was evaporated, and then water (2 mL) was added. The aqueous phase was firstly washed
36
37 with diethyl ether in order to purify the reaction mixture from the unreacted starting material,
38
39 and then treated with 1N HCl (0.5 mL). The acid was extracted with ethyl acetate (3×1 mL),
40
41 the organic phase was dried over anhydrous sodium sulfate and the solvent was evaporated
42
43 under reduced pressure. The crude product was purified by flash chromatography eluting
44
45 with dichloromethane/methanol (95:5) to afford the desired derivatives.⁵⁰
46
47
48

49
50 **General Procedure E.** To a solution of the proper methoxynaphthalene (0.180 mmol) in
51
52 dry dichloromethane (2 mL), BBr₃ (1M in dichloromethane, 0.945 mmol) was added
53
54 dropwise under N₂. The reaction was carried out at room temperature for all the synthesized
55
56 compounds. The starting solution was firstly cooled at -78°C and BBr₃ was carefully added
57
58 dropwise to the reaction mixture. After 20 minutes, the resulting solution was warmed to
59
60

1
2
3 room temperature and the stirring was continued for further 3 hours. The reaction was then
4
5 quenched at 0°C with water (4 mL), and extracted with ethyl acetate (3×2 mL). The
6
7 combined organic phases were washed with brine (3×1 mL) and dried over anhydrous
8
9 sodium sulfate. The subsequent filtration and evaporation of the organic solvent provided a
10
11 crude product, which was purified by flash chromatography eluting firstly with
12
13 dichloromethane/methanol (95:5) and then with dichloromethane/ methanol (80:20) to afford
14
15 the final naphthol.⁴⁹
16
17

18
19 **General Procedures F. Procedure F1.** To an ice-cold solution of the proper *tert*-butyl-
20
21 naphthylcarbamate (1.67 mmol) in dry 1,4-dioxane (1 mL), HCl (4M in 1,4-dioxane, 1 mL)
22
23 was added dropwise, under N₂. The reaction was stirred at room temperature for 24 hours.
24
25 After completion of the reaction, monitored by TLC, diethyl ether was added to the reaction
26
27 mixture and it was stirred. After cooling at 0°C, the formed precipitate was collected by
28
29 filtration, washed with cold diethyl ether and dried to afford the hydrochloride salt of
30
31 compound **7i** or **7j**.
32
33

34
35 *Procedure F2.* Trifluoroacetic acid (0.65 mmol) was added to a solution of the suitable
36
37 *tert*-butyl-naphthylcarbamate (0.13 mmol) in dichloromethane (1 mL) and the reaction was
38
39 stirred at room temperature for 60 min. The solvent was removed *in vacuo*; then, a 2M
40
41 sodium hydroxide solution (2 mL) was added and extracted with ethyl acetate (3×1 mL). The
42
43 organic layers were dried over anhydrous sodium sulfate and the solvent was evaporated
44
45 under reduced pressure. Products **10** and **11** were isolated as hydrochloride salts by treatment
46
47 with 1.25 M HCl in methanol.
48
49

50
51 **General Procedure G.** To a solution of the opportune benzoic acid (2.487 mmol) in
52
53 ethanol (1 mL), a catalytic amount of concentrated sulfuric acid was added dropwise. The
54
55 resulting mixture was stirred under microwave irradiation for 90 min at 80°C, and then the
56
57 solvent was evaporated under reduced pressure. Ethyl acetate (3 mL) was added, and the
58
59
60

1
2
3 organic layer was firstly washed with a saturated solution of sodium bicarbonate (1×2 mL)
4 and then with water (2×2 mL). The organic solvent was dried over anhydrous sodium sulfate
5 and evaporated under *vacuum*. The crude product was purified by flash chromatography.⁵²
6
7

8
9
10 **General Procedure H.** To a solution of the required bromonaphthol (0.672 mmol) in dry
11 *N,N*-dimethylformamide (1 mL) sodium hydride (60% dispersion in mineral oil, 29.6 mg,
12 0.739 mmol) was added under N₂. After the evolution of H₂, iodomethane (0.17 mL, 2.688
13 mmol) was added, and the reaction mixture was stirred at room temperature for 3 hours. After
14 the evaporation of *N,N*-dimethylformamide, the resulting residue was extracted with ethyl
15 acetate (3×2 mL). The collected organic phase was dried over anhydrous sodium sulfate and
16 the solvent was evaporated under reduced pressure to give the desired derivatives. The crude
17 oils were purified by flash chromatography (cyclohexane/ethyl acetate 90:10) to provide
18 compounds **16a** and **16b**.
19
20
21
22
23
24
25
26
27
28
29

30
31 **General Procedure I.** To a solution of the proper bromomethoxynaphthalene (0.422
32 mmol) in anhydrous THF (4 mL) cooled to -78°C under N₂ was added *n*-BuLi (2.7M in
33 heptane, 0.39 mL, 1.055 mmol) and the resulting mixture was stirred for 1 hour. Anhydrous
34 *N,N*-dimethylformamide (0.20 mL, 2.532 mmol) was added, and the reaction was stirred for a
35 further 1 hour at -78°C. The reaction was quenched by a slow addition of cold water (0.5
36 mL), in order to neutralize the unreacted *n*-BuLi, and THF and DMF were evaporated. The
37 residue was poured into 3N HCl (3 mL) and extracted with diethyl ether (6×2 mL). The
38 combined organic layers were washed firstly with water, then with a saturated sodium
39 hydrogen carbonate solution and, finally, with a saturated sodium chloride solution. The
40 organic phase was dried, filtered and concentrated. The crude oils were purified by flash
41 chromatography (cyclohexane/ethyl acetate 9:1) to provide compounds **17a** and **17b**.
42
43
44
45
46
47
48
49
50
51
52
53
54
55

56 **General Procedure J.** To a solution of compound **19** (0.787 mmol) in dry diethyl ether
57 (1 mL) at -78°C was added dropwise 0.58 mL of a 2.7 M solution of *n*-BuLi in heptane
58
59
60

1
2
3 (1.574 mmol), under N₂, obtaining intermediate **20**. The solution was stirred at -78°C for 1
4
5 hour, then the suitable methoxy-1-naphthaldehyde (0.787 mmol) was added and the reaction
6
7 mixture was stirred at room temperature overnight. To quench the unreacted *n*-BuLi, cold
8
9 water (1 mL) was dropped in the reaction mixture and then the aqueous phase was extracted
10
11 with ethyl acetate (3×2 mL). The organic phase was dried over anhydrous sodium sulfate and
12
13 the solvent was evaporated under reduced pressure. The obtained oil (284.3 mg) was
14
15 dissolved in a solution of 3N HCl (1.5 mL), and the mixture was heated at reflux for 4.5
16
17 hours. After cooling, the solid was collected and washed with water, in order to be taken up
18
19 in aqueous 10% NaOH (1.5 mL) and heated at reflux for 1 hour. The product was collected
20
21 upon acidification with 3N HCl (2 mL), extracted into ethyl acetate, washed with water and
22
23 dried over anhydrous sodium sulfate. The solvent was evaporated under reduced pressure to
24
25 give a crude solid, which was purified by flash chromatography eluting with
26
27 cyclohexane/ethyl acetate (80:20).⁴⁸
28
29
30
31
32

33 **General Procedure K.** To a solution of the suitable 1-nitronaphthalene (1.155 mmol)
34
35 and triethylsilane (0.74 mL, 4.633 mmol) in ethanol (5 mL) a catalytic amount of palladium
36
37 (II) chloride (10 mol %) was added under an N₂ atmosphere. The resulting mixture was kept
38
39 under stirring and a change of color was observed. The solvent was evaporated and then
40
41 water was added and decanted. The aqueous phase was extracted with diethyl ether (3×2
42
43 mL). The organic phase was firstly treated with 3N HCl (2 mL) and then the collected acidic
44
45 aqueous solution, containing the hydrochloride salt of the naphthylamine, was basified with
46
47 25% NaOH (2 mL) and extracted with diethyl ether (6×2 mL). The organic phase was dried
48
49 over anhydrous sodium sulfate and the solvent was evaporated under reduced pressure.⁴⁷
50
51
52
53

54 **General Procedure L.** To a solution of the proper bromo-1-naphthalenamine (1.351
55
56 mmol) in ethanol (2.5 mL) di-*tert*-butyl dicarbonate (442.3 mg, 2.026 mmol) was added. The
57
58 resulting mixture was kept under stirring for 24 hours at 30°C. Then, the solvent was
59
60

1
2
3 evaporated under reduced pressure and the crude oil was purified by flash chromatography,
4
5 eluting with cyclohexane/ethyl acetate (90:10) to afford the products.
6
7

8 **Synthesis of 2-(1-naphthoyl)benzoic acid (1).** A mixture of 1-bromonaphthalene (200
9 mg, 0.966 mmol), magnesium turnings (47 mg, 1.931 mmol), and a catalytic amount of
10 iodine in dry THF (2 mL) was refluxed under N₂ until the formation of the Grignard reagent.
11 The latter was added dropwise, under N₂, to a solution of phthalic anhydride (143.1 mg,
12 0.966 mmol) in dry THF (1.5 mL), and the resulting mixture was heated under reflux for 48
13 hours. The reaction mixture was quenched with 0.5 mL of a saturated aqueous solution of
14 ammonium chloride. The solvent was evaporated and then the aqueous layer was extracted
15 with ethyl acetate (3×2 mL). In order to purify the reaction mixture from the unreacted
16 starting material, the organic phase was firstly treated with a saturated solution of sodium
17 bicarbonate (1 mL) and then the collected alkaline aqueous layer, which contained the
18 sodium salt of compound **1**, was acidified with 3N HCl and extracted with ethyl acetate (3×2
19 mL). The organic phase was dried over anhydrous sodium sulfate, filtered, and the solvent
20 was evaporated under reduced pressure. The crude oil was purified by flash chromatography
21 eluting firstly with cyclohexane/ethyl acetate (80:20) and then with
22 dichloromethane/methanol (95:5) to afford compound **1**. Pale green solid, m.p. 175-176°C,
23 73% yield. Molecular formula: C₁₈H₁₂O₃. Molecular Weight: 276.29 g/mol. R_f = 0.28
24 (dichloromethane/methanol 95:5). ¹H NMR (300 MHz, CD₃OD) δ 8.94 (d, *J* = 8.1 Hz, 1H,
25 ArH), 7.98 (d, *J* = 8.1 Hz, 1H, ArH), 7.94-7.82 (m, 2H, ArH), 7.62-7.30 (m, 7H, ArH) ppm.
26 ESI-MS (*m/z*) Calcd: 276 Found: 275 [M-H]⁻. Anal. Calcd for C₁₈H₁₂O₃: C, 78.61; H, 4.86.
27 Found: C, 78.45; H, 4.88.
28
29
30
31
32
33
34
35
36
37
38
39
40
41
42
43
44
45
46
47
48
49
50
51
52
53

54 **2-(3-Methoxy-1-naphthoyl)benzoic acid (1a).** Procedure A: starting from **21a**. White
55 solid, m.p. 167-168°C, 71 % yield. Molecular formula: C₁₉H₁₄O₄. Molecular Weight: 306.31
56 g/mol. R_f = 0.31 (dichloromethane/methanol 95:5). ¹H NMR (300 MHz, CD₃OD) δ 8.81 (d, *J*
57
58
59
60

1
2
3 = 8.5 Hz, 1H, ArH), 7.89 (dd, $J_1 = 7.0$ Hz, $J_2 = 2.0$ Hz, 1H, ArH), 7.80 (d, $J = 8.5$ Hz, 1H,
4 ArH), 7.60-7.40 (m, 6H, ArH), 6.99 (d, $J = 2.0$ Hz, 1H, ArH), 3.82 (s, 3H, CH₃) ppm. ESI-
5 MS (m/z) Calcd: 306 Found: 305 [M-H]⁻. Anal. Calcd for C₁₉H₁₄O₄: C, 74.50; H, 4.61.
6 Found: C, 74.36; H, 4.63.
7

8
9
10
11
12 **2-(4-Methoxy-1-naphthoyl)benzoic acid (1b)**. Procedure A: starting from **21b**. Brown
13 solid, m.p. 196-197°C, 36 % yield. Molecular formula: C₁₉H₁₄O₄. Molecular Weight: 306.31
14 g/mol. Rf = 0.20 (dichloromethane/methanol 95:5). ¹H NMR (300 MHz, CD₃OD) δ 9.12 (d, J
15 = 8.5 Hz, 1H, ArH), 8.28 (d, $J = 8.5$ Hz, 1H, ArH), 7.90-7.87 (m, 1H, ArH), 7.62 (dt, $J_1 = 7.2$
16 Hz, $J_2 = 1.5$ Hz, 1H, ArH), 7.54-7.45 (m, 4H, ArH), 7.39-7.36 (m, 1H, ArH), 6.76 (d, $J = 8.1$
17 Hz, 1H, ArH), 4.02 (s, 3H, CH₃) ppm. ESI-MS (m/z) Calcd: 306 Found: 305 [M-H]⁻. Anal.
18 Calcd for C₁₉H₁₄O₄: C, 74.50; H, 4.61 Found: C, 74.39; H, 4.59.
19
20
21
22
23
24
25
26
27

28
29 **2-(3-Hydroxy-1-naphthoyl)benzoic acid (1c)**. Procedure E: starting from **1a**. Reaction
30 time: 60 min. Foam, 6 % yield. Molecular formula: C₁₈H₁₂O₄. Molecular Weight: 292.29
31 g/mol. Rf = 0.10 (dichloromethane/methanol 95:5). ¹H NMR (300 MHz, CD₃OD) δ 8.78 (d, J
32 = 8.1 Hz, 1H, ArH), 8.01 (dd, $J_1 = 7.5$ Hz, $J_2 = 1.2$ Hz, 1H, ArH), 7.72-7.64 (m, 3H, ArH),
33 7.53-7.37 (m, 3H, ArH), 7.28 (d, $J = 2.6$ Hz, 1H, ArH), 7.00 (d, $J = 2.7$ Hz, 1H, ArH) ppm.
34 ESI-MS (m/z) Calcd: 292 Found: 291 [M-H]⁻. Anal. Calcd for C₁₈H₁₂O₄: C, 73.97; H, 4.14.
35 Found: C, 73.81; H, 4.12.
36
37
38
39
40
41
42
43

44
45 **Ethyl 2-(2-naphthoyl)benzoate (2)**. Procedure B: starting from **1**. Yellow oil, 60 %
46 yield. Molecular formula: C₂₀H₁₆O₃. Molecular Weight: 304.34 g/mol. Rf = 0.38
47 (cyclohexane/ethyl acetate 90:10). ¹H NMR (300 MHz, CDCl₃) δ 9.07 (d, $J = 8.4$ Hz, 1H,
48 ArH), 8.0-7.97 (m, 2H, ArH), 7.90 (d, $J = 8.4$ Hz, 1H, ArH), 7.60-7.50 (m, 5H, ArH), 7.45 (d,
49 $J = 7.5$ Hz, 1H, ArH), 7.36 (t, $J = 8.4$ Hz, 1H, ArH), 3.90 (q, $J = 7.2$ Hz, 2H, CH₂), 0.91 (t, J
50 = 7.2 Hz, 3H, CH₃) ppm. ESI-MS (m/z) Calcd: 304 Found: 303 [M-H]⁻. Anal. Calcd for
51 C₂₀H₁₆O₃: C, 78.93; H, 5.30; Found: C, 78.81; H, 5.35.
52
53
54
55
56
57
58
59
60

Ethyl 2-(naphthalen-1-ylamino)benzoate (3). Procedure C1: starting from 1-bromonaphthalene and ethyl-2-amino-benzoate. Reaction time: 17 hours. Silver foam, quantitative yield. Molecular formula: C₁₉H₁₇NO₂. Molecular Weight: 291.34 g/mol. R_f = 0.47 (cyclohexane/ethyl acetate 98:2). Eluent for chromatography: firstly only cyclohexane, then cyclohexane/ ethyl acetate from (98:2) to till (90:10). ¹H NMR (300 MHz, CDCl₃) δ 9.85 (br s, 1H, NH, exchangeable with D₂O), 8.13-8.10 (m, 1H, ArH), 8.05 (dd, *J*₁ = 7.8 Hz, *J*₂ = 1.2 Hz 1H, ArH), 7.91-7.88 (m, 1H, ArH), 7.71 (d, *J* = 7.8 Hz, 1H, ArH), 7.55-7.45 (m, 4H, ArH), 7.27-7.22 (m, 1H, ArH), 6.96 (dd, *J*₁ = 8.7 Hz, *J*₂ = 0.9 Hz, 1H, ArH), 6.73 (dt, *J*₁ = 7.8 Hz, *J*₂ = 1.2 Hz, 1H, ArH), 4.43 (q, *J* = 7.2 Hz, 2H, CH₂), 1.45 (t, *J* = 7.2 Hz, 3H, CH₃) ppm. ESI-MS (*m/z*) Calcd: 291 Found: 290 [M-H]⁻. Anal. Calcd for C₁₉H₁₇NO₂: C, 78.33; H, 5.88; N, 4.81. Found: C, 78.78; H, 5.87; N, 4.79.

Ethyl-2-(3-methoxy-1-naphthylamino)benzoate (3a). Procedure C1: starting from 1-bromo-3-methoxynaphthalene (**16a**) and ethyl-2-aminobenzoate. Reaction time: 18 hours. Yellow oil, 71% yield. Molecular formula: C₂₀H₁₉NO₃. Molecular Weight: 321.37 g/mol. R_f = 0.62 (cyclohexane/ethyl acetate 90:10). Eluent for chromatography: cyclohexane/ethyl acetate (90:10). ¹H NMR (300 MHz, CDCl₃) δ 9.98 (br s, 1H, NH, exchangeable with D₂O), 8.08 (d, *J* = 8.1 Hz, 2H, ArH), 7.79 (d, *J* = 8.1 Hz, 1H, ArH), 7.50 (t, *J* = 8.1 Hz, 1H, ArH), 7.41-7.28 (m, 3H, ArH), 7.19 (d, *J* = 8.4 Hz, 1H, ArH), 7.02 (d, *J* = 2.4 Hz, 1H, ArH), 6.79 (t, *J* = 7.8 Hz, 1H, ArH), 4.45 (q, *J* = 6.9 Hz, 2H, CH₂), 3.95 (s, 3H, OCH₃), 1.47 (t, *J* = 6.9 Hz, 3H, CH₃) ppm. ESI-MS (*m/z*) Calcd: 321 Found: 320 [M-H]⁻. Anal. Calcd for C₂₀H₁₉NO₃: C, 74.75; H, 5.96; N, 4.36. Found: C, 74.61; H, 5.94; N, 4.38.

Ethyl-2-(4-methoxy-1-naphthylamino)benzoate (3b). Procedure C2: starting from 1-amino-4-methoxynaphthalene (**25**) and ethyl-2-bromobenzoate (**22**). Reaction time: 18 hours. Yellow oil, 98% yield. Molecular formula: C₂₀H₁₉NO₃. Molecular Weight: 321.37 g/mol. R_f = 0.40 (cyclohexane/ethyl acetate 98:2). Eluent for chromatography: cyclohexane/ethyl

1
2
3 acetate (98:2). ¹H NMR (300 MHz, CDCl₃) δ 9.49 (br s, 1H, NH, exchangeable with D₂O),
4
5 8.30 (d, *J* = 8.8 Hz, 1H, ArH), 8.06-7.89 (m, 2H, ArH), 7.55-7.42 (m, 2H, ArH), 7.37 (d, *J* =
6
7 8.2 Hz, 1H, ArH), 7.15 (t, *J* = 8.4 Hz, 1H, ArH), 6.82 (d, *J* = 8.3 Hz, 1H, ArH), 6.67-6.57 (m,
8
9 2H, ArH), 4.41 (q, *J* = 7.1 Hz, 2H, CH₂), 4.03 (s, 3H, OCH₃), 1.44 (t, *J* = 7.1 Hz, 3H, CH₃)
10
11 ppm. ESI-MS (*m/z*) Calcd: 321 Found: 320 [M-H]⁻. Anal. Calcd for C₂₀H₁₉NO₃: C, 74.75; H,
12
13 5.96; N, 4.36. Found: C, 74.63; H, 5.98; N, 4.31.

14
15
16
17 **Ethyl 2-(5-methoxy-1-naphthylamino)benzoate (3c)**. Procedure C2: starting from 1-
18 amino-5-methoxynaphthalene and ethyl-2-bromobenzoate (**22**). Reaction time: 18 hours.
19 Yellow oil, 72.66% yield. Molecular formula: C₂₀H₁₉NO₃. Molecular Weight: 321.37 g/mol.
20 R_f = 0.58 (cyclohexane/ethyl acetate 95:5). Eluent for chromatography: cyclohexane/ethyl
21 acetate (95:5). ¹H NMR (300 MHz, CDCl₃) δ 9.80 (br s, 1H, NH exchangeable with D₂O),
22 8.13 (dd, *J*₁ = 8.5 Hz, *J*₂ = 0.8 Hz, 1H, ArH), 8.02 (dd, *J*₁ = 7.8 Hz, *J*₂ = 1.2 Hz, 1H, ArH),
23 7.67 (d, *J* = 8.5 Hz, 1H, ArH), 7.58-7.32 (m, 3H, ArH), 7.23-7.20 (m, 1H, ArH), 6.96-6.79
24 (m, 2H, ArH), 6.70 (t, *J* = 7.8 Hz, 1H, ArH), 4.41 (q, *J* = 7.1 Hz, 2H, CH₂), 4.02 (s, 3H,
25 OCH₃), 1.44 (t, *J* = 7.1 Hz, 3H, CH₃).
26
27
28
29
30
31
32
33
34
35
36

37 **Ethyl 2-(5-((*tert*-butoxycarbonyl)amino)-1-naphthylamino)benzoate (3h)**. Procedure
38 C1: starting from *tert*-butyl (5-bromonaphthalen-1-yl)carbamate (**27**) and ethyl-2-
39 aminobenzoate. Reaction time: 18 hours. Foam, 76% yield. Molecular formula: C₂₄H₂₆N₂O₄.
40 Molecular Weight: 406.47 g/mol. R_f = 0.58 (cyclohexane/ethyl acetate 80:20). Eluent for
41 chromatography: cyclohexane/ethyl acetate (80:20). ¹H NMR (300 MHz, CDCl₃) δ 9.84 (br s,
42 1H, NH exchangeable with D₂O), 8.03 (dd, *J*₁ = 7.9 Hz, *J*₂ = 1.2 Hz, 1H, ArH), 7.91 (dd, *J*₁ =
43 8.4 Hz, *J*₂ = 1.6 Hz, 1H, ArH), 7.72 (d, *J* = 7.9 Hz, 1H, ArH), 7.56-7.38 (m, 3H, ArH), 7.31-
44 7.17 (m, 2H, ArH and NHCO exchangeable with D₂O), 7.00-6.79 (m, 2H, ArH), 6.73 (t, *J* =
45 7.5 Hz, 1H, ArH), 4.41 (q, *J* = 7.1 Hz, 2H, CH₂), 1.57 (s, 9H, CH₃), 1.44 (t, *J* = 7.1 Hz, 3H,
46 CH₃).
47
48
49
50
51
52
53
54
55
56
57
58
59
60

1
2
3 **Ethyl 3-(naphthalen-1-ylamino)benzoate (4)**. Procedure C1: starting from 1-
4 bromonaphthalene and ethyl-3-aminobenzoate. Reaction time: 17 hours. Yellow-brown oil,
5 83% yield. Molecular formula: C₁₉H₁₇NO₂. Molecular Weight: 291.34 g/mol. R_f = 0.39
6 (cyclohexane/ethyl acetate 90:10). Eluent for chromatography: cyclohexane/ethyl acetate
7 (95:5). ¹H NMR (300 MHz, CDCl₃) δ 8.01 (dd, *J*₁ = 8.4 Hz, *J*₂ = 1.2 Hz, 1H, ArH), 7.88 (dd,
8 *J*₁ = 7.0 Hz, *J*₂ = 2.5 Hz, 1H, ArH), 7.71-7.67 (m, 1H, ArH), 7.64-7.36 (m, 6H, ArH), 7.28 (t,
9 *J* = 8.1 Hz, 1H, ArH), 7.12 (dd, *J*₁ = 8.1 Hz, *J*₂ = 2.4 Hz, 1H, ArH), 6.06 (br s, 1H, NH,
10 exchangeable with D₂O), 4.36 (q, *J* = 7.1 Hz, 2H, CH₂), 1.38 (t, *J* = 7.1 Hz, 3H, CH₃) ppm.
11 ESI-MS (*m/z*) Calcd: 291 Found: 290 [M-H]⁻. Anal. Calcd for C₁₉H₁₇NO₂: C, 78.33; H, 5.88;
12 N, 4.81. Found: C, 78.35; H, 5.80; N, 4.79.
13
14
15
16
17
18
19
20
21
22
23
24
25

26 **Ethyl-3-(3-methoxy-1-naphthylamino)benzoate (4a)**. Procedure C1: starting from 1-
27 bromo-3-methoxynaphthalene (**16a**) and ethyl-3-aminobenzoate. Reaction time: 18 hours.
28 Yellow oil, 85% yield. Molecular formula: C₂₀H₁₉NO₃. Molecular Weight: 321.37 g/mol. R_f
29 = 0.36 (cyclohexane/ethyl acetate 90:10). Eluent for chromatography: cyclohexane/ethyl
30 acetate (98:2). ¹H NMR (300 MHz, CDCl₃) δ 7.91 (d, *J* = 8.1 Hz, 1H, ArH), 7.78-7.74 (m,
31 2H, ArH), 7.63 (dt, *J*₁ = 7.5 Hz, *J*₂ = 1.2 Hz, 1H, ArH), 7.49- 7.44 (m, 1H, ArH), 7.36-7.21
32 (m, 3H, ArH), 7.04 (d, *J* = 2.4 Hz, 1H, ArH), 6.90 (d, *J* = 2.1 Hz, 1H, ArH), 6.13 (br s, 1H,
33 NH, exchangeable with D₂O), 4.37 (q, *J* = 6.9 Hz, 2H, CH₂), 3.90 (s, 3H, OCH₃), 1.39 (t, *J* =
34 6.9 Hz, 3H, CH₃) ppm. ESI-MS (*m/z*) Calcd: 321 Found: 320 [M-H]⁻. Anal. Calcd for
35 C₂₀H₁₉NO₃: C, 74.75; H, 5.96; N, 4.36. Found: C, 74.62; H, 5.98; N, 4.32.
36
37
38
39
40
41
42
43
44
45
46
47
48

49 **Ethyl-3-(4-methoxy-1-naphthylamino)benzoate (4b)**. Procedure C1: starting from 1-
50 bromo-4-methoxynaphthalene (**16b**) and ethyl-3-aminobenzoate. Reaction time: 40 hours,
51 40% yield. Procedure C2: starting from 1-amino-4-methoxynaphthalene (**25**) and ethyl-3-
52 bromobenzoate (**23**). Reaction time: 24 hours, 94% yield. Brown oil. Molecular formula:
53 C₂₀H₁₉NO₃. Molecular Weight: 321.37 g/mol. R_f = 0.25 (cyclohexane/ethyl acetate 90:10).
54
55
56
57
58
59
60

1
2
3 Eluent for chromatography: cyclohexane/ethyl acetate (90:10). ^1H NMR (300 MHz,
4 $\text{CO}(\text{CD}_3)_2$) δ 8.30-8.26 (m, 1H, ArH), 8.05-8.02 (m, 1H, ArH), 7.53-7.46 (m, 3H, ArH), 7.39-
5
6 7.34 (m, 1H, NH, exchangeable with D_2O ; 2H, ArH), 7.23 (t, $J = 7.8$ Hz, 1H, ArH), 7.00-6.95
7
8 (m, 2H, ArH), 4.28 (q, $J = 7.1$ Hz, 2H, CH_2), 4.05 (s, 3H, OCH_3), 1.31 (t, $J = 7.1$ Hz, 3H,
9
10 CH_3) ppm. ESI-MS (m/z) Calcd: 321 Found: 320 $[\text{M}-\text{H}]^-$. Anal. Calcd for $\text{C}_{20}\text{H}_{19}\text{NO}_3$: C,
11
12 74.75; H, 5.96; N, 4.36. Found: C, 74.64; H, 5.93; N, 4.38.

13
14
15
16
17 **Ethyl 3-(5-methoxy-1-naphthylamino)benzoate (4c)**. Procedure C2: starting from 1-
18 amino-5-methoxynaphthalene and ethyl-3-bromobenzoate (**23**). Reaction time: 18 hours.
19 Brown oil, 47% yield. Molecular formula: $\text{C}_{20}\text{H}_{19}\text{NO}_3$. Molecular Weight: 321.37 g/mol. Rf
20 = 0.31 (cyclohexane/ethyl acetate 90:10). Eluent for chromatography: cyclohexane/ethyl
21 acetate (90:10). ^1H NMR (300 MHz, CDCl_3) δ 8.05 (t, $J = 4.8$ Hz, 1H, ArH), 7.65 (s, 1H,
22 ArH), 7.56 (t, $J = 7.2$ Hz, 1H, ArH), 7.44-7.36 (m, 3H, ArH, 1H, NH), 7.30-7.24 (m, 2H,
23 ArH), 7.12-7.08 (m, 1H, ArH), 6.86 (d, $J = 7.6$ Hz, 1H, ArH), 4.35 (q, $J = 7.1$ Hz, 2H, CH_2),
24 4.02 (s, 3H, OCH_3), 1.37 (t, $J = 7.1$ Hz, 3H, CH_3).

25
26
27
28
29
30
31
32
33
34
35 **Ethyl-3-(4-((*tert*-butoxycarbonyl)amino)-1-naphthylamino)benzoate (4g)**. Procedure
36 C1: starting from *tert*-butyl (4-bromonaphthalen-1-yl)carbamate (**26**) and ethyl-3-
37 aminobenzoate. Reaction time: 18 hours. Silver foam, 83% yield. Molecular formula:
38 $\text{C}_{24}\text{H}_{26}\text{N}_2\text{O}_4$. Molecular Weight: 406.47 g/mol. Rf = 0.40 (cyclohexane/ethyl acetate 80:20).
39 Eluent for chromatography: cyclohexane/ethyl acetate (80:20). ^1H NMR (300 MHz, CD_3OD)
40 δ 8.09 (d, $J = 8.1$ Hz, 1H, ArH), 8.02 (d, $J = 8.4$ Hz, 1H, ArH), 7.57-7.41 (m, 5H, ArH), 7.34
41 (d, $J = 8.1$ Hz, 1H, ArH), 7.25 (t, $J = 7.8$ Hz, 1H, ArH), 7.11 (dd, $J_1 = 8.1$ Hz, $J_2 = 2.1$ Hz,
42 1H, ArH), 4.30 (q, $J = 7.2$ Hz, 2H, CH_2), 1.55 (s, 9H, CH_3), 1.34 (t, $J = 7.2$ Hz, 3H, CH_3)
43
44 ppm.

45
46
47
48
49
50
51
52
53
54
55 **Ethyl-3-(5-((*tert*-butoxycarbonyl)amino)-1-naphthylamino)benzoate (4h)**. Procedure
56 C1: starting from *tert*-butyl (5-bromonaphthalen-1-yl)carbamate (**27**) and ethyl-3-
57
58
59
60

aminobenzoate. Reaction time: 18 hours. Foam, 85% yield. Molecular formula: $C_{24}H_{26}N_2O_4$. Molecular Weight: 406.47 g/mol. $R_f = 0.33$ (cyclohexane/ethyl acetate 80:20). Eluent for chromatography: cyclohexane/ethyl acetate (80:20). 1H NMR (300 MHz, $CDCl_3$) δ 7.82 (d, $J = 7.5$ Hz, 1H, ArH), 7.70 (d, $J = 8.4$ Hz, 1H, ArH), 7.59 (t, $J = 1.8$ Hz, 1H, ArH), 7.54-7.47 (m, 2H, ArH), 7.35-7.26 (m, 4H, ArH), 7.18 (t, $J = 7.5$ Hz, 1H, ArH), 7.02 (dd, $J_1 = 8.4$ Hz, $J_2 = 1.5$ Hz, 1H, ArH), 6.83 (br s, 1H, NH, exchangeable with D_2O), 6.02 (br s, 1H, NH, exchangeable with D_2O), 4.26 (q, $J = 6.9$ Hz, 2H, CH_2), 1.48 (s, 9H, CH_3), 1.28 (t, $J = 6.9$ Hz, 3H, CH_3) ppm.

1-(*N*-Phenylamino)naphthalene (5). Procedure C1: starting from 1-bromonaphthalene and aniline. Reaction time: 18 hours. Yellow-brown solid, m.p. 61-63°C, 34 % yield. Molecular formula: $C_{16}H_{13}N$. Molecular Weight: 219.28 g/mol. $R_f = 0.58$ (cyclohexane/ethyl acetate 90:10). Eluent for chromatography: firstly only cyclohexane and then cyclohexane/ethyl acetate (95:5). 1H NMR (300 MHz, $CDCl_3$) δ 8.04 (dd, $J_1 = 7.2$ Hz, $J_2 = 2.1$ Hz, 1H, ArH), 7.89 (dd, $J_1 = 7.2$ Hz, $J_2 = 2.1$ Hz, 1H, ArH), 7.59 (dd, $J_1 = 7.2$ Hz, $J_2 = 2.1$ Hz, 1H, ArH), 7.53-7.40 (m, 4H, ArH), 7.31-7.26 (m, 2H, ArH), 7.03-7.00 (m, 2H, ArH), 6.94 (t, $J_1 = 7.2$ Hz, $J_2 = 1.2$ Hz, 1H, ArH), 5.95 (br s, 1H, NH, exchangeable with D_2O) ppm. ESI-MS (m/z) Calcd: 219 Found: 218 $[M-H]^-$. Anal. Calcd for $C_{16}H_{13}N$: C, 87.64; H, 5.98; N, 6.39. Found: C, 87.54; H, 5.97; N, 6.36.

2-(Naphthalen-1-ylamino)benzoic acid (6). Procedure D: starting from **3**. Reaction time: 60 min. Yellow solid, m.p. 230°C, 98 % yield. Molecular formula: $C_{17}H_{13}NO_2$. Molecular Weight: 263.29 g/mol. $R_f = 0.39$ (dichloromethane/methanol 95:5). 1H NMR (300 MHz, $CO(CD_3)_2$) δ 10.09 (br s, 1H, NH, exchangeable with D_2O), 8.09-8.07 (m, 2H, ArH), 7.97-7.95 (m, 1H, ArH), 7.77 (d, $J = 7.5$ Hz, 1H, ArH), 7.58-7.51 (m, 4H, ArH), 7.33 (t, $J = 8.7$ Hz, 1H, ArH), 6.97 (d, $J = 8.7$ Hz, 1H, ArH), 6.78 (t, $J = 7.5$ Hz, 1H, ArH) ppm. ESI-MS

(*m/z*) Calcd: 263 Found: 262 [M-H]⁻. Anal. Calcd for C₁₇H₁₃NO₂: C, 77.55; H, 4.98; N, 5.32. Found: C, 77.46; H, 4.99; N, 5.29.

2-(3-Methoxy-1-naphthylamino)benzoic acid (6a). Procedure D: starting from **3a**.

Reaction time: 30 min. Yellow foam, quantitative yield. Molecular formula: C₁₈H₁₅NO₃. Molecular Weight: 293.32 g/mol. R_f = 0.34 (dichloromethane/methanol 95:5). ¹H NMR (300 MHz, CO(CD₃)₂) δ 10.15 (br s, 1H, NH, exchangeable with D₂O), 7.96 (d, *J* = 8.4 Hz, 1H, ArH), 7.85 (d, *J* = 8.4 Hz, 1H, ArH), 7.71 (d, *J* = 8.1 Hz, 1H, ArH), 7.35 (t, *J* = 7.2 Hz, 1H, ArH), 7.24-7.20 (m, 2H, ArH), 7.08 (d, *J* = 2.1 Hz, 1H, ArH), 7.02-6.99 (m, 2H, ArH), 6.68 (d, *J* = 7.2 Hz, 1H, ArH), 3.80 (s, 3H, CH₃) ppm. ESI-MS (*m/z*) Calcd: 293 Found: 292 [M-H]⁻. Anal. Calcd for C₁₈H₁₅NO₃: C, 73.71; H, 5.15; N, 4.78. Found: C, 73.57; H, 5.13; N, 4.76.

2-(4-Methoxy-1-naphthylamino)benzoic acid (6b). Procedure D: starting from **3b**.

Reaction time: 90 min. Oil, 53 % yield. Molecular formula: C₁₈H₁₅NO₃. Molecular Weight: 293.32 g/mol. R_f = 0.54 (dichloromethane/methanol 95:5). ¹H NMR (300 MHz, CO(CD₃)₂) δ 9.72 (br s, 1H, NH, exchangeable with D₂O), 8.34-8.25 (m, 1H, ArH), 8.03 (dd, *J*₁ = 8.0 Hz, *J*₂ = 1.6 Hz, 1H, ArH), 7.96-7.89 (m, 1H, ArH), 7.58-7.48 (m, 2H, ArH), 7.44 (d, *J* = 8.1 Hz, 1H, ArH), 7.23 (dt, *J*₁ = 8.4 Hz, *J*₂ = 1.6 Hz, 1H, ArH), 7.01 (d, *J* = 8.1 Hz, 1H, ArH), 6.69 (t, *J* = 7.6 Hz, 1H, ArH), 6.58 (d, *J* = 8.5 Hz, 1H, ArH), 4.07 (s, 3H, CH₃) ppm. ESI-MS (*m/z*) Calcd: 293 Found: 292 [M-H]⁻. Anal. Calcd for C₁₈H₁₅NO₃: C, 73.71; H, 5.15; N, 4.78. Found: C, 73.59; H, 5.13; N, 4.77.

2-(5-Methoxy-1-naphthylamino)benzoic acid (6c). Procedure D: starting from **3c**.

Reaction time: 90 min. Solid, m.p. 203-205°C, 82% yield. Molecular formula: C₁₈H₁₅NO₃. Molecular Weight: 293.32 g/mol. R_f = 0.48 (dichloromethane/methanol 95:5). Eluent for chromatography: dichloromethane/methanol (95:5). ¹H NMR (300 MHz, CDCl₃) δ 9.58 (br s, 1H, NH, exchangeable with D₂O), 8.17 (d, *J* = 8.2 Hz, 1H, ArH), 8.04 (d, *J* = 8.2 Hz, 1H,

ArH), 7.64 (d, $J = 8.5$ Hz, 1H, ArH), 7.54-7.37 (m, 4H, ArH), 6.87-6.82 (m, 2H, ArH), 6.71 (t, $J = 7.5$ Hz, 1H, ArH), 4.03 (s, 3H, CH₃).

2-(3-Hydroxy-1-naphthylamino)benzoic acid (6d). Procedure E: starting from **6a**. Reaction time: 30 min. Brown-purple foam, 90% yield. Molecular formula: C₁₇H₁₃NO₃. Molecular Weight: 279.29 g/mol. Rf = 0.17 (dichloromethane/methanol 95:5). ¹H NMR (300 MHz, CO(CD₃)₂) δ 10.00 (br s, 1H, NH, exchangeable with D₂O), 7.95 (dd, $J_1 = 7.8$ Hz, $J_2 = 1.5$ Hz, 1H, ArH), 7.81 (d, $J = 8.4$ Hz, 1H, ArH), 7.59 (d, $J = 7.8$ Hz, 1H, ArH), 7.32-7.10 (m, 4H, ArH), 6.99 (d, $J = 8.4$ Hz, 1H, ArH), 6.93 (d, $J = 1.8$ Hz, 1H, ArH), 6.67 (t, $J = 7.5$ Hz, 1H, ArH) ppm. ESI-MS (m/z) Calcd: 279 Found: 278 [M-H]⁻. Anal. Calcd for C₁₇H₁₃NO₃: C, 73.11; H, 4.69; N, 5.02. Found: C, 73.01; H, 4.71; N, 5.04.

2-(4-Hydroxy-1-naphthylamino)benzoic acid (6e). Procedure E: starting from **6b**. Reaction time: 2 h. Dark solid, m.p. 214-215°C, 98% yield. Molecular formula: C₁₇H₁₃NO₃. Molecular Weight: 279.30 g/mol. Rf = 0.18 (dichloromethane/methanol 95:5). Eluent for chromatography: dichloromethane/methanol (95:5). ¹H NMR (300 MHz, CO(CD₃)₂) δ 11.21 (br s, 1H, COOH, exchangeable with D₂O), 9.66 (br s, 1H, NH, exchangeable with D₂O), 9.13 (br s, 1H, OH, exchangeable with D₂O), 8.34-8.28 (m, 1H, ArH), 8.02 (dd, $J_1 = 8.1$ Hz, $J_2 = 1.6$ Hz, 1H, ArH), 7.92-7.85 (m, 1H, ArH), 7.55-7.47 (m, 2H, ArH), 7.32 (d, $J = 8.1$ Hz, 1H, ArH), 7.21 (dt, $J_1 = 8.5$ Hz, $J_2 = 1.5$ Hz, 1H, ArH), 6.98 (d, $J = 8.1$ Hz, 1H, ArH), 6.67 (t, $J = 8.1$ Hz, 1H, ArH), 6.54 (d, $J = 8.5$ Hz, 1H, ArH). ESI-MS (m/z) Calcd: 279 Found: 278 [M-H]⁻. Anal. Calcd for C₁₇H₁₃NO₃: C, 73.11; H, 4.69; N, 5.02. Found: C, 73.15; H, 4.68; N, 5.04.

2-(5-Hydroxy-1-naphthylamino)benzoic acid (6f). Procedure E: starting from **6c**. Reaction time: 30 min. Green foam, 72 % yield. Molecular formula: C₁₇H₁₃NO₃. Molecular Weight: 279.29 g/mol. Rf = 0.30 (dichloromethane/methanol 95:5). ¹H NMR (300 MHz, CO(CD₃)₂) δ 10.05 (br s, 1H, COOH, exchangeable with D₂O), 8.13 (d, $J = 8.3$ Hz, 1H,

ArH), 8.06 (dd, $J_1 = 8.0$ Hz, $J_2 = 1.6$ Hz, 1H, ArH), 7.61-7.41 (m, 3H, ArH), 7.39-7.24 (m, 2H, ArH), 6.97 (d, $J = 7.6$ Hz, 2H, ArH), 6.76 (td, $J_1 = 7.5$ Hz, $J_2 = 1.5$ Hz, 1H, ArH). ESI-MS (m/z) Calcd: 279 Found: 278 [M-H]⁻. Anal. Calcd for C₁₇H₁₃NO₃: C, 73.11; H, 4.69; N, 5.02. Found: C, 73.04; H, 4.71; N, 5.00.

3-(1-Naphthylamino)benzoic acid (7). Procedure D: starting from **4**. Reaction time: 60 min. Oil, 96 % yield. Molecular formula: C₁₇H₁₃NO₂. Molecular Weight: 263.29 g/mol. Rf = 0.25 (dichloromethane/methanol 95:5). ¹H NMR (300 MHz, CD₃OD) δ 8.12 (d, $J = 7.5$ Hz, 1H, ArH), 7.82 (d, $J = 7.5$ Hz, 1H, ArH), 7.64 (s, 1H, ArH), 7.52-7.32 (m, 6H, ArH), 7.20 (t, $J = 7.5$ Hz, 1H, ArH), 7.08 (d, $J = 7.5$ Hz, 1H, ArH) ppm. ESI-MS (m/z) Calcd: 263 Found: 262 [M-H]⁻. Anal. Calcd for C₁₇H₁₃NO₂: C, 77.55; H, 4.98; N, 5.32. Found: C, 77.43; H, 4.96; N, 5.31.

3-(3-Methoxy-1-naphthylamino)benzoic acid (7a). Procedure D: starting from **4a**. Reaction time: 40 min. Oil, 96 % yield. Molecular formula: C₁₈H₁₅NO₃. Molecular Weight: 293.32 g/mol. Rf = 0.19 (dichloromethane/methanol 95:5). ¹H NMR (300 MHz, CO(CD₃)₂) δ 7.95 (d, $J = 8.4$ Hz, 1H, ArH), 7.68-7.64 (m, 2H, ArH), 7.59 (br s, 1H, NH, exchangeable with D₂O), 7.44-7.41 (m, 1H, ArH), 7.33-7.14 (m, 4H, ArH), 6.91 (d, $J = 2.1$ Hz, 1H, ArH), 6.87 (d, $J = 2.1$ Hz, 1H, ArH), 3.74 (s, 3H, CH₃) ppm. ESI-MS (m/z) Calcd: 293 Found: 292 [M-H]⁻. Anal. Calcd for C₁₈H₁₅NO₃: C, 73.71; H, 5.15; N, 4.78. Found: C, 73.59; H, 5.16; N, 4.76.

3-(4-Methoxy-1-naphthylamino)benzoic acid (7b). Procedure D: starting from **4b**. Reaction time: 60 min. Oil, 73 % yield. Molecular formula: C₁₈H₁₅NO₃. Molecular Weight: 293.32 g/mol. Rf = 0.16 (dichloromethane/methanol 95:5). ¹H NMR (300 MHz, CO(CD₃)₂) δ 11.00 (bs, 1H, OH, exchangeable with D₂O), 8.31-8.25 (m, 1H, ArH), 8.07-7.99 (m, 1H, ArH), 7.55-7.45 (m, 3H, ArH), 7.42-7.36 (m, 2H, ArH), 7.34 (bs, 1H, NH, exchangeable with D₂O), 7.24 (t, $J = 7.8$ Hz, 1H, ArH), 7.00 (dd, $J = 8.1$, $J_2 = 1.6$ Hz, 1H, ArH), 6.96 (d, $J = 8.2$

1
2
3 Hz, 1H, ArH), 4.04 (s, 3H, CH₃) ppm. ESI-MS (*m/z*) Calcd: 293 Found: 292 [M-H]⁻. Anal.
4
5 Calcd for C₁₈H₁₅NO₃: C, 73.71; H, 5.15; N, 4.78. Found: C, 73.52; H, 5.14; N, 4.81.
6
7

8 **2-(5-Methoxy-1-naphthylamino)benzoic acid (7c).** Procedure D: starting from **4c**.
9
10 Reaction time: 30 min. Solid, 203-205°C, 70% yield. Molecular formula: C₁₈H₁₅NO₃.
11
12 Molecular Weight: 293.32 g/mol. R_f = 0.30 (dichloromethane/methanol 95:5). Eluent for
13
14 chromatography: dichloromethane/methanol (95:5). ¹H NMR (300 MHz, CD₃OD) δ 7.98-
15
16 7.95 (m, 1H, ArH), 7.64 (d, *J* = 8.4 Hz, 1H, ArH), 7.59 (s, 1H, ArH), 7.43 (d, *J* = 7.2 Hz, 1H,
17
18 ArH), 7.38-7.33 (m, 3H, ArH), 7.25 (t, *J* = 7.7 Hz, 1H, ArH), 7.13 (d, *J* = 8.4 Hz, 1H, ArH),
19
20 6.92 (d, *J* = 7.7 Hz, 1H, ArH), 4.01 (s, 3H, CH₃).
21
22
23

24 **3-((3-Hydroxynaphthalen-1-yl)amino)benzoic acid (7d).** Procedure E: starting from
25
26 **7a**. Reaction time: 210 minutes. Oil, 91 % yield. Molecular formula: C₁₇H₁₃NO₃. Molecular
27
28 Weight: 279.29 g/mol. R_f = 0.17 (dichloromethane/methanol 95:5). ¹H NMR (300 MHz,
29
30 CO(CD₃)₂) δ 7.93 (d, *J* = 8.0 Hz, 1H, ArH), 7.67 (s, 1H, ArH), 7.60-7.53 (m, 2H, ArH), 7.44-
31
32 7.40 (m, 1H, ArH), 7.30-7.20 (m, 3H, ArH, NH, exchangeable with D₂O), 7.14-7.08 (m, 1H,
33
34 ArH), 6.96 (d, *J* = 2.7 Hz, 1H, ArH), 6.81 (s, 1H, ArH) ppm. ESI-MS (*m/z*) Calcd: 279
35
36 Found: 278 [M-H]⁻. Anal. Calcd for C₁₇H₁₃NO₃: C, 73.11; H, 4.69; N, 5.02. Found: C, 73.02;
37
38 H, 4.70; N, 5.01.
39
40
41

42 **3-(4-Hydroxy-1-naphthylamino)benzoic acid (7e).** Procedure E: starting from **7b**.
43
44 Reaction time: 60 min. Yellow oil, 89 % yield. Molecular formula: C₁₇H₁₃NO₃. Molecular
45
46 Weight: 279.29 g/mol. R_f = 0.13 (dichloromethane/methanol 95:5). ¹H NMR (300 MHz,
47
48 CO(CD₃)₂) δ 8.99 (br s, 1H, exchangeable with D₂O), 8.32-8.26 (m, 1H, ArH), 8.03-7.96 (m,
49
50 1H, ArH), 7.51-7.44 (m, 3H, ArH), 7.39-7.33 (m, 1H, ArH), 7.30-7.18 (m, 2H, ArH), 6.99-
51
52 6.90 (m, 2H, ArH) ppm. ESI-MS (*m/z*) Calcd: 279 Found: 278 [M-H]⁻. Anal. Calcd for
53
54 C₁₇H₁₃NO₃: C, 73.11; H, 4.69; N, 5.02. Found: C, 73.13; H, 4.69; N, 5.02.
55
56
57
58
59
60

1
2
3 **3-(5-Hydroxy-1-naphthylamino)benzoic acid (7f)**. Procedure E: starting from **7c**.
4
5 Reaction time: 4 h. Yellow oil, 98% yield. Molecular formula: C₁₇H₁₃NO₃. Molecular
6
7 Weight: 279.30 g/mol. R_f = 0.13 (dichloromethane/methanol 95:5). Eluent for
8
9 chromatography: dichloromethane/methanol (95:5). ¹H NMR (300 MHz, CO(CD₃)₂) δ 9.14
10
11 (br s, 1H, NH exchangeable with D₂O), 8.03-8.00 (m, 1H, ArH), 7.72-7.62 (m, 2H, ArH, 1H,
12
13 OH exchangeable with D₂O), 7.51-7.22 (m, 6H, ArH), 6.95 (dd, *J*₁ = 7.5 Hz, *J*₂ = 1.0 Hz, 1H,
14
15 ArH). ESI-MS (*m/z*) Calcd: 279 Found: 278 [M-H]⁻. Anal. Calcd for C₁₇H₁₃NO₃: C, 73.11; H,
16
17 4.69; N, 5.02. Found: C, 73.05; H, 4.68; N, 5.04.
18
19
20
21

22 **3-(4-((tert-Butoxycarbonyl)amino)-1-naphthylamino)benzoic acid (7g)**. Procedure D:
23
24 starting from **4g**. Reaction time: 30 min. Silver foam, quantitative yield. Molecular formula:
25
26 C₂₂H₂₂N₂O₄. Molecular Weight: 378.42 g/mol. R_f = 0.17 (dichloromethane/methanol 95:5).
27
28 ¹H NMR (300 MHz, CD₃OD) δ 8.09 (d, *J* = 7.8 Hz, 1H, ArH), 8.01 (d, *J* = 8.7 Hz, 1H, ArH),
29
30 7.59-7.42 (m, 5H, ArH), 7.32 (d, *J* = 8.1 Hz, 1H, ArH), 7.24 (t, *J* = 7.8 Hz, 1H, ArH), 7.10-
31
32 7.16 (m, 1H, ArH), 1.54 (s, 9H, CH₃) ppm.
33
34

35 **3-(5-((tert-Butoxycarbonyl)amino)-1-naphthylamino)benzoic acid (7h)**. Procedure D:
36
37 starting from **4h**. Reaction time: 30 min. Green-brown oil, 79 % yield. Molecular formula:
38
39 C₂₂H₂₂N₂O₄. Molecular Weight: 378.42 g/mol. R_f = 0.20 (dichloromethane/methanol 95:5).
40
41 ¹H NMR (300 MHz, CO(CD₃)₂) δ 8.19 (br s, 1H, NH, exchangeable with D₂O), 7.84 (d, *J* =
42
43 8.7 Hz, 1H, ArH), 7.75 (dd, *J*₁ = 6.9 Hz, *J*₂ = 3.0 Hz, 1H, ArH), 7.70 (d, *J* = 7.5 Hz, 1H,
44
45 ArH), 7.58 (t, *J* = 2.1 Hz, 1H, ArH), 7.55 (br s, 1H, NH, exchangeable with D₂O), 7.40-7.28
46
47 (m, 4H, ArH), 7.20 (t, *J* = 7.5 Hz, 1H, ArH), 7.17-7.12 (m, 1H, ArH), 1.39 (s, 9H, CH₃) ppm.
48
49
50

51 **3-(4-Amino-1-naphthylamino)benzoic acid hydrochloride (7i)**. Procedure F1: starting
52
53 from **7g**. Foam, 58% yield. Molecular formula: C₁₇H₁₄N₂O₂ · HCl. Molecular Weight: 314.77
54
55 g/mol. ¹H NMR (300 MHz, CD₃OD) δ 8.32 (d, *J* = 8.4 Hz, 1H, ArH), 7.93 (d, *J* = 8.4 Hz, 1H,
56
57 ArH), 7.81-7.69 (m, 2H, ArH), 7.72-7.60 (m, 1H, ArH), 7.58 (d, *J* = 7.0 Hz, 1H, ArH), 7.47
58
59
60

(d, $J = 8.4$ Hz, 1H, ArH), 7.41-7.24 (m, 3H, ArH) ppm. ESI-MS (m/z) Calcd: 278 Found: 277 [M-H]⁻. Anal. Calcd for C₁₇H₁₅ClN₂O₂: C, 64.87; H, 4.80; Cl, 11.26. Found: C, 64.71; H, 4.82; Cl, 11.25.

3-(5-Amino-1-naphthylamino)benzoic acid hydrochloride (7j). Procedure F1: starting from **7h**. Foam, 66 % yield. Molecular formula: C₁₇H₁₄N₂O₂ · HCl. Molecular Weight: 314.77 g/mol. ¹H NMR (300 MHz, CD₃OD) δ 8.28 (dd, $J_1 = 8.1$ Hz, $J_2 = 1.2$ Hz, 1H, ArH), 7.66 (t, $J = 2.1$ Hz, 1H, ArH), 7.63-7.49 (m, 6H, ArH), 7.34 (t, $J = 7.8$ Hz, 1H, ArH), 7.28-7.24 (m, 1H, ArH) ppm. ESI-MS (m/z) Calcd: 278 Found: 277 [M-H]⁻. Anal. Calcd for C₁₇H₁₅ClN₂O₂: C, 64.87; H, 4.80; Cl, 11.26. Found: C, 64.94; H, 4.81; Cl, 11.24.

Ethyl-2-(5-hydroxy-1-naphthylamino)benzoate (8). Procedure G: starting from **6f**. Green foam, 30% yield. Molecular formula: C₁₉H₁₇NO₃. Molecular Weight: 307.34 g/mol. R_f = 0.54 (cyclohexane/ethyl acetate 70:30). Eluent for chromatography: cyclohexane/ethyl acetate 70:30. ¹H NMR (300 MHz, CDCl₃) δ 9.80 (br s, 1H, NH exchangeable with D₂O), 8.1-8.0 (m, 2H, ArH), 7.68 (d, $J = 8.6$ Hz, 1H, ArH), 7.54 (d, $J = 7.3$ Hz, 1H, ArH), 7.46 (t, $J = 7.8$ Hz, 1H, ArH), 7.33-7.22 (m, 2H, ArH), 6.96 (d, $J = 8.6$ Hz, 1H, ArH), 6.85 (d, $J = 7.4$ Hz, 1H, ArH), 6.72 (t, $J = 7.6$ Hz, 1H, ArH), 4.40 (q, $J = 7.1$ Hz, 2H, CH₂), 1.44 (t, $J = 7.1$ Hz, 3H, CH₃), 1.25 (br s, 1H, OH exchangeable with D₂O). ESI-MS (m/z) Calcd: 307 Found: 306 [M-H]⁻. Anal. Calcd for C₁₉H₁₇NO₃: C, 74.25; H, 5.58; N, 4.56. Found: C, 74.29; H, 5.56; N, 4.54.

Ethyl-3-(5-hydroxy-1-naphthylamino)benzoate (9). Procedure G: starting from **7f**. Yellow foam, 41% yield. Molecular formula: C₁₉H₁₇NO₃. Molecular Weight: 307.34 g/mol. R_f = 0.51 (cyclohexane/ethyl acetate 70:30). Eluent for chromatography: cyclohexane/ethyl acetate 70:30. ¹H NMR (300 MHz, CDCl₃) δ 8.64 (br s, 1H, NH exchangeable with D₂O), 8.15-8.05 (m, 1H, ArH), 7.85-7.70 (m, 2H, ArH), 7.64-7.50 (m, 2H, ArH), 7.46-7.40 (m, 2H, ArH), 7.38-7.30 (m, 2H, ArH), 7.15 (t, $J = 7.1$ Hz, 1H, ArH), 6.02 (br s, 1H, OH

exchangeable with D₂O), 4.10 (q, $J = 7.0$ Hz, 2H, CH₂), 1.40 (t, $J = 7.0$ Hz, 3H, CH₃). ESI-MS (m/z) Calcd: 307 Found: 306 [M-H]⁻. Anal. Calcd for C₁₉H₁₇NO₃: C, 74.25; H, 5.58; N, 4.56. Found: C, 74.09; H, 5.61; N, 4.55.

Ethyl 2-(5-amino-1-naphthyamino)benzoate hydrochloride (10). Procedure F2: starting from **3h**. Green solid, 71.6% yield. Molecular formula: C₁₉H₁₈N₂O₂·HCl. Molecular Weight: 342.82 g/mol. Rf = 0.22 (cyclohexane/ethyl acetate 80:20). ¹H NMR (300 MHz, CD₃OD) δ 8.15-8.21 (m, 1H, ArH), 8.04 (dd, $J_1=8.0$ Hz, $J_2=1.6$ Hz, 1H, ArH), 7.65-7.83 (m, 3H, ArH), 7.55-7.61 (m, 2H, ArH), 7.25-7.37 (m, 1H, ArH), 7.00 (dd, $J_1=8.5$ Hz, $J_2=0.8$ Hz, 1H, ArH), 6.77-6.86 (m, 1H, ArH), 4.42 (q, $J=7.1$ Hz, 2H, CH₂), 1.43 (t, $J=7.1$ Hz, 3H, CH₃). ¹³C-NMR (CD₃OD) δ 169.01, 148.09, 137.64, 134.06, 131.31, 129.94, 128.68, 128.04, 127.49, 125.41, 122.84, 120.49, 120.02, 117.60, 116.80, 114.13, 112.31, 60.81, 13.26. ESI-MS (m/z) Calcd: 306 Found: 305 [M-H]⁻. Anal. Calcd for C₁₉H₁₉ClN₂O₂: C, 66.57; H, 5.59; Cl, 10.34; N, 8.17. Found: C, 66.69; H, 5.58; Cl, 10.43; N, 8.19.

Ethyl 3-(5-amino-1-naphthylamino)benzoate hydrochloride (11). Procedure F2: starting from **7j**. Blue solid, 86.4% yield. Molecular formula: C₁₉H₁₈N₂O₂·HCl. Molecular Weight: 342.82 g/mol. Rf = 0.17 (cyclohexane/ethyl acetate 80:20). ¹H NMR (300 MHz, CD₃OD) δ 8.28 (d, $J = 8.1$ Hz, 1H, ArH), 7.67-7.46 (m, 7H, ArH), 7.37-7.21 (m, 2H, ArH), 4.32 (q, $J = 7.1$ Hz, 2H, CH₂), 1.35 (t, $J=7.1$ Hz, 3H, CH₃). ¹³C-NMR (CD₃OD) δ 166.79, 145.26, 140.44, 131.23, 128.98, 128.51, 128.00, 127.78, 127.47, 124.27, 123.70, 121.59, 120.85, 120.32, 117.63, 116.15, 114.24, 60.67, 13.14. ESI-MS (m/z) Calcd: 306 Found: 305 [M-H]⁻. Anal. Calcd for C₁₉H₁₉ClN₂O₂: C, 66.57; H, 5.59; Cl, 10.34; N, 8.17. Found: C, 66.40; H, 5.58; Cl, 10.38; N, 8.13.

2-((5-Aminonaphthalen-1-yl)amino)benzoic acid hydrochloride (12). Procedure D: starting from **10**. Reaction time: 30 min. Grey solid, 48% yield. Molecular formula: C₁₇H₁₄N₂O₂·HCl. Molecular Weight: 314.77 g/mol. Rf = 0.26 (dichloromethane/methanol

95:5). Eluent for chromatography: dichloromethane/methanol (95:5). ^1H NMR (300 MHz, $(\text{CD}_3)_2\text{SO}$) δ 10.03 (br s, 1H, NH, exchangeable with D_2O), 8.00-7.76 (m, 3H, ArH), 7.68-7.42 (m, 4H, ArH), 7.31 (t, $J = 7.8$ Hz, 1H, ArH), 6.90 (d, $J = 8.4$ Hz, 1H, ArH), 6.77 (t, $J = 7.5$ Hz, 1H, ArH), 3.65 (br s, 2H, NH_2 , exchangeable with D_2O hidden under water peak) ^{13}C -NMR ($(\text{CD}_3)_2\text{SO}$) δ 170.73, 148.64, 137.14, 134.72, 132.24, 129.85, 127.58, 126.89, 126.90, 126.60, 120.65, 118.98, 118.99, 117.87, 117.88, 114.42, 112.85. ESI-MS (m/z) Calcd: 278 Found: 277 $[\text{M}-\text{H}]^-$. Anal. Calcd for $\text{C}_{17}\text{H}_{14}\text{N}_2\text{O}_2$: C, 73.37; H, 5.07; N, 10.07. Found: C, 73.48; H, 5.09; N, 10.09.

Synthesis of 1-amino-2,4-dibromonaphthalene (13). To a solution of 1-aminonaphthalene (**24**) (250 mg, 1.745 mmol) in acetic acid (1 mL) was added a 0-5°C solution of Br_2 (0.27 mL, 5.235 mmol) in acetic acid (2 mL). Another 1 mL of acetic acid was added and the mixture was warmed at 60°C for 15 min, during which the color solution changed from purple to orange. Then, the mixture was cooled, and the salt was filtered, washed with acetic acid, and suspended in an excess of 1M NaOH. The product was collected by filtration, washed with water and dried to give a purple solid. The crude residue was purified by flash chromatography (cyclohexane/ethyl acetate 90:10) to provide compound **13**.⁴⁷ Violet solid m.p. 114-116°C, 86 % yield. Molecular formula: $\text{C}_{10}\text{H}_7\text{Br}_2\text{N}$. Molecular Weight: 300.98 g/mol. $R_f = 0.33$ (cyclohexane/ethyl acetate 8:2). ^1H NMR (300 MHz, CDCl_3) δ 8.20-8.17 (m, 1H, ArH) 7.8-7.76 (m, 2H, ArH), 7.62-7.50 (m, 2H, ArH), 4.63 (br s, 2H, NH_2 , exchangeable with D_2O).

Synthesis of 4-bromo-2-hydroxynaphthalene-1-diazonium salt (14). To a stirred solution of compound **13** (250 mg, 0.831 mmol) in acetic acid (4 mL) and propionic acid (0.67 mL) at 8-10°C was gradually added sodium nitrite (86 mg, 1.246 mmol). After stirring for 10 min the yellow-brown solution was poured into 6 mL of ice water and the resulting mixture was rapidly filtered to remove a black tar. The aqueous phase was extracted with

dichloromethane (6×2 mL). The collected organic phase was dried over anhydrous sodium sulfate, filtered and the solvent was evaporated under *vacuum* to give compound **14**.⁴⁷ Yellow-orange solid (melting point: 118-125°C), 98 % yield. Molecular formula: C₁₀H₆BrN₂O⁺. Molecular Weight: 250.96 g/mol. ¹H NMR (300 MHz, CDCl₃) δ 8.08 (d, *J* = 9 Hz, 1H, ArH), 7.58 (t, *J* = 9 Hz, 1H, ArH), 7.37 (t, *J* = 9 Hz, 1H, ArH), 7.28 (d, *J* = 9 Hz, 1H, ArH), 7.18 (s, 1H, ArH) ppm.

Synthesis of 4-bromonaphthalen-2-ol (15a). To a suspension of compound **14** (200 mg, 0.803 mmol) in ethanol (3.5 mL), NaBH₄ (30.4 mg, 0.803 mmol) was added at 0-10°C. The solution was stirred until gas evolution ceased and the mixture appeared darker. After evaporating ethanol, the remaining residue was poured into water, basified with 10% NaOH and then extracted with dichloromethane (2×2 mL), in order to purify the reaction mixture from the unreacted materials and impurities. Then, the collected alkaline aqueous solution, which contained the sodium salt of compound **15a**, was acidified with 3M HCl and extracted with ethyl acetate (2×2 mL). The organic layer was dried over anhydrous sodium sulfate and evaporated under reduced pressure, to afford a crude brown solid. The residue was purified by flash chromatography (cyclohexane/ethyl acetate 90:10 - R_f = 0.18) to provide the intermediate **15a**. Brown solid m.p. 118-119°C, 75 % yield. Molecular formula: C₁₀H₇BrO. Molecular Weight: 223.06 g/mol. ¹H NMR (300 MHz, CDCl₃) δ 8.14 (d, *J* = 7.8 Hz, 1H, ArH), 7.67 (d, *J*₁ = 6.9 Hz, *J*₂ = 1.8 Hz, 1H, ArH), 7.41-7.50 (m, 3H, ArH), 7.14 (d, *J* = 1.8 Hz, 1H, ArH), 4.98 (s, 1H, OH, exchangeable with D₂O) ppm.

1-Bromo-3-methoxynaphthalene (16a). Procedure H: starting from **15a**. Brown solid, m.p. 67-68°C, 97 % yield. Molecular formula: C₁₁H₉BrO. Molecular Weight: 237.09 g/mol. R_f = 0.66 (cyclohexane/ethyl acetate 90:10). ¹H NMR (300 MHz, CDCl₃) δ 8.15 (d, *J* = 7.5 Hz, 1H, ArH), 7.72 (d, *J* = 7.5 Hz, 1H, ArH), 7.52-7.41 (m, 3H, ArH), 7.12 (d, *J* = 2.4 Hz, 1H, ArH), 3.91 (s, 3H, CH₃) ppm.

1
2
3 **1-Bromo-4-methoxynaphthalene (16b).** Procedure H: starting from 4-
4 bromonaphthalen-1-ol. Brown solid, m.p. 64-66°C, 98% yield. Molecular formula:
5 C₁₁H₉BrO. Molecular Weight: 237.09 g/mol. Rf = 0.56 (cyclohexane/ethyl acetate 90:10). ¹H
6 NMR (300 MHz, CDCl₃) δ 8.28 (d, *J* = 8.4 Hz, 1H, ArH), 8.18 (d, *J* = 8.4 Hz, 1H, ArH),
7 7.67-7.50 (m, 3H, ArH), 6.67 (d, *J* = 8.4 Hz, 1H, ArH), 3.98 (s, 3H, CH₃) ppm.

8
9
10
11
12
13
14 **3-Methoxy-1-naphthaldehyde (17a).** Procedure I: starting from **16a**. Yellow-brown
15 solid, m.p. 59-61°C, 56% yield. Molecular formula: C₁₂H₁₀O₂. Molecular Weight: 186.21
16 g/mol. Rf = 0.38 (cyclohexane/ethyl acetate 90:10). ¹H NMR (300 MHz, CDCl₃) δ 10.36 (s,
17 1H, CHO), 9.16-9.02 (m, 1H, ArH), 7.84-7.75 (m, 1H, ArH), 7.68-7.60 (m, 1H, ArH), 7.57-
18 7.47 (m, 2H, ArH), 7.38 (d, *J* = 2.5 Hz, 1H, ArH), 3.95 (s, 3H, CH₃) ppm.

19
20
21
22
23
24
25 **4-Methoxy-1-naphthaldehyde (17b).** Procedure I: starting from **16b**. Yellow-brown
26 semi-solid, m.p. 34°C, 89 % yield. Molecular formula: C₁₂H₁₀O₂. Molecular Weight: 186.21
27 g/mol. Rf = 0.25 (cyclohexane/ethyl acetate 90:10). ¹H NMR (300 MHz, CDCl₃) δ 10.18 (s,
28 1H, CHO), 9.30 (d, *J* = 8.5 Hz, 1H, ArH), 8.32 (d, *J* = 8.5 Hz, 1H, ArH), 7.88 (d, *J* = 8.0 Hz,
29 1H, ArH), 7.69 (t, *J* = 7.9 Hz, 1H, ArH), 7.56 (t, *J* = 7.9 Hz, 1H, ArH), 6.88 (d, *J* = 8.0 Hz,
30 1H, ArH), 4.04 (s, 3H, OCH₃) ppm.

31
32
33
34
35
36
37
38
39
40 **Synthesis of 4,4-dimethyl-2-(2-bromophenyl)oxazoline (19).** Thionyl chloride (1.09
41 mL, 14.924 mmol) was added to 2-bromobenzoic acid (1000 mg, 4.975 mmol) under N₂ and
42 the mixture was refluxed for 6 hours. Then, the excess of thionyl chloride was removed under
43 *vacuum*. The ice-cold solution of the remaining acyl chloride in dry dichloromethane (2 mL)
44 was added dropwise to a solution of 2-amino-2-methyl-1-propanol (886.9 mg, 9.950 mmol)
45 in dichloromethane (2 mL) at 0°C. The mixture was stirred at room temperature for 2 hours.
46 In order to purify the reaction mixture from the unreacted 2-amino-2-methyl-1-propanol, the
47 organic phase was washed with 3N HCl (3×1 mL), dried over anhydrous sodium sulfate,
48 filtered and the solvent was evaporated under reduced pressure. The crude **18** was used in the
49
50
51
52
53
54
55
56
57
58
59
60

1
2
3 following reaction without further purification. White foam, 98% yield. Molecular formula:
4
5 $C_{11}H_{14}BrNO_2$. Molecular weight: 272.14 g/mol. $R_f = 0.67$ (dichloromethane/methanol
6
7 90:10). 1H NMR (300 MHz, $CDCl_3$) δ 7.51 (dd, $J_1 = 8.1$ Hz, $J_2 = 1.1$ Hz, 1H, ArH), 7.43 (dd,
8
9 $J_1 = 7.7$ Hz, $J_2 = 1.8$ Hz, 1H, ArH), 7.29 (dt, $J_1 = 8.1$ Hz, $J_2 = 1.1$ Hz, 1H, ArH), 7.20 (dt, $J_1 =$
10
11 7.7 Hz, $J_2 = 1.8$ Hz, 1H, ArH), 5.97 (br s, 1H, exchangeable with D_2O), 3.96 (br s, 1H,
12
13 exchangeable with D_2O), 3.63 (s, 2H, CH_2), 1.35 (s, 6H, CH_3) ppm.
14
15

16
17 Subsequently, thionyl chloride (1.07 mL, 14.625 mmol) was added dropwise to the
18
19 benzamide **18** (1326.8 mg, 4.875 mmol). When the vigorous reaction subsided, 6 mL of dry
20
21 diethyl ether was added to the yellow solution. After 6 hours, the excess of thionyl chloride
22
23 was evaporated under reduced pressure to provide white crystals of the hydrochloride salt,
24
25 which was neutralized with cold 20% sodium hydroxide (2 mL) and extracted with diethyl
26
27 ether (3 \times 2 mL). The organic phase was dried over anhydrous sodium sulfate and the solvent
28
29 was evaporated under reduced pressure. The crude brown oil was purified by flash
30
31 chromatography eluting firstly with cyclohexane/ethyl acetate (98:2) and then with
32
33 cyclohexane/ethyl acetate (9:1) to afford intermediate **19**. Pale yellow solid, m.p. 36-38°C, 79
34
35 % yield. Molecular formula: $C_{11}H_{12}BrNO$. Molecular weight: 254.12 g/mol. $R_f = 0.15$
36
37 (cyclohexane / ethyl acetate 90:10). 1H NMR (300 MHz, $CDCl_3$) δ 8.02 (s, 1H, ArH), 7.79 (d,
38
39 $J_1 = 8.1$ Hz, 1H, ArH), 7.56 (d, $J = 8.1$ Hz, 1H, ArH), 7.19 (t, $J_1 = 8.1$ Hz, 1H, ArH), 4.05 (s,
40
41 2H, CH_2), 1.35 (s, 6H, CH_3).
42
43
44
45
46

47 **3-(3-Methoxynaphthalen-1-yl)isobenzofuran-1(3H)-one (21a)**. Procedure J: starting
48
49 from **17a**. Foam, 52 % yield. Molecular formula: $C_{19}H_{14}O_3$. Molecular Weight: 290.31 g/mol.
50
51 $R_f = 0.37$ (cyclohexane/ethyl acetate 80:20). 1H NMR (300 MHz, $CDCl_3$) δ 8.15 (d, $J = 8.0$
52
53 Hz, 1H, ArH), 7.97 (d, $J = 8.0$ Hz, 1H, ArH), 7.78 (d, $J = 7.7$ Hz, 1H, ArH), 7.60-7.37 (m,
54
55 5H, ArH), 7.17-7.06 (m, 2H, ArH), 6.86 (d, $J = 2.5$ Hz, 1H, ArH), 3.79 (s, 3H, CH_3) ppm.
56
57
58
59
60

1
2
3 **3-(4-Methoxynaphthalen-1-yl)isobenzofuran-1(3H)-one (21b)**. Procedure J: starting
4 from **17b**. White solid, m.p. 194-197°C, 21 % yield. Molecular formula: C₁₉H₁₄O₃. Molecular
5 Weight: 290.31 g/mol. R_f = 0.41 (cyclohexane/ethyl acetate 80:20). ¹H NMR (300 MHz,
6 CDCl₃) δ 8.29 (d, *J* = 8.1 Hz, 1H, ArH), 8.09 (d, *J* = 8.4 Hz, 1H, ArH), 7.94 (d, *J* = 7.2 Hz,
7 1H, ArH), 7.62-7.46 (m, 4H, ArH), 7.36 (d, *J* = 7.8 Hz, 1H, ArH), 7.09-7.06 (m, 2H, ArH),
8 6.63 (d, *J* = 8.1 Hz, 1H, ArH), 3.91 (s, 3H, CH₃) ppm.

9
10
11
12
13
14
15
16
17 **Ethyl-2-bromobenzoate (22)**. Procedure B: starting compound: 2-bromobenzoic acid.
18 Pail brown oil, 56 % yield. Molecular formula: C₉H₉BrO₂. Molecular Weight: 229.07 g/mol.
19 R_f = 0.63 (cyclohexane/ethyl acetate 90:10). ¹H NMR (300 MHz, CDCl₃) δ 7.73 (dd, *J*₁ = 7.6
20 Hz, *J*₂ = 2.0 Hz, 1H, ArH), 7.60 (dd, *J*₁ = 7.6 Hz, *J*₂ = 2.0 Hz, 1H, ArH), 7.28 (m, 2H, ArH),
21 4.36 (q, *J* = 7.2 Hz, 2H, CH₂), 1.36 (t, *J* = 7.2 Hz, 3H, CH₃) ppm.

22
23
24
25
26
27
28
29 **Ethyl-3-bromobenzoate (23)**. Procedure B: starting compound: 3-bromobenzoic acid.
30 Pail brown oil, 65% yield. Molecular formula: C₉H₉BrO₂. Molecular Weight: 229.07 g/mol.
31 R_f = 0.72 (cyclohexane/ethyl acetate 90:10). ¹H NMR (300 MHz, CDCl₃) δ 8.18 (t, *J* = 1.2
32 Hz, 1H, ArH), 7.97 (dd, *J*₁ = 8.1 Hz, *J*₂ = 1.2 Hz, 1H, ArH), 7.67 (dd, *J*₁ = 8.1 Hz, *J*₂ = 1.2
33 Hz, 1H, ArH), 7.30 (t, *J* = 8.1 Hz, 1H, ArH), 4.37 (q, *J* = 7.2 Hz, 2H, CH₂), 1.39 (t, *J* = 7.2
34 Hz, 3H, CH₃) ppm.

35
36
37
38
39
40
41
42 **1-Aminonaphthalene (24)**. Procedure K: starting from 1-nitronaphthalene. Reaction
43 time: 10 min. Purple solid m.p. 47-50°C, 74 % yield. Molecular formula: C₁₀H₉N. Molecular
44 Weight: 143.19 g/mol. R_f = 0.47 (cyclohexane/ethyl acetate 70:30). The product was purified
45 by flash chromatography, eluting with cyclohexane/ethyl acetate from (80:20) to (70:30). ¹H
46 NMR (300 MHz, CDCl₃) δ 8.00-7.80 (m, 2H, ArH), 7.60-7.40 (m, 2H, ArH), 6.82 (d, *J* = 6
47 Hz, 1H, ArH), 4.10 (br s, 2H, NH₂, exchangeable with D₂O) ppm.

48
49
50
51
52
53
54
55
56 **1-Amino-4-methoxynaphthalene (25)**. Procedure K: starting from 1-methoxy-4-
57 nitronaphthalene. Reaction time: 60 min. Light tan solid m.p. 38-40°C, 49 % yield. Molecular
58
59
60

1
2
3 formula: $C_{11}H_{11}NO$. Molecular Weight: 173.21 g/mol. $R_f = 0.43$ (cyclohexane/ethyl acetate
4 80:20). The product was used in the next reaction without any further purification. 1H NMR
5 (300 MHz, $CDCl_3$) δ 8.49-8.42 (m, 1H, ArH), 7.85-7.80 (m, 1H, ArH), 7.57-7.50 (m, 2H,
6 ArH), 6.70-6.65 (m, 2H, ArH), 3.98 (s, 3H, CH_3), 3.80 (br s, 2H, NH_2 , exchangeable with
7 D_2O) ppm.

8
9
10
11
12
13
14
15 ***tert*-Butyl (4-bromonaphthalen-1-yl)carbamate (26)**. Procedure L: starting from 1-
16 amino-4-bromonaphthalene. White Solid, m.p. 138-140°C, 98 % yield. Molecular formula:
17 $C_{15}H_{16}BrNO_2$. Molecular Weight: 322.20 g/mol. $R_f = 0.33$ (cyclohexane/ethyl acetate 90:10).
18 1H NMR (300 MHz, $CDCl_3$) δ 8.25 (d, $J = 8.1$ Hz, 1H, ArH), 7.86 (d, $J = 8.0$ Hz, 1H, ArH),
19 7.77-7.71 (m, 2H, ArH), 7.62-7.51 (m, 2H, ArH), 6.89 (br s, 1H, NH, exchangeable with
20 D_2O), 1.56 (s, 9H, CH_3) ppm.

21
22
23
24
25
26
27
28
29
30
31
32
33 ***tert*-Butyl (5-bromonaphthalen-1-yl)carbamate (27)**. Procedure L: starting from 1-
34 amino-5-bromonaphthalene. Light pink foam, 85 % yield. Molecular formula: $C_{15}H_{16}BrNO_2$.
35 Molecular Weight: 322.20 g/mol. $R_f = 0.53$ (cyclohexane/ethyl acetate 80:20). 1H NMR (300
36 MHz, $CDCl_3$) δ 8.06 (d, $J = 8.7$ Hz, 1H, ArH), 7.98-7.84 (m, 2H, ArH), 7.80 (d, $J = 7.5$ Hz,
37 1H, ArH), 7.57 (t, $J = 8.1$ Hz, 1H, ArH), 7.35 (t, $J = 8.1$ Hz, 1H, ArH), 6.78 (br s, 1H, NH,
38 exchangeable with D_2O), 1.55 (s, 9H, CH_3) ppm.
39
40
41
42
43

44 **Biological Methods.**

45
46
47 **Materials and Reagents.** Stock solutions of the active compounds were prepared in
48 dimethylsulfoxide (DMSO) at 20 mM concentration; when diluted in the aqueous solution,
49 the final concentration of the various compounds never exceeded 50 μM . For the production
50 of the recombinant forms of CDC25A, -B and -C catalytic domain, a heterologous expression
51 system was used, constituted by the vectors pET28a-CDC25A-cd, pET28a-CDC25B-cd or
52 pET28a-CDC25C-cd, kindly provided by H. Bhattacharjee (Florida International University,
53
54
55
56
57
58
59
60

Herbert Wertheim College of Medicine, Miami, Florida) and the *Escherichia coli* BL21(DE3) strain from Novagen. In the preparation of the recombinant enzyme,⁷⁰ the buffers used for the purification procedure and storage were slightly modified by thoroughly replacing 10 mM β -mercaptoethanol as a reducing agent with 0.5 mM Tris-(2-carboxyethyl)-phosphine hydrochloride (TCEP). The phosphate-buffered saline (PBS) contained 10 mM Na_2HPO_4 , 2 mM KH_2PO_4 , pH 7.4, supplemented with 137 mM NaCl and 2.7 mM KCl. Dulbecco's modified Eagle's medium (DMEM), fetal bovine serum (FBS), L-glutamine, penicillin G, streptomycin and trypsin were purchased from Lonza (Milano, Italy). OMFP, propidium iodide (PI), crystal violet, and all other chemicals of analytical grade were purchased from Sigma. Rabbit polyclonal antibody against p-Cdk1 was purchased from Cell Signaling Technology (Boston, USA), whereas rabbit polyclonal antibody against β -actin, as well as HRP conjugated secondary antibody, were purchased from Santa Cruz Biotechnology (Heidelberg, Germany).

Kinetic Studies of the CDC25 Phosphatase Activity. A fluorimetric assay method was used to measure the dephosphorylation of OMFP catalyzed by the recombinant CDC25 forms, essentially as previously described.^{27, 38} Briefly, the formation of the fluorescent product O-methylfluorescein was monitored continuously at 30°C, using a computer-assisted Cary Eclipse spectrofluorimeter (Varian) equipped with an electronic temperature controller. Excitation and emission wavelengths were set at 485 and 530 nm, respectively. Both excitation and emission slits were set at 10 nm. The 500- μL final volume of the reaction mixture, containing a fixed concentration of CDC25A, -B or -C ranging between 15 and 25 nM in 20 mM Tris-HCl, pH 7.8, 0.5 mM TCEP, was prepared in the absence or in the presence of various concentrations of each among thirty-one inhibitors. The reaction mixture also contained 1% (v/v) DMSO carried over from the inhibitors. After the addition of 0.5-25 μM OMFP, the velocity of OMFP hydrolysis (v_i) was measured and expressed as Arbitrary

1
2
3 Units per min (AU/min). The data of v_i were analyzed as a function of [OMFP] in double
4
5 reciprocal Lineweaver-Burk plots, thus allowing the extrapolation of the maximum velocity
6
7 of OMFP hydrolysis (V_{\max}) and affinity for the substrate OMFP (K_M).
8
9

10 To measure the inhibition constant (K_i) of CDC25 forms towards the various compounds,
11
12 the Lineweaver-Burk plot of phosphatase activity in the absence of inhibitor was compared
13
14 with those obtained in the presence of different concentrations of inhibitor. The resulting
15
16 values of K_M for OMFP and V_{\max} in the presence of the inhibitor were then used to calculate
17
18 the K_i according to the following equations. When the K_M remained essentially unchanged,
19
20 but the V_{\max} decreased after the addition of the inhibitor (non-competitive inhibition), the K_i
21
22 was calculated with the equation: $K_i = V_{\max+I} \cdot [I]/(V_{\max} - V_{\max+I})$, where $V_{\max+I}$ represents the
23
24 V_{\max} measured in the presence of the inhibitor (I). When both K_M and V_{\max} underwent a
25
26 similar and progressive decrease after the addition of the inhibitor (un-competitive
27
28 inhibition), the K_i could be calculated with either the former equation or an alternate
29
30 equation: $K_i = K_{M+I} \cdot [I]/(K_M - K_{M+I})$, where K_{M+I} represents the K_M measured in the presence
31
32 of the inhibitor. On the other hand, in the case of mixed inhibition, only a rough evaluation of
33
34 the K_i value was possible on the basis of the decrease of V_{\max} and increase of K_M after the
35
36 addition of the inhibitor.
37
38
39
40
41

42 **Intrinsic Fluorescence Studies on CDC25B.** Fluorescence spectra were recorded at 20°C,
43
44 using a computer-assisted Cary Eclipse spectrofluorimeter (Varian) equipped with an
45
46 electronic temperature controller. Unless otherwise indicated, the excitation wavelength was
47
48 set at 280 nm; both excitation and emission slits were set at 10 nm. Briefly, a 500- μ L final
49
50 volume of a 1 μ M solution of the recombinant CDC25B dissolved in 20 mM Tris•HCl, pH
51
52 7.8 buffer containing 0.5 mM TCEP and 0.5% (v/v) DMSO was directly prepared in a
53
54 fluorimetric cuvette in the absence or in the presence of various NPA derivatives. Spectra
55
56
57
58
59
60

1
2
3 were recorded at a scan speed of 120 nm/min and corrected for the inner-filter effect due to
4
5 the absorbance of the NPA derivatives at 280 nm.
6

7
8 **Cell Cultures.** The human melanoma cell lines A375 and A2058, deriving from a primary
9
10 tumor or lymph nodal metastasis, respectively, were kindly provided from CEINGE (Naples,
11
12 Italy). Cells were grown in DMEM supplemented with 10% FBS, 2 mM L-glutamine, 100
13
14 IU/mL penicillin G and 100 µg/mL streptomycin in humidified incubator at 37°C under 5%
15
16 CO₂ atmosphere. The human skin fibroblast cell line BJ-5ta immortalized with the human
17
18 telomerase reverse transcriptase⁷¹ was cultured in a 4:1 mixture of DMEM and Medium 199
19
20 supplemented with 4 mM L-glutamine, 4.5 g/L glucose, 1.5 g/L sodium bicarbonate, 10%
21
22 FBS, 100 IU/mL penicillin G, 100 mg/mL streptomycin and 0.01 mg/mL hygromycin B in
23
24 humidified incubator at 37 C under 5% CO₂ atmosphere. All cells were split and seeded
25
26 every three days, and used during their exponential phase of growth. Cell treatments were
27
28 usually carried out after 24 h from plating.
29
30
31

32
33 **MTT Assay.** The 3-(4,5-dimethylthiazole-2-yl)-2,5-biphenyltetrazolium bromide (MTT)
34
35 assay was used to detect cell viability essentially as previously described.⁷² A2058 cells were
36
37 plated in 96-well microtiter plates at 4×10⁴ cells/well. After 24 h, cells were treated with
38
39 different concentrations of the various inhibitors or with 0.5% (v/v) DMSO as a control
40
41 vehicle. After 24, 48 or 72 h treatment and upon addition of 10 µL MTT solution in the dark,
42
43 plates were incubated for 3 h at 37°C under 5% CO₂ atmosphere. After medium aspiration
44
45 and solubilization of formazan crystals, the absorbance was measured at a wavelength of 570
46
47 nm using an ELISA plate reader (Bio-Rad, Milano, Italy).
48
49
50

51
52 **Cell Cycle Analysis.** Cells were seeded into 6-well plates at 3 × 10⁵ cells/well for 24 h at
53
54 37°C; after the addition of 10 µM FP-21 or 0.5% (v/v) DMSO, the incubation of treated cells
55
56 continued for 8 or 16 h. After each treatment, cells were harvested with trypsin, centrifuged
57
58 and the pellet was resuspended in PBS. For cell cycle analysis, cells were fixed with 70%
59
60

1
2
3 (v/v) cold ethanol and stored at -20°C for 1 h. Then, cells were washed with cold PBS,
4
5 centrifuged and the pellet was resuspended in 200 µL of a non-lysis solution containing 50
6
7 µg/mL PI. After incubation at 4°C for 30 min, cells were analyzed with a FACScan flow
8
9 cytometer (Becton Dickinson) to evaluate the distribution of cell cycle phases.

10
11
12 **Colony Formation Assay.** Colony-forming assay was performed as previously described
13
14 with some modifications.⁷³ Briefly, cells were seeded in duplicate in 6-well plates at a density
15
16 of 4×10^2 cells per well. After 2/3-days, cells were treated with 0.5% (v/v) DMSO or different
17
18 FP-21 concentrations and incubated for additional 10 days at 37°C. Then, colonies were
19
20 stained with 1% (w/v) crystal violet in 50% (v/v) ethanol for 1 h at room temperature. Cells
21
22 were photographed with a digital camera (Canon PowerShot G9); the number of colonies (\geq
23
24 50 cells per colony) was counted using ImageJ 1.42q software.

25
26
27
28 **Total cell lysates and Western blotting.** A2058 and A375 cells were seeded into 6-well-
29
30 plates (3×10^5 cells/plate) for 24 h at 37 °C and then treated for 8 h with 10 µM compound
31
32 **4a** or 0.5% DMSO. After treatment, cells were harvested, washed with PBS and then lysed in
33
34 ice-cold modified radio immunoprecipitation assay (RIPA) buffer (50 mM Tris-HCl, pH 7.4,
35
36 150 mM NaCl, 1% Nonidet P-40, 0.25% sodium deoxycholate, 1 mM Na_3VO_4 and 1 mM
37
38 NaF), supplemented with protease inhibitors and incubated for 30 min on ice. The
39
40 supernatant obtained after centrifugation at 12,000 rpm for 30 min at 4°C constituted the total
41
42 protein extract. Protein concentration was determined by the Bradford method, using bovine
43
44 serum albumin (BSA) as standard.⁷⁴ Western blotting analysis was performed with equal
45
46 amounts of total protein extracts. Briefly, protein samples were dissolved in SDS-reducing
47
48 loading buffer, run on 12% SDS/PAGE and then transferred to Immobilon P membrane
49
50 (Millipore). The filter was incubated with the specific primary antibody at 4°C overnight and
51
52 then with the secondary antibody at room temperature for 1 h. Membranes were then
53
54
55
56
57
58
59
60

1
2
3 analyzed by an enhanced chemiluminescence reaction, using WesternBright ECL (Advansta)
4 according to manufacturer's instruction; signals were visualized by autoradiography.
5
6

7
8 **Statistical Analysis.** Data are reported as the mean \pm standard error (SE). The statistical
9 significance of differences among groups was evaluated using ANOVA, with the Bonferroni
10 correction as post hoc test or the Student *t* test where appropriate. The significance was
11
12
13
14
15 accepted at the level of $p < 0.05$.
16
17
18

19 **Molecular Modeling.**

20
21 **Ligand and Protein Preparation.** The molecular structures of compounds **1-12** were
22 sketched using the Molecular Builder module implemented in Maestro (Maestro,
23 Schrödinger, LLC, New York, NY, 2018) and then preprocessed with LigPrep (LigPrep,
24 Schrödinger, LLC, New York, NY, 2018). Multiple protonation and tautomerization states at
25
26
27
28
29
30
31
32
33
34
35
36
37
38
39
40
41
42
43
44
45
46
47
48
49
50
51
52
53
54
55
56
57
58
59
60
pH of 7.0 \pm 2.0 were requested, although no additional ionization states were generated. The
obtained structures were then energy-minimized by means of MacroModel 11.7
(MacroModel, Schrödinger, LLC, New York, NY, 2018) using the MMFF force field with
the steepest descent (1000 steps) followed by truncated Newton conjugate gradient (500
steps) methods. Partial atomic charges were computed using the OPLS3 force field.⁷⁵

Docking experiments were performed employing the crystal structure of the human
Cdc25B catalytic domain (PDB ID: 1QB0).²² This structure was selected because of its
completeness, the absence of mutations, and the reasonably high resolution (1.9 Å). The
protein setup was carried out using the Protein Preparation Wizard implemented in Maestro.
Crystallographic water molecules and other chemical components were removed; hydrogen
atoms were added to the protein consistent with the neutral physiologic pH. Arginine, lysine,
aspartic and glutamic residues were considered ionized. Hydrogen bonds were optimized
with PropKa (at pH 7.0), and a restrained minimization of the protein hydrogen atoms only

1
2
3 was conducted with the OPLS3 force field until an RMSD of 0.30 Å using the Impref module
4
5 of Impact.
6

7
8 **Docking Calculations.** Since the receptor likely experiences conformational movements
9
10 upon binding of ligands, docking simulations were performed with IFD module.^{57, 58} Briefly,
11
12 each ligand is first docked using a softened potential by means of Glide, which outputs a set
13
14 of plausible poses. During this step, binding site residues are temporarily mutated to alanine,
15
16 on the basis of the B-factors of the side chain atoms. A selected set of poses is then refined by
17
18 Prime, which backmutates alanines to the original residues and performs a rotamer-based
19
20 library optimization of the protein side chain conformations, to better accommodate the
21
22 ligand. The best receptor structures are passed back to Glide for redocking of the ligand using
23
24 the Glide XP scoring function. In this work, the docking grid was defined as the approximate
25
26 center of the swimming pool, with an inner box size of 10 × 10 × 10 Å and an outer box of 30
27
28 × 30 × 30 Å.
29
30
31
32

33
34 With the aim to obtain a set of non-redundant poses and to save CPU time, the output
35
36 poses from IFD simulations were clustered into separate self-organizing maps (SOMs) based
37
38 on the Structural Interaction Fingerprints (SIFt)⁷⁶ contact similarity, as implemented in the
39
40 Schrodinger Suite. The clusters were arranged in a 3 × 3 square matrix. Each cell in the
41
42 cluster map contains a group of poses that are similar to one another in structural interaction
43
44 fingerprint pattern. For each cluster, one representative was chosen for the subsequent
45
46 binding pose metadynamics protocol. In this protocol, the selected poses underwent a series
47
48 of metadynamics simulations by means of Desmond module, to determine the most stable
49
50 one and provide a more reliable binding mode. The stability is assessed in terms of the
51
52 fluctuations of the ligand RMSD over the course of the simulation, and the persistence of
53
54 important contacts between the ligand and the receptor (and any other cofactors or solvent
55
56 molecules), such as hydrogen bonds and π interactions. The collective variable for the
57
58
59
60

1
2
3 metadynamics simulation is the ligand RMSD from its initial pose. Since a biasing potential
4 is applied to the ligand RMSD, an incorrect pose would easily be displaced than a more
5 stable one. To improve the statistics, 10 metadynamics runs for each of the candidate poses
6 were performed, and the results were averaged over the simulations. The poses were rank
7 ordered by a Composite Score, linearly combining the average energy-weighted expectation
8 of the pose RMSD over the course of metadynamics trajectories and the persistence of
9 contacts between the protein and the ligand.

10
11
12 **PAINS Filtering.** All the tested compounds were screened for known classes of pan-assay
13 interference compounds (PAINS)⁷⁷ by using Faf-Drugs4.⁷⁸ None of the compounds was
14 found as potential PAINS. Furthermore, all the compounds were examined for known classes
15 of molecular aggregators by using <http://zinc15.docking.org/patterns/home/>,⁷⁹ and none of
16 them was found as a potential aggregator at the used final concentration. In addition, none of
17 the compounds emitted fluorescence at the same wavelength as the substrate ligand OMFP in
18 the fluorimetric assays.

19
20
21
22
23
24
25
26
27
28
29
30
31
32
33
34
35
36
37
38
39
40
41
42
43
44
45
46
47
48
49
50
51
52
53
54
55
56
57
58
59
60

Supporting Information

Kinetic parameters of the CDC25B phosphatase activity in the presence of compounds **1-12**, Lineweaver-Burk plots of non-competitive, un-competitive and mixed inhibitors, and structural analysis of Cdc25B crystal structures (PDF)

Molecular formula strings and the associated biological data (CSV)

Corresponding Author Information

Maria Rosaria Ruocco, Department of Molecular Medicine and Medical Biotechnology, University of Naples Federico II, 80131 Naples, Italy; Phone: +39-081-7463121; Fax: +39-081-7463653. E-mail: mariarosaria.ruocco2@unina.it

Antonio Lavecchia, Department of Pharmacy, “Drug Discovery” Laboratory, University of Naples Federico II, 80131 Naples, Italy; Phone: +39-081-678613/623; Fax: +39-081-678012. E-mail: antonio.lavecchia@unina.it

Author Contributions

[†]These authors contributed equally to this work

Acknowledgments

This study was supported by grants “Combattere la resistenza tumorale: piattaforma integrata multidisciplinare per un approccio tecnologico innovativo alle oncoterapie - CAMPANIA ONCOTERAPIE” (Project N. B61G18000470007) and “SATIN grant 2018-2020” of Regione Campania (Italy). The authors would like to thank Dr. Federica Porta, Marianna Porcino and Ilaria D’Andrea for their precious collaboration.

Abbreviations Used

BSA, bovine serum albumin; CDC25, cell division cycle 25; Cdk, cyclin-dependent kinases; DMEM, Dulbecco's modification of Eagle's medium; DMSO, dimethyl sulfoxide; DSP, dual-specificity phosphatase; FBS, foetal bovine serum; IFD, Induced Fit Docking; MTT, 3-[4,5-dimethylthiazol-2-yl]-2,5 diphenyl tetrazolium bromide; *n*-BuLi, *n*-Butyllithium; NPA, naphthylphenylamine; NPK, naphthylphenylketone; OMFP, 3-O-methyl fluorescein phosphate; PBS, phosphate-buffered saline; PDB, protein data bank; PI, propidium iodide; ROS, reactive oxygen species; SAR, structure-activity relationships; SDS/PAGE, sodium dodecyl sulfate polyacrylamide gel electrophoresis; SOMs, self-organizing maps; SIFT, Structural Interaction Fingerprints; TCEP, Tris-(2-carboxyethyl)-phosphine hydrochloride.

REFERENCES

- (1) Russell, P.; Nurse, P. Cdc25+ Functions as an Inducer in the Mitotic Control of Fission Yeast. *Cell* **1986**, 45, 145-153.
- (2) Strausfeld, U.; Labbe, J. C.; Fesquet, D.; Cavadore, J. C.; Picard, A.; Sadhu, K.; Russell, P.; Doree, M. Dephosphorylation and Activation of a P34cdc2/Cyclin B Complex in Vitro by Human Cdc25 Protein. *Nature* **1991**, 351, 242-245.
- (3) Aressy, B.; Bugler, B.; Valette, A.; Biard, D.; Ducommun, B. Moderate Variations in Cdc25b Protein Levels Modulate the Response to DNA Damaging Agents. *Cell Cycle* **2008**, 7, 2234-2240.
- (4) Molinari, M.; Mercurio, C.; Dominguez, J.; Goubin, F.; Draetta, G. F. Human Cdc25 a Inactivation in Response to S Phase Inhibition and Its Role in Preventing Premature Mitosis. *EMBO Rep.* **2000**, 1, 71-79.
- (5) Karlsson-Rosenthal, C.; Millar, J. B. A. Cdc25: Mechanisms of Checkpoint Inhibition and Recovery. *Trends Cell Biol.* **2006**, 16, 285-292.
- (6) Terada, Y.; Tatsuka, M.; Jinno, S.; Okayama, H. Requirement for Tyrosine Phosphorylation of Cdk4 in G1 Arrest Induced by Ultraviolet Irradiation. *Nature* **1995**, 376, 358-362.
- (7) Massagué, J. Repression of the Cdk Activator Cdc25a and Cell-Cycle Arrest by Cytokine Tgf-B in Cells Lacking the Cdk Inhibitor P15. *Nature* **1997**, 387, 417-422.
- (8) Lindqvist, A.; Rodríguez-Bravo, V.; Medema, R. H. The Decision to Enter Mitosis: Feedback and Redundancy in the Mitotic Entry Network. *J. Cell Biol.* **2009**, 185, 193-202.
- (9) Bartek, J.; Lukas, J. Mammalian G1- and S-Phase Checkpoints in Response to DNA Damage. *Curr. Opin. Cell Biol.* **2001**, 13, 738-747.

- 1
2
3 (10) Boutros, R.; Lobjois, V.; Ducommun, B. Cdc25 Phosphatases in Cancer Cells: Key
4 Players? Good Targets? *Nat. Rev. Cancer* **2007**, *7*, 495-507.
5
6
7
8 (11) Fauman, E. B.; Saper, M. A. Structure and Function of Theprotein Tyrosine
9 Phosphatases. *Trends Biochem. Sci* **1996**, *21*, 413-417.
10
11
12 (12) Gabrielli, B. G.; De Souza, C. P.; Tonks, I. D.; Clark, J. M.; Hayward, N. K.; Ellem, K.
13 A. Cytoplasmic Accumulation of Cdc25b Phosphatase in Mitosis Triggers Centrosomal
14 Microtubule Nucleation in Hela Cells. *J. Cell Sci.* **1996**, *109*, 1081-1093.
15
16
17 (13) Izumi, T.; Maller, J. L. Phosphorylation and Activation of the Xenopus Cdc25
18 Phosphatase in the Absence of Cdc2 and Cdk2 Kinase Activity. *Mol. Biol. Cell* **1995**, *6*,
19 215-226.
20
21
22 (14) Zwicker, J.; Lucibello, F. C.; Wolfrain, L. A.; Gross, C.; Truss, M.; Engeland, K.;
23 Müller, R. Cell Cycle Regulation of the Cyclin a, Cdc25c and Cdc2 Genes Is Based on
24 a Common Mechanism of Transcriptional Repression. *EMBO J.* **1995**, *14*, 4514-4522.
25
26
27 (15) Boutros, R.; Dozier, C.; Ducommun, B. The When and Wheres of Cdc25 Phosphatases.
28 *Curr. Opin. Cell Biol.* **2006**, *18*, 185-191.
29
30
31 (16) Liu, J. C.; Granieri, L.; Shrestha, M.; Wang, D.-Y.; Vorobieva, I.; Rubie, E. A.; Jones,
32 R.; Ju, Y.; Pellicchia, G.; Jiang, Z. Identification of Cdc25 as a Common Therapeutic
33 Target for Triple-Negative Breast Cancer. *Cell Rep.* **2018**, *23*, 112-126.
34
35
36 (17) Hernández, S.; Bessa, X.; Beà, S.; Hernández, L.; Nadal, A.; Mallofré, C.; Muntane, J.;
37 Castells, A.; Fernández, P. L.; Cardesa, A. Differential Expression of Cdc25 Cell-
38 Cycle-Activating Phosphatases in Human Colorectal Carcinoma. *Lab. Invest.* **2001**, *81*,
39 465-473.
40
41
42 (18) Wang, Z.; Trope, C. G.; Flørenes, V. A.; Suo, Z.; Nesland, J. M.; Holm, R.
43 Overexpression of Cdc25b, Cdc25c and Phospho-Cdc25c (Ser216) in Vulvar
44
45
46
47
48
49
50
51
52
53
54
55
56
57
58
59
60

- 1
2
3 Squamous Cell Carcinomas Are Associated with Malignant Features and Aggressive
4 Cancer Phenotypes. *BMC Cancer* **2010**, 10, 233.
5
6
7
8 (19) Kristjansdottir, K.; Rudolph, J. Cdc25 Phosphatases and Cancer. *Chem. Biol.* **2004**, 11,
9 1043-1051.
10
11
12 (20) Albert, H.; Santos, S.; Battaglia, E.; Brito, M.; Monteiro, C.; Bagrel, D. Differential
13 Expression of Cdc25 Phosphatases Splice Variants in Human Breast Cancer Cells. *Clin.*
14 *Chem. Lab. Med.* **2011**, 49, 1707-1714.
15
16
17 (21) Fauman, E. B.; Cogswell, J. P.; Lovejoy, B.; Rocque, W. J.; Holmes, W.; Montana, V.
18 G.; Piwnica-Worms, H.; Rink, M. J.; Saper, M. A. Crystal Structure of the Catalytic
19 Domain of the Human Cell Cycle Control Phosphatase, Cdc25a. *Cell* **1998**, 93, 617-
20 625.
21
22
23 (22) Reynolds, R. A.; Yem, A. W.; Wolfe, C. L.; Deibel, M. R., Jr.; Chidester, C. G.;
24 Watenpaugh, K. D. Crystal Structure of the Catalytic Subunit of Cdc25b Required for
25 G2/M Phase Transition of the Cell Cycle. *J. Mol. Biol.* **1999**, 293, 559-568.
26
27
28 (23) Rudolph, J. Targeting the Neighbor's Pool. *Mol. Pharmacol.* **2004**, 66, 780-782.
29
30
31 (24) Lavecchia, A.; Di Giovanni, C.; Novellino, E. Cdc25 Phosphatase Inhibitors: An
32 Update. *Mini-Rev. Med. Chem.* **2012**, 12, 62-73.
33
34
35 (25) Lavecchia, A.; Coluccia, A.; Di Giovanni, C.; Novellino, E. Cdc25b Phosphatase
36 Inhibitors in Cancer Therapy: Latest Developments, Trends and Medicinal Chemistry
37 Perspective. *Anti-Cancer Agents Med. Chem.* **2008**, 8, 843-856.
38
39
40 (26) Brenner, A. K.; Reikvam, H.; Lavecchia, A.; Bruserud, Ø. Therapeutic Targeting the
41 Cell Division Cycle 25 (Cdc25) Phosphatases in Human Acute Myeloid Leukemia—
42 the Possibility to Target Several Kinases through Inhibition of the Various Cdc25
43 Isoforms. *Molecules* **2014**, 19, 18414-18447.
44
45
46
47
48
49
50
51
52
53
54
55
56
57
58
59
60

- 1
2
3 (27) Capasso, A.; Cerchia, C.; Di Giovanni, C.; Granato, G.; Albano, F.; Romano, S.; De
4
5 Vendittis, E.; Ruocco, M. R.; Lavecchia, A. Ligand-Based Chemoinformatic Discovery
6
7 of a Novel Small Molecule Inhibitor Targeting Cdc25 Dual Specificity Phosphatases
8
9 and Displaying in Vitro Efficacy against Melanoma Cells. *Oncotarget* **2015**, *6*, 40202-
10
11 40222.
12
13
14 (28) Kar, S.; Lefterov, I. M.; Wang, M.; Lazo, J. S.; Scott, C. N.; Wilcox, C. S.; Carr, B. I.
15
16 Binding and Inhibition of Cdc25 Phosphatases by Vitamin K Analogues. *Biochemistry*
17
18 **2003**, *42*, 10490-10497.
19
20
21 (29) Pu, L.; Amoscato, A. A.; Bier, M. E.; Lazo, J. S. Dual G1 and G2 Phase Inhibition by a
22
23 Novel, Selective Cdc25 Inhibitor 6-Chloro-7-[Corrected](2-Morpholin-4-
24
25 Ylethylamino)-Quinoline-5,8-Dione. *J. Biol. Chem.* **2002**, *277*, 46877-46885.
26
27
28 (30) Brisson, M.; Nguyen, T.; Wipf, P.; Joo, B.; Day, B. W.; Skoko, J. S.; Schreiber, E. M.;
29
30 Foster, C.; Bansal, P.; Lazo, J. S. Redox Regulation of Cdc25b by Cell-Active
31
32 Quinolinediones. *Mol. Pharmacol.* **2005**, *68*, 1810-1820.
33
34
35 (31) Zhou, Y. B.; Feng, X.; Wang, L. N.; Du, J. Q.; Zhou, Y. Y.; Yu, H. P.; Zang, Y.; Li, J.
36
37 Y.; Li, J. Lgh00031, a Novel Ortho-Quinonoid Inhibitor of Cell Division Cycle 25b,
38
39 Inhibits Human Cancer Cells Via Ros Generation. *Acta Pharmacol. Sin.* **2009**, *30*,
40
41 1359-1368.
42
43
44 (32) Bolton, J. L.; Trush, M. A.; Penning, T. M.; Dryhurst, G.; Monks, T. J. Role of
45
46 Quinones in Toxicology. *Chem. Res. Toxicol.* **2000**, *13*, 135-160.
47
48
49 (33) Sohn, J.; Kiburz, B.; Li, Z.; Deng, L.; Safi, A.; Pirrung, M. C.; Rudolph, J. Inhibition of
50
51 Cdc25 Phosphatases by Indolyldihydroxyquinones. *J. Med. Chem.* **2003**, *46*, 2580-
52
53 2588.
54
55
56 (34) Brisson, M.; Nguyen, T.; Vogt, A.; Yalowich, J.; Giorgianni, A.; Tobi, D.; Bahar, I.;
57
58 Stephenson, C. R.; Wipf, P.; Lazo, J. S. Discovery and Characterization of Novel Small
59
60

- 1
2
3 Molecule Inhibitors of Human Cdc25b Dual Specificity Phosphatase. *Mol. Pharmacol.*
4
5 **2004**, 66, 824-833.
6
7
8 (35) Kim, K. R.; Kwon, J. L.; Kim, J. S.; No, Z.; Kim, H. R.; Cheon, H. G. Ek-6136 (3-
9
10 Methyl-4-(O-Methyl-Oximino)-1-Phenylpyrazolin-5-One): A Novel Cdc25b Inhibitor
11
12 with Antiproliferative Activity. *Eur. J. Pharmacol.* **2005**, 528, 37-42.
13
14
15 (36) Kolb, S.; Mondesert, O.; Goddard, M. L.; Jullien, D.; Villoutreix, B. O.; Ducommun,
16
17 B.; Garbay, C.; Braud, E. Development of Novel Thiazolopyrimidines as Cdc25b
18
19 Phosphatase Inhibitors. *ChemMedChem* **2009**, 4, 633-648.
20
21
22 (37) George Rosenker, K. M.; Paquette, W. D.; Johnston, P. A.; Sharlow, E. R.; Vogt, A.;
23
24 Bakan, A.; Lazo, J. S.; Wipf, P. Synthesis and Biological Evaluation of 3-
25
26 Aminoisoquinolin-1(2h)-One Based Inhibitors of the Dual-Specificity Phosphatase
27
28 Cdc25b. *Bioorg. Med. Chem.* **2015**, 23, 2810-2818.
29
30
31 (38) Lavecchia, A.; Di Giovanni, C.; Pesapane, A.; Montuori, N.; Ragno, P.; Martucci, N.
32
33 M.; Masullo, M.; De Vendittis, E.; Novellino, E. Discovery of New Inhibitors of
34
35 Cdc25b Dual Specificity Phosphatases by Structure-Based Virtual Screening. *J. Med.*
36
37 *Chem.* **2012**, 55, 4142-4158.
38
39
40 (39) Cerchia, C.; Lavecchia, A. Small Molecule Drugs and Targeted Therapy for Melanoma:
41
42 Current Strategies and Future Directions. *Curr. Med. Chem.* **2017**, 24, 2312-2344.
43
44
45 (40) Bales, E. S.; Dietrich, C.; Bandyopadhyay, D.; Schwahn, D. J.; Xu, W.; Didenko, V.;
46
47 Leiss, P.; Conrad, N.; Pereira-Smith, O.; Orengo, I. High Levels of Expression of
48
49 P27kip1 and Cyclin E in Invasive Primary Malignant Melanomas. *J. Invest. Dermatol.*
50
51 **1999**, 113, 1039-1046.
52
53
54 (41) Tang, L.; Li, G.; Tron, V. A.; Trotter, M. J.; Ho, V. C. Expression of Cell Cycle
55
56 Regulators in Human Cutaneous Malignant Melanoma. *Melanoma Res.* **1999**, 9, 148-
57
58 154.
59
60

- 1
2
3 (42) Muthusamy, V.; Hobbs, C.; Nogueira, C.; Cordon-Cardo, C.; McKee, P. H.; Chin, L.;
4 Bosenberg, M. W. Amplification of Cdk4 and Mdm2 in Malignant Melanoma. *Genes,*
5
6 *Chromosomes Cancer* **2006**, 45, 447-454.
7
8
9
10 (43) Lyons, J.; Bastian, B. C.; McCormick, F. Mc1r and Camp Signaling Inhibit Cdc25b
11
12 Activity and Delay Cell Cycle Progression in Melanoma Cells. *Proc. Natl. Acad. Sci.*
13
14 *U.S.A.* **2013**, 110, 13845-13850.
15
16
17 (44) Yazdanian, M.; Glynn, S. L.; Wright, J. L.; Hawi, A. Correlating Partitioning and Caco-
18
19 2 Cell Permeability of Structurally Diverse Small Molecular Weight Compounds.
20
21 *Pharm. Res.* **1998**, 15, 1490-1494.
22
23
24 (45) Platt, K. L.; Oesch, F. Reductive Cyclization of Keto Acids to Polycyclic Aromatic
25
26 Hydrocarbons by Hydroiodic Acid-Red Phosphorus. *J. Org. Chem.* **1981**, 46, 2601-
27
28 2603.
29
30
31 (46) Badger, G. M. Derivatives of O-1-Naphthoylbenzoic Acid and 1-Benzyl-naphthalene-2-
32
33 Carboxylic Acid. *J. Chem. Soc.* **1941**, 351-352.
34
35
36 (47) Newman, M. S.; Sankaran, V.; Olson, D. R. Phenolic and Ketonic Tautomers in
37
38 Polycyclic Aromatic Hydrocarbons. *J. Am. Chem. Soc.* **1976**, 98, 3237-3242.
39
40
41 (48) Harvey, R. G.; Cortez, C. Fluorine-Substituted Derivatives of the Carcinogenic
42
43 Dihydrodiol and Diol Epoxide Metabolites of 7-Methyl-, 12-Methyl-and 7, 12-
44
45 Dimethylbenz [a] Anthracene. *Tetrahedron* **1997**, 53, 7101-7118.
46
47
48 (49) Di Santo, R.; Costi, R.; Cuzzucoli Crucitti, G.; Pescatori, L.; Rosi, F.; Scipione, L.;
49
50 Celona, D.; Vertechy, M.; Ghirardi, O.; Piovesan, P. Design, Synthesis, and Structure-
51
52 Activity Relationship of N-Arylnaphthylamine Derivatives as Amyloid Aggregation
53
54 Inhibitors. *J. Med. Chem.* **2012**, 55, 8538-8548.
55
56
57 (50) Vilaivan, T. A Rate Enhancement of Tert-Butoxycarbonylation of Aromatic Amines
58
59 with Boc₂O in Alcoholic Solvents. *Tetrahedron Lett.* **2006**, 47, 6739-6742.
60

- 1
2
3 (51) Pini, E.; Poli, G.; Tuccinardi, T.; Chiarelli, L.; Mori, M.; Gelain, A.; Costantino, L.;
4
5 Villa, S.; Meneghetti, F.; Barlocco, D. New Chromane-Based Derivatives as Inhibitors
6
7 of Mycobacterium Tuberculosis Salicylate Synthase (MbtI): Preliminary Biological
8
9 Evaluation and Molecular Modeling Studies. *Molecules* **2018**, *23*, 1506.
10
11
12 (52) Chiarelli, L. R.; Mori, M.; Barlocco, D.; Beretta, G.; Gelain, A.; Pini, E.; Porcino, M.;
13
14 Mori, G.; Stelitano, G.; Costantino, L.; Lapillo, M.; Bonanni, D.; Poli, G.; Tuccinardi,
15
16 T.; Villa, S.; Meneghetti, F. Discovery and Development of Novel Salicylate Synthase
17
18 (MbtI) Furanic Inhibitors as Antitubercular Agents. *Eur. J. Med. Chem.* **2018**, *155*, 754-
19
20 763.
21
22
23 (53) Ge, Y.; van der Kamp, M.; Malaisree, M.; Liu, D.; Liu, Y.; Mulholland, A. J.
24
25 Identification of the Quinolinedione Inhibitor Binding Site in Cdc25 Phosphatase B
26
27 through Docking and Molecular Dynamics Simulations. *J. Comput.-Aided Mol. Des.*
28
29 **2017**, *31*, 995-1007.
30
31
32 (54) Sarkis, M.; Miteva, M. A.; Dasso Lang, M. C.; Jaouen, M.; Sari, M. A.; Galcéra, M. O.;
33
34 Ethève-Quellejeu, M.; Garbay, C.; Bertho, G.; Braud, E. Insights into the Interaction
35
36 of High Potency Inhibitor Irc-083864 with Phosphatase Cdc25. *Proteins: Struct.,*
37
38 *Funct., Bioinf.* **2017**, *85*, 593-601.
39
40
41 (55) Lazo, J. S.; Nemoto, K.; Pestell, K. E.; Cooley, K.; Southwick, E. C.; Mitchell, D. A.;
42
43 Furey, W.; Gussio, R.; Zaharevitz, D. W.; Joo, B. Identification of a Potent and
44
45 Selective Pharmacophore for Cdc25 Dual Specificity Phosphatase Inhibitors. *Mol.*
46
47 *Pharmacol.* **2002**, *61*, 720-728.
48
49
50 (56) Sohn, J.; Kristjánssdóttir, K.; Safi, A.; Parker, B.; Kiburz, B.; Rudolph, J. Remote Hot
51
52 Spots Mediate Protein Substrate Recognition for the Cdc25 Phosphatase. *Proc. Natl.*
53
54 *Acad. Sci. U.S.A.* **2004**, *101*, 16437-16441.
55
56
57
58
59
60

- 1
2
3 (57) Sherman, W.; Day, T.; Jacobson, M. P.; Friesner, R. A.; Farid, R. Novel Procedure for
4 Modeling Ligand/Receptor Induced Fit Effects. *J. Med. Chem.* **2006**, 49, 534-553.
5
6
7 (58) Sherman, W.; Beard, H. S.; Farid, R. Use of an Induced Fit Receptor Structure in
8 Virtual Screening. *Chem. Biol. Drug Des.* **2006**, 67, 83-84.
9
10
11
12 (59) Clark, A. J.; Tiwary, P.; Borrelli, K.; Feng, S.; Miller, E. B.; Abel, R.; Friesner, R. A.;
13 Berne, B. J. Prediction of Protein–Ligand Binding Poses Via a Combination of Induced
14 Fit Docking and Metadynamics Simulations. *J. Chem. Theory Comput.* **2016**, 12, 2990-
15 2998.
16
17
18
19
20
21 (60) Sohn, J.; Kiburz, B.; Li, Z.; Deng, L.; Safi, A.; Pirrung, M. C.; Rudolph, J. Inhibition of
22 Cdc25 Phosphatases by Indolyldihydroxyquinones. *J. Med. Chem.* **2003**, 46, 2580-
23 2588.
24
25
26
27
28 (61) Lavecchia, A.; Cosconati, S.; Limongelli, V.; Novellino, E. Modeling of Cdc25b Dual
29 Specificity Protein Phosphatase Inhibitors: Docking of Ligands and Enzymatic Inhibition
30 Mechanism. *ChemMedChem* **2006**, 1, 540-550.
31
32
33
34
35 (62) Taylor, N. R.; Borhani, D.; Epstein, D.; Rudolph, J.; Ritter, K.; Fujimori, T.; Robinson,
36 S.; Eckstein, J.; Haupt, A.; Walker, N.; Dixon, R. W.; Choquette, D.; Blanchard, J.;
37 Kluge, A.; Pal, K.; Bockovich, N.; Come, J.; Hediger, M. Method of Identifying
38 Inhibitors of Cdc25. WO0116300 (A2), Mar 8, 2001.
39
40
41
42
43
44 (63) Cheng, L.; Lopez-Beltran, A.; Massari, F.; MacLennan, G. T.; Montironi, R. Molecular
45 Testing for Braf Mutations to Inform Melanoma Treatment Decisions: A Move toward
46 Precision Medicine. *Mod. Pathol.* **2018**, 31, 24-38.
47
48
49
50
51 (64) Franken, N. A. P.; Rodermond, H. M.; Stap, J.; Haveman, J.; Van Bree, C. Clonogenic
52 Assay of Cells in Vitro. *Nat. Protoc.* **2006**, 1, 2315-2319.
53
54
55
56 (65) Rudolph, J. Cdc25 Phosphatases: Structure, Specificity, and Mechanism. *Biochemistry*
57 **2007**, 46, 3595-3604.
58
59
60

- 1
2
3 (66) Aressy, B.; Ducommun, B. Cell Cycle Control by the Cdc25 Phosphatases. *Anti-*
4 *Cancer Agents Med. Chem.* **2008**, *8*, 818-824.
5
6
7 (67) Morgan, D. O. Principles of Cdk Regulation. *Nature* **1995**, *374*, 131-134.
8
9
10 (68) Hoffmann, I.; Clarke, P. R.; Marcote, M. J.; Karsenti, E.; Draetta, G. Phosphorylation
11 and Activation of Human Cdc25-C by Cdc2--Cyclin B and Its Involvement in the Self-
12 Amplification of Mpf at Mitosis. *EMBO J.* **1993**, *12*, 53-63.
13
14
15 (69) Yamaura, M.; Mitsushita, J.; Furuta, S.; Kiniwa, Y.; Ashida, A.; Goto, Y.; Shang, W.
16 H.; Kubodera, M.; Kato, M.; Takata, M.; Saida, T.; Kamata, T. Nadph Oxidase 4
17 Contributes to Transformation Phenotype of Melanoma Cells by Regulating G2-M Cell
18 Cycle Progression. *Cancer Res.* **2009**, *69*, 2647-2654.
19
20
21 (70) Bhattacharjee, H.; Sheng, J.; Ajees, A. A.; Mukhopadhyay, R.; Rosen, B. P.
22 Adventitious Arsenate Reductase Activity of the Catalytic Domain of the Human
23 Cdc25b and Cdc25c Phosphatases. *Biochemistry* **2010**, *49*, 802-809.
24
25
26 (71) Albano, F.; Arcucci, A.; Granato, G.; Romano, S.; Montagnani, S.; De Vendittis, E.;
27 Ruocco, M. R. Markers of Mitochondrial Dysfunction During the Diclofenac-Induced
28 Apoptosis in Melanoma Cell Lines. *Biochimie* **2013**, *95*, 934-945.
29
30
31 (72) Gelzo, M.; Granato, G.; Albano, F.; Arcucci, A.; Russo, A. D.; De Vendittis, E.;
32 Ruocco, M. R.; Corso, G. Evaluation of Cytotoxic Effects of 7-Dehydrocholesterol on
33 Melanoma Cells. *Free Radical Biol. Med.* **2014**, *70*, 129-140.
34
35
36 (73) Rafahi, H.; Orlowski, C.; Georgiadis, G. T.; Ververis, K.; El-Osta, A.; Karagiannis, T.
37 C. Clonogenic Assay: Adherent Cells. *J. Visualized Exp.* **2011**, *49*, 2573.
38
39
40 (74) Bradford, M. M. A Rapid and Sensitive Method for the Quantitation of Microgram
41 Quantities of Protein Utilizing the Principle of Protein-Dye Binding. *Anal. Biochem.*
42 **1976**, *72*, 248-254.
43
44
45
46
47
48
49
50
51
52
53
54
55
56
57
58
59
60

- 1
2
3 (75) Harder, E.; Damm, W.; Maple, J.; Wu, C.; Reboul, M.; Xiang, J. Y.; Wang, L.; Lupyan,
4 D.; Dahlgren, M. K.; Knight, J. L. Opls3: A Force Field Providing Broad Coverage of
5 Drug-Like Small Molecules and Proteins. *J. Chem. Theory Comput.* **2015**, 12, 281-296.
6
7
8
9
10 (76) Deng, Z.; Chuaqui, C.; Singh, J. Structural Interaction Fingerprint (Sift): A Novel
11 Method for Analyzing Three-Dimensional Protein–Ligand Binding Interactions. *J.*
12 *Med. Chem.* **2004**, 47, 337-344.
13
14
15
16 (77) Baell, J. B.; Holloway, G. A. New Substructure Filters for Removal of Pan Assay
17 Interference Compounds (Pains) from Screening Libraries and for Their Exclusion in
18 Bioassays. *J. Med. Chem.* **2010**, 53, 2719-2740.
19
20
21
22
23 (78) Lagorce, D.; Sperandio, O.; Baell, J. B.; Miteva, M. A.; Villoutreix, B. O. Faf-Drugs3:
24 A Web Server for Compound Property Calculation and Chemical Library Design.
25 *Nucleic Acids Res.* **2015**, 43, W200-W207.
26
27
28
29
30 (79) Sterling, T.; Irwin, J. J. Zinc 15 – Ligand Discovery for Everyone. *J. Chem. Inf. Model.*
31 **2015**, 55, 2324-2337.
32
33
34
35
36
37
38
39
40
41
42
43
44
45
46
47
48
49
50
51
52
53
54
55
56
57
58
59
60

FIGURE LEGENDS

Figure 1. Known reversible CDC25 Inhibitors.

Figure 2. Structure-based optimization of lead NSC28620. (A) Predicted binding mode of NSC28620 (green) in the CDC25B binding cavity. For clarity, only interacting residues are displayed and labeled. Ligand and interacting key residues (white) are represented as stick models, while the protein is a transparent Connolly surface model. H-bonds and salt bridges are shown as dashed black lines. (B) Schematic overview of the rationally designed NSC28620 derivatives.

Figure 3. Effect of compound **7j** or **3** on the Lineweaver-Burk plots of the CDC25B phosphatase activity. The activity, measured through the OMFP hydrolysis rate as described in the Experimental Section, was determined in the absence (open circles in both panels) or in the presence of 1.0 μM or 2.0 μM compound **7j** (filled triangles or filled circles, respectively; panel A) or 1.5 μM or 3.0 μM compound **3** (filled triangles or filled circles, respectively; panel B).

Figure 4. Effect of some NPA derivatives on the intrinsic fluorescence of CDC25B. The emission spectrum of 1 μM recombinant CDC25B in 20 mM Tris•HCl, pH 7.8 buffer containing 0.5 mM TCEP and 0.5% (v/v) DMSO was recorded at 20°C using the excitation wavelength of 280 nm, either in the absence (black line) or in the presence of 1.5 μM **7j** (purple line), 3 μM **7i** (green line), 4 μM **3** (red line), or 10 μM **4a** (blue line).

Figure 5. (A) Binding mode of compound **7j** (green) into the swimming pool site of CDC25B (PDB ID: 1QB0). (B) Binding mode of compound **3** (cyan) to CDC25B in complex with the

1
2
3 artificial OMFP substrate. For clarity, only interacting residues are displayed and labeled.
4
5 Ligands and interacting key residues (white) are represented as stick models, while the
6
7 protein is a slate ribbon model. The catalytic site and the adjacent deeper and larger
8
9 swimming pool site are displayed as bluewhite Connolly surface. H-bonds and salt bridges
10
11 are shown as dashed grey lines.
12
13
14
15
16

17 **Figure 6.** Cell toxicity of NPA derivatives. Panels A and B. A2058 cells were incubated for
18
19 48 or 72 h with 0.5 % (v/v) DMSO (open bars), 2.5 μM (gray bars) or 5.0 μM (black bars) of
20
21 compound **4** (panel A) or **4a** (panel B). Panel C. BJ-5ta cells were incubated for 24, 48 or 72
22
23 h with 0.5 % (v/v) DMSO (open bars), 2.5 μM (light gray bars), 5.0 μM (dark gray bars) or
24
25 10 μM (black bars) of compound **4a**. Data of cell viability were obtained from at least three
26
27 independent experiments and expressed in arbitrary units (AU), as the mean \pm SE. **, $p <$
28
29 0.01; ***, $p <$ 0.001 compared to control cells. Other details are in the Experimental Section.
30
31
32
33
34

35 **Figure 7.** Effect of **4a** on the colony formation of melanoma cells. A2058 and A375 cells
36
37 were treated with vehicle alone or 0.625, 1.25, 2.5, 5.0, or 10 μM **4a**. After 10-days
38
39 treatment, plates were photographed and images of representative experiments are shown.
40
41 The bottom plots report the number of colonies counted as indicated in the Experimental
42
43 Section; values are expressed in percentages and reported as the mean \pm SE from at least
44
45 three different experiments.
46
47
48
49
50

51 **Figure 8.** Effect of **4a** on the distribution of cell cycle phases of A2058 cells. The distribution
52
53 of cells in the different phases was evaluated after 8 h (panels **A** and **C**) or 16 h (panels **B** and
54
55 **D**) from treatment with 0.5% DMSO (Panels **A** and **B**) or 10 μM **4a** (Panels **C** and **D**) as
56
57 described in the Experimental Section. Cell cycle phases colours: sub G1, light blue; G0/G1,
58
59
60

1
2
3 red; S, green; G2/M, dark blue. Histograms show the cell percentage distribution among the
4 various phases after 8 h (Panel E) or 16 h (Panel F). Data obtained from triplicate
5 experiments in the presence of DMSO (open bars) or **4a** (black bars) are reported as the mean
6 \pm SE. ****, $p < 0.0001$ compared to control cells.
7
8
9
10
11
12
13
14

15 **Figure 9.** Effect of **4a** on the distribution of cell cycle phases of A375 cells. The same
16 protocol described in the legend to Fig. 8 was followed for analyzing the cell phases
17 distribution of A375 cells. **, $p < 0.01$; ****, $p < 0.0001$ compared to control cells.
18
19
20
21
22
23

24 **Figure 10.** Effect of **4a** on p-Cdk1 protein levels. A2058 and A375 cells were incubated in
25 the absence or in the presence of 10 μ M **4a** for 8 h and total protein extracts were used to
26 detect p-Cdk1 levels through Western blot. β -actin was used as an internal loading control. *,
27 $p < 0.05$ compared to control cells.
28
29
30
31
32
33
34
35
36
37
38
39
40
41
42
43
44
45
46
47
48
49
50
51
52
53
54
55
56
57
58
59
60

SCHEME LEGENDS**Scheme 1. Synthesis of 2-(1-naphthoyl)benzoic acid 1 and its ethyl ester 2.^a**

^aReagents and conditions: i) a. Mg, dry THF, N₂, reflux, 1h; b. phthalic anhydride, dry THF, N₂, reflux, 48 h; ii) EtOH, H₂SO₄, reflux, 24 h.

Scheme 2. Synthesis of 2-(3(4)-methoxy-1-naphthyl)benzoic acids 1a,b and 2-(3-hydroxy-1-naphthoyl)benzoic acid 1c.^a

^aReagents and conditions: i) Br₂, AcOH, 60°C, 15 min; ii) NaNO₂, AcOH, 8-10°C, 10 min; iii) NaBH₄, EtOH, 0-10°C, 2-3 h; iv) a. NaH, dry DMF, N₂, rt, 15 min; b. CH₃I, dry DMF, N₂, rt, 3h; v) *n*-BuLi, dry THF, N₂, -78°C, 1 h; vi) dry DMF, dry THF, N₂, -78°C, 1 h; vii) a. SOCl₂, N₂, reflux, 6 h; b. 2-amino-2-methyl-1-propanol, dry DCM, N₂, rt, 2 h; viii) a. SOCl₂, N₂, rt, 30 min; b. dry Et₂O, 30 min; c. 20% NaOH; ix) *n*-BuLi, dry Et₂O, N₂, -78°C, 1 h; x) a. dry Et₂O, N₂, rt, overnight; b. 3M HCl, reflux, 4.5 h; c. 10% NaOH, reflux, 1 h; xi) 25% KOH, KMnO₄, Py, reflux, 5 h; xii) BBr₃ (1M in DCM), dry DCM, N₂, rt, 30-210 min.

Scheme 3. Synthesis of ethyl-(naphthylamino)benzoates 3, 3a-c, 3h, 4, 4a-c, 4g,h and 5.^a

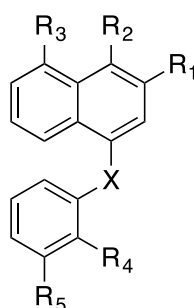
^aReagents and conditions: i) Pd(OAc)₂, (±)-BINAP, Cs₂CO₃, dry toluene, Ar, 80°C, 17-40 h.

Scheme 4. Synthesis of (naphthylamino)benzoic acid derivatives 6, 6a-f, 7, 7a-j, 8-12.^a

^aReagents and conditions: i) 1M NaOH, THF/EtOH (1:1), reflux, 30-90 min; ii) a) HCl (4M in 1,4-dioxane), dry 1,4-dioxane, r.t., 24 h, or trifluoroacetic acid, dichloromethane, r.t., 60 min. (for **10** and **11**); b) BBr₃ (1M in dichloromethane), dry dichloromethane, N₂, r.t., 30-210 min; iii) H₂SO₄, EtOH, MW 80°C, 90 min (for **8** and **9**).

TABLES

Table 1. Rationally Designed Compounds **1-12** and their Inhibition Kinetic Parameters against CDC25B.

**1-12**

Cpd	R ¹	R ²	R ³	R ⁴	R ⁵	X	<i>K_i</i> ^a (μ M)	Putative inhibition mechanism
1	H	H	H	COOH	H	CO	69	mixed
1a	OCH ₃	H	H	COOH	H	CO	36	mixed
1b	H	OCH ₃	H	COOH	H	CO	7.1 \pm 0.9	non-competitive
1c	OH	H	H	COOH	H	CO	34 \pm 3	non-competitive
2	H	H	H	COOC ₂ H ₅	H	CO	54	mixed
3	H	H	H	COOC ₂ H ₅	H	NH	2.8 \pm 0.7	un-competitive
3a	OCH ₃	H	H	COOC ₂ H ₅	H	NH	12.5 \pm 2.6	un-competitive
3b	H	OCH ₃	H	COOC ₂ H ₅	H	NH	6.9 \pm 2.0	non-competitive
4	H	H	H	H	COOC ₂ H ₅	NH	7.3 \pm 0.6	un-competitive
4a	OCH ₃	H	H	H	COOC ₂ H ₅	NH	8.5 \pm 1.2	un-competitive
4b	H	OCH ₃	H	H	COOC ₂ H ₅	NH	11.9 \pm 4.2	non-competitive
5	H	H	H	H	H	NH	32	mixed
6	H	H	H	COOH	H	NH	22 \pm 3	un-competitive
6a	OCH ₃	H	H	COOH	H	NH	16.9 \pm 0.3	non-competitive
6b	H	OCH ₃	H	COOH	H	NH	6.1 \pm 0.7	un-competitive
6d	OH	H	H	COOH	H	NH	5.1 \pm 0.7	non-competitive
6e	H	OH	H	COOH	H	NH	2.7 \pm 1.1	non-competitive
6f	H	H	OH	COOH	H	NH	13.4 \pm 1.1	non-competitive
7	H	H	H	H	COOH	NH	30	mixed
7a	OCH ₃	H	H	H	COOH	NH	55 \pm 7	un-competitive

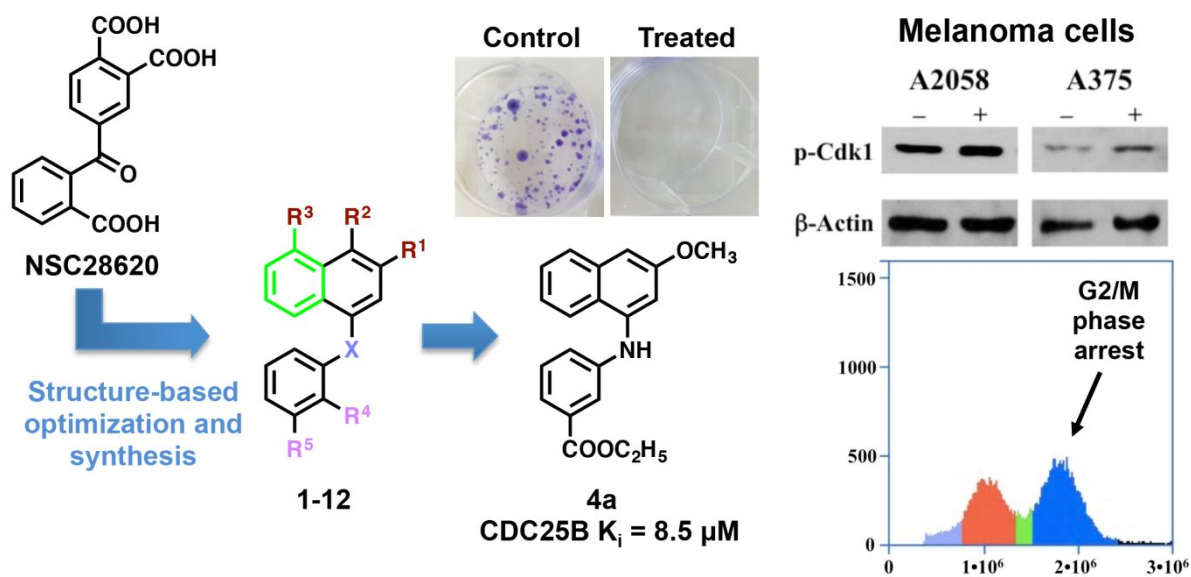
1
2
3
4
5
6
7
8
9
10
11
12
13
14
15
16
17
18
19
20
21
22
23
24
25
26
27
28
29
30
31
32
33
34
35
36
37
38
39
40
41
42
43
44
45
46
47
48
49
50
51
52
53
54
55
56
57
58
59
60

7b	H	OCH ₃	H	H	COOH	NH	45 ± 3	un-competitive
7d	OH	H	H	H	COOH	NH	5.8 ± 0.8	non-competitive
7e	H	OH	H	H	COOH	NH	6.4 ± 0.8	un-competitive
7f	H	H	OH	H	COOH	NH	2.9 ± 0.3	non-competitive
7i^b	H	NH ₂	H	H	COOH	NH	1.4 ± 0.3	non-competitive
7j^b	H	H	NH ₂	H	COOH	NH	0.8 ± 0.2	non-competitive
8	H	H	OH	COOC ₂ H ₅	H	NH	7.4 ± 2.2	non-competitive
9	H	H	OH	H	COOC ₂ H ₅	NH	4.9 ± 1.3	non-competitive
10^b	H	H	NH ₂	COOC ₂ H ₅	H	NH	9.9 ± 3.2	non-competitive
11^b	H	H	NH ₂	H	COOC ₂ H ₅	NH	36 ± 3	non-competitive
12	H	H	NH ₂	COOH	H	NH	6.5 ± 1.4	non-competitive
NSC28620 ³⁸							5.3 ± 2.4	competitive

^a The values of K_i , calculated as indicated in the Experimental Section, are an average from at least three independent experiments. The missing standard deviation for mixed inhibitors is due to the fact that the K_i value indicated is just a rough evaluation of the inhibition power.

^b Compounds were tested as hydrochloride salts.

Table of Contents graphic



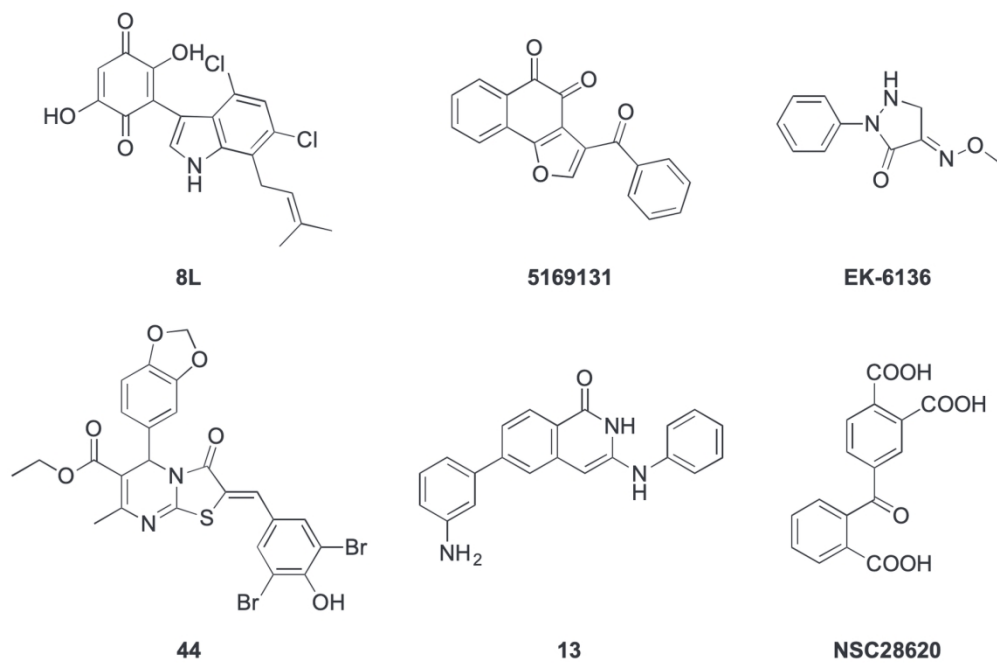


Figure 1. Known reversible CDC25 Inhibitors.

159x105mm (300 x 300 DPI)

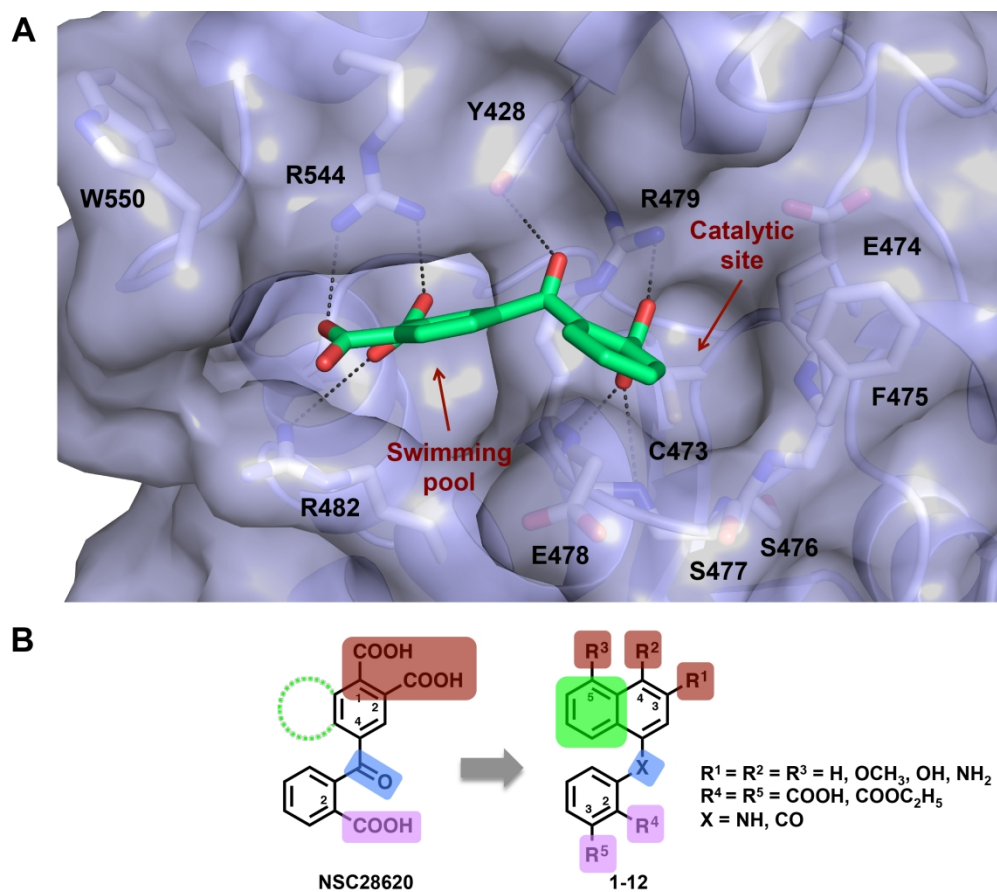
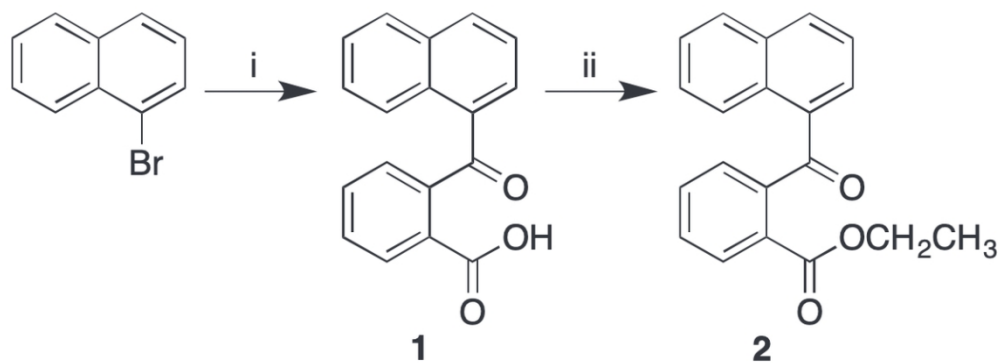
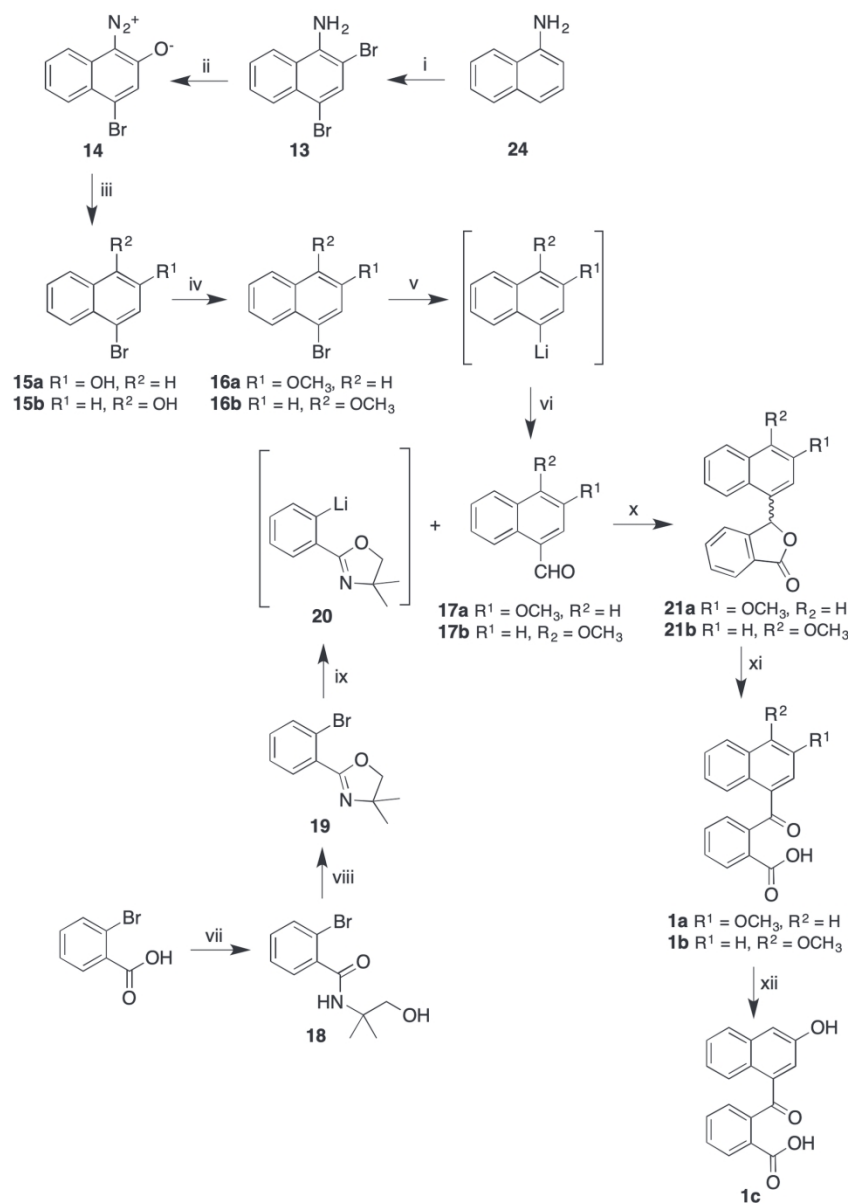


Figure 2. Structure-based optimization of lead NSC28620. (A) Predicted binding mode of NSC28620 (green) in the CDC25B binding cavity. For clarity, only interacting residues are displayed and labeled. Ligand and interacting key residues (white) are represented as stick models, while the protein is a transparent Connolly surface model. H-bonds and salt bridges are shown as dashed black lines. (B) Schematic overview of the rationally designed NSC28620 derivatives.



Scheme 1. Synthesis of 2-(1-naphthoyl)benzoic acid 1 and its ethyl ester 2.
a) Reagents and conditions: i) a. Mg, dry THF, N₂, reflux, 1h; b. phthalic anhydride, dry THF, N₂, reflux, 48 h; ii) EtOH, H₂SO₄, reflux, 24 h.

101x37mm (300 x 300 DPI)

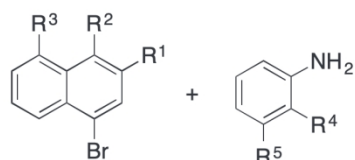


Scheme 2. Synthesis of 2-(3(4)-methoxy-1-naphthyl)benzoic acids 1a,b and 2-(3-hydroxy-1-naphthyl)benzoic acid 1c.a

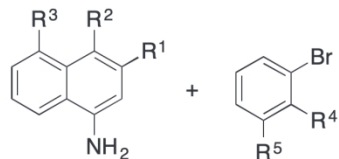
aReagents and conditions: i) Br₂, AcOH, 60°C, 15 min; ii) NaNO₂, AcOH, 8-10°C, 10 min; iii) NaBH₄, EtOH, 0-10°C, 2-3 h; iv) a. NaH, dry DMF, N₂, rt, 15 min; b. CH₃I, dry DMF, N₂, rt, 3h; v) n-BuLi, dry THF, N₂, -78°C, 1 h; vi) dry DMF, dry THF, N₂, -78°C, 1 h; vii) a. SOCl₂, N₂, reflux, 6 h; b. 2-amino-2-methyl-1-propanol, dry DCM, N₂, rt, 2 h; viii) a. SOCl₂, N₂, rt, 30 min; b. dry Et₂O, 30 min; c. 20% NaOH; ix) n-BuLi, dry Et₂O, N₂, -78°C, 1 h; x) a. dry Et₂O, N₂, rt, overnight; b. 3M HCl, reflux, 4.5 h; c. 10% NaOH, reflux, 1 h; xi) 25% KOH, KMnO₄, Py, reflux, 5 h; xii) BBr₃ (1M in DCM), dry DCM, N₂, rt, 30-210 min.

158x226mm (300 x 300 DPI)

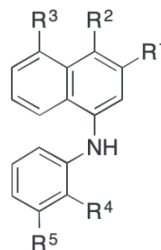
Procedure C1



Procedure C2



i

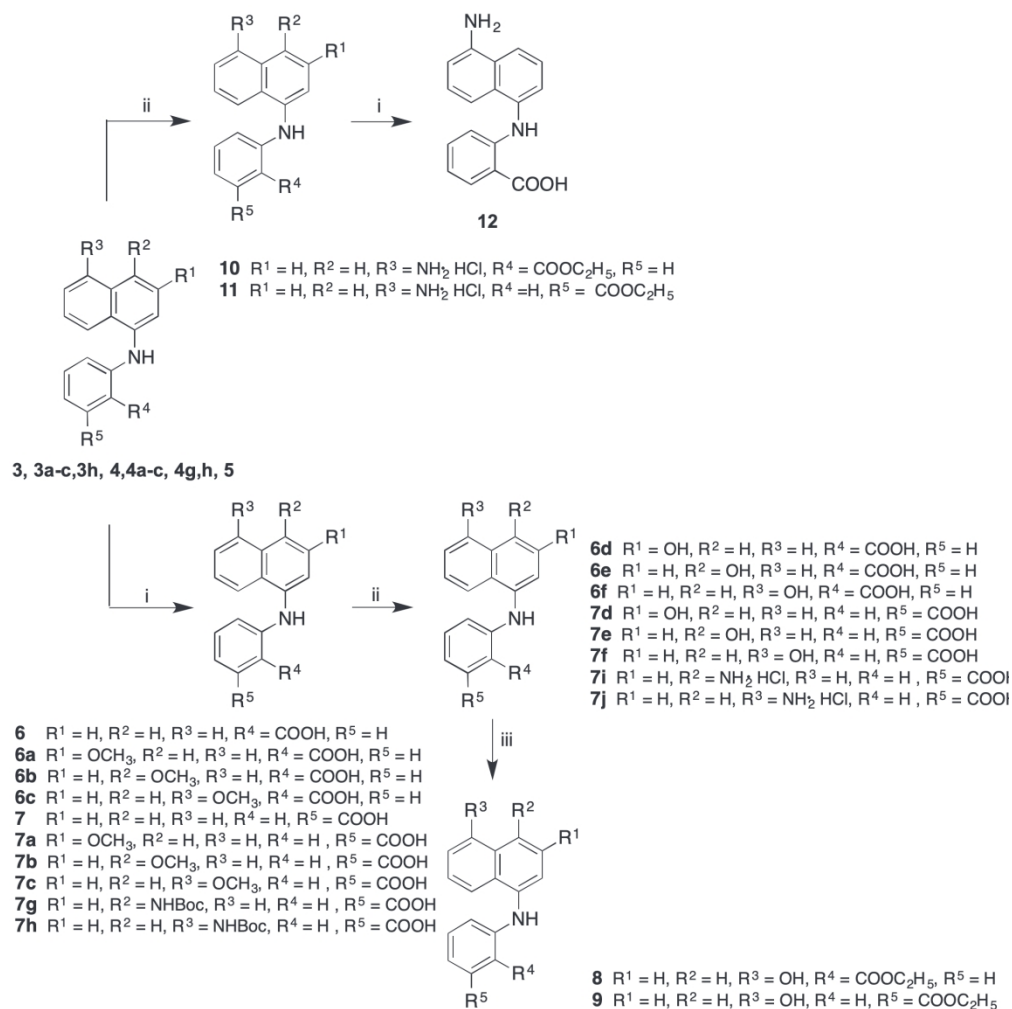


Procedure

3	R ¹ = H, R ² = H, R ³ = H, R ⁴ = COOC ₂ H ₅ , R ⁵ = H	C1
3a	R ¹ = OCH ₃ , R ² = H, R ³ = H, R ⁴ = COOC ₂ H ₅ , R ⁵ = H	C1
3b	R ¹ = H, R ² = OCH ₃ , R ³ = H, R ⁴ = COOC ₂ H ₅ , R ⁵ = H	C2
3c	R ¹ = H, R ² = H, R ³ = OCH ₃ , R ⁴ = COOC ₂ H ₅ , R ⁵ = H	C2
3h	R ¹ = H, R ² = H, R ³ = NHBoc, R ⁴ = COOC ₂ H ₅ , R ⁵ = H	C1
4	R ¹ = H, R ² = H, R ³ = H, R ⁴ = H, R ⁵ = COOC ₂ H ₅	C1
4a	R ¹ = OCH ₃ , R ² = H, R ³ = H, R ⁴ = H, R ⁵ = COOC ₂ H ₅	C1
4b	R ¹ = H, R ² = OCH ₃ , R ³ = H, R ⁴ = H, R ⁵ = COOC ₂ H ₅	C1/C
4c	R ¹ = H, R ² = H, R ³ = OCH ₃ , R ⁴ = H, R ⁵ = COOC ₂ H ₅	C2
4g	R ¹ = H, R ² = NHBoc, R ³ = H, R ⁴ = H, R ⁵ = COOC ₂ H ₅	C1
4h	R ¹ = H, R ² = H, R ³ = NHBoc, R ⁴ = H, R ⁵ = COOC ₂ H ₅	C1
5	R ¹ = H, R ² = H, R ³ = H, R ⁴ = H, R ⁵ = H	C1

Scheme 3. Synthesis of ethyl-(naphthylamino)benzoates **3**, **3a-c**, **3h**, **4**, **4a-c**, **4g,h** and **5**. aReagents and conditions: i) Pd(OAc)₂, (±)-BINAP, Cs₂CO₃, dry toluene, Ar, 80°C, 17-40 h.

159x106mm (300 x 300 DPI)



Scheme 4. Synthesis of (naphthylamino)benzoic acid derivatives **6**, **6a-f**, **7**, **7a-j**, **8-12.a**
 Reagents and conditions: i) 1M NaOH, THF/EtOH (1:1), reflux, 30-90 min; ii) a) HCl (4M in 1,4-dioxane), dry 1,4-dioxane, r.t., 24 h, or trifluoroacetic acid, dichloromethane, r.t., 60 min. (for **10** and **11**); b) BBr₃ (1M in dichloromethane), dry dichloromethane, N₂, r.t., 30-210 min; iii) H₂SO₄, EtOH, MW 80°C, 90 min (for **8** and **9**).

187x188mm (300 x 300 DPI)

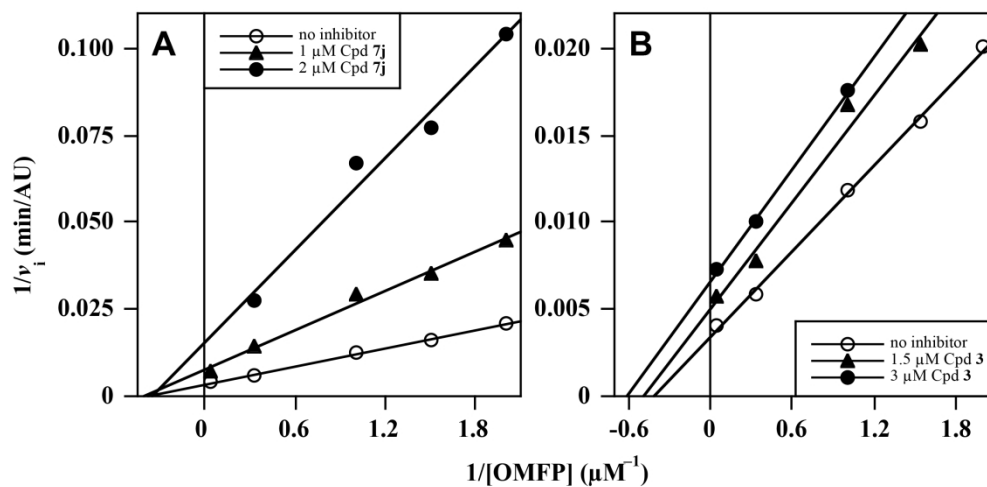


Figure 3. Effect of compound 7j or 3 on the LineweaverBurk plots of the CDC25B phosphatase activity. The activity, measured through the OMFP hydrolysis rate as described in the Experimental Section, was determined in the absence (open circles in both panels) or in the presence of 1.0 μM or 2.0 μM compound 7j (filled triangles or filled circles, respectively; panel A) or 1.5 μM or 3.0 μM compound 3 (filled triangles or filled circles, respectively; panel B).

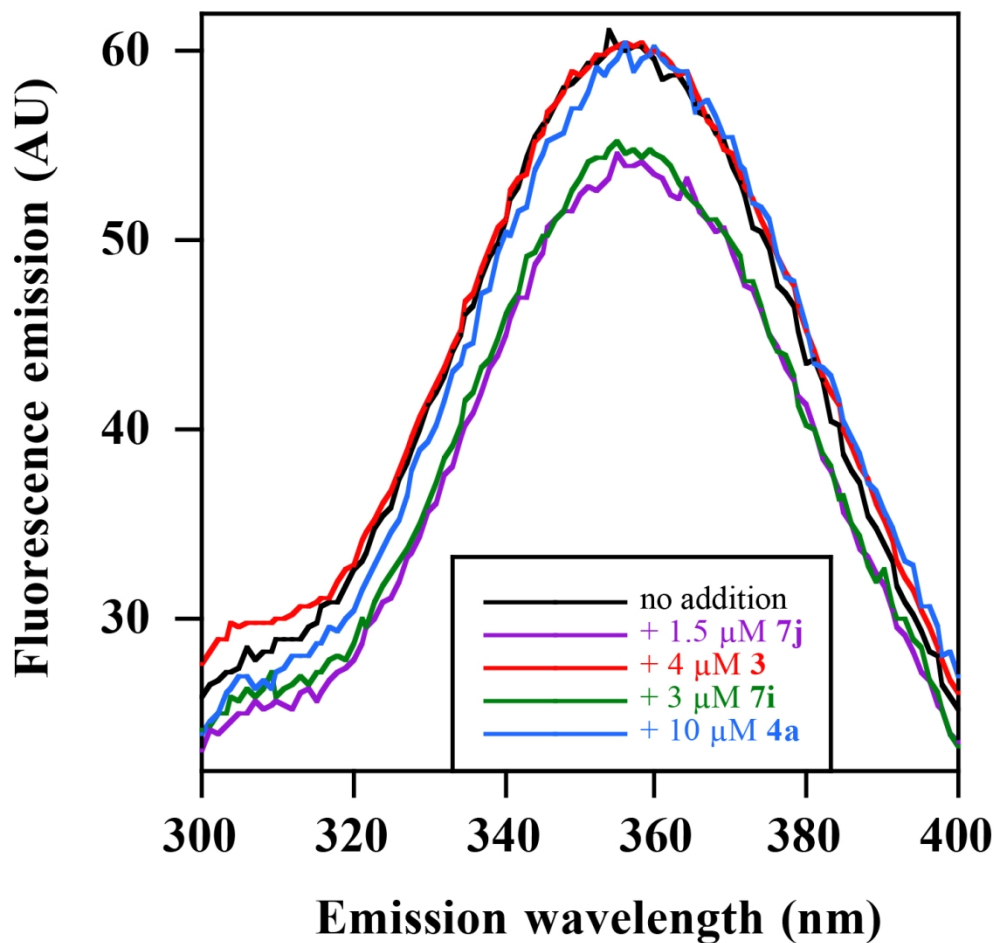


Figure 4. Effect of some NPA derivatives on the intrinsic fluorescence of CDC25B. The emission spectrum of 1 μM recombinant CDC25B in 20 mM Tris•HCl, pH 7.8 buffer containing 0.5 mM TCEP and 0.5% (v/v) DMSO was recorded at 20°C using the excitation wavelength of 280 nm, either in the absence (black line) or in the presence of 1.5 μM 7j (purple line), 3 μM 7i (green line), 4 μM 3 (red line), or 10 μM 4a (blue line).

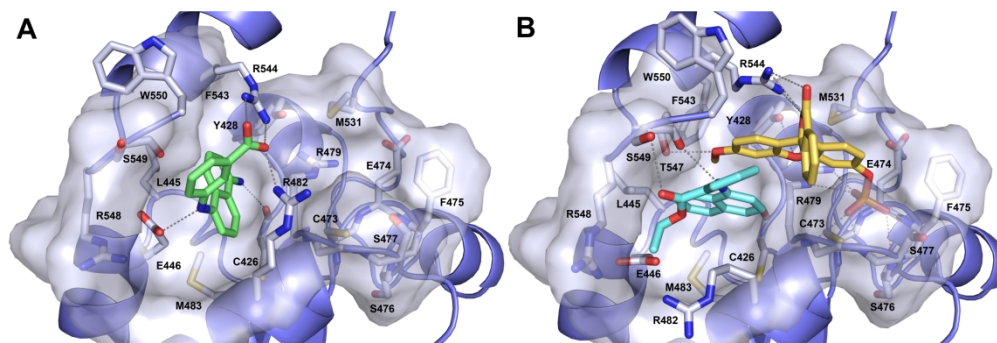


Figure 5. (A) Binding mode of compound 7j (green) into the swimming pool site of CDC25B. (B) Binding mode of compound 3 (cyan) to CDC25B in complex with the artificial OMFP substrate. For clarity, only interacting residues are displayed and labeled. Ligands and interacting key residues (white) are represented as stick models, while the protein is a slate ribbon model. The catalytic site and the adjacent deeper and larger swimming pool site are displayed as bluewhite Connolly surface. H-bonds and salt bridges are shown as dashed grey lines.

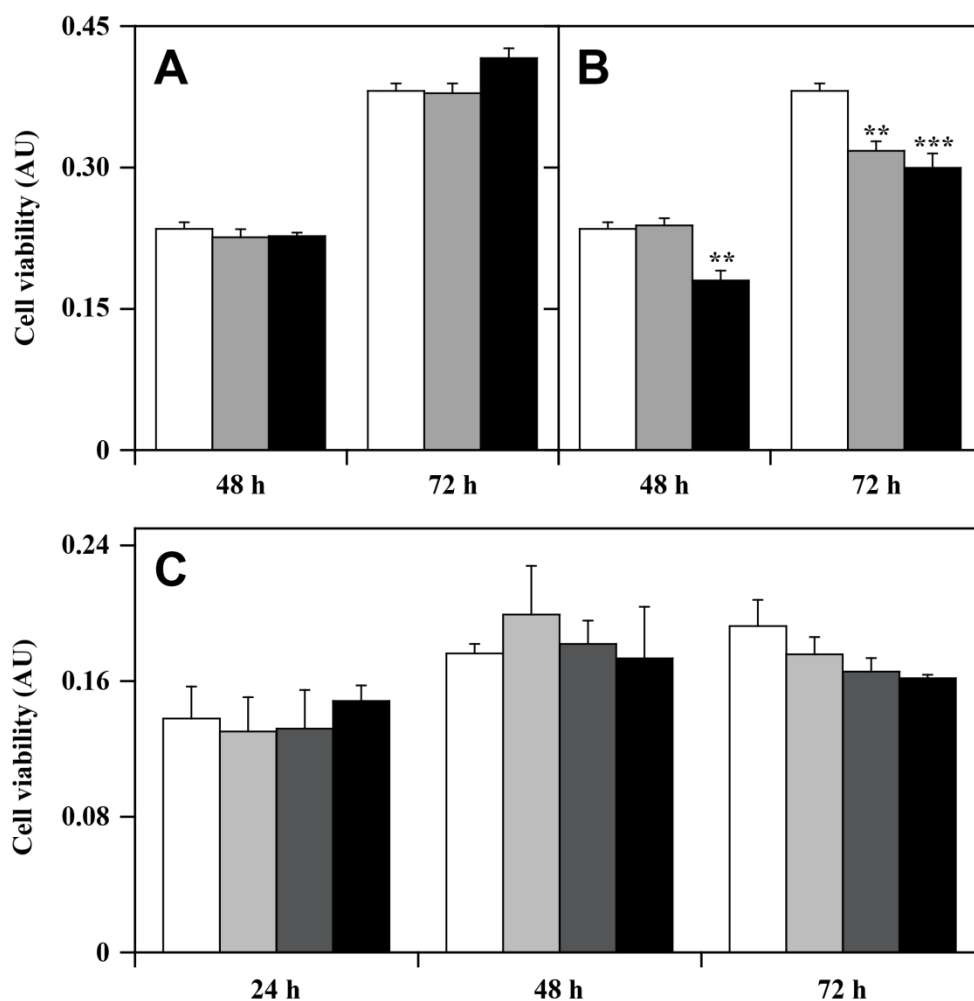
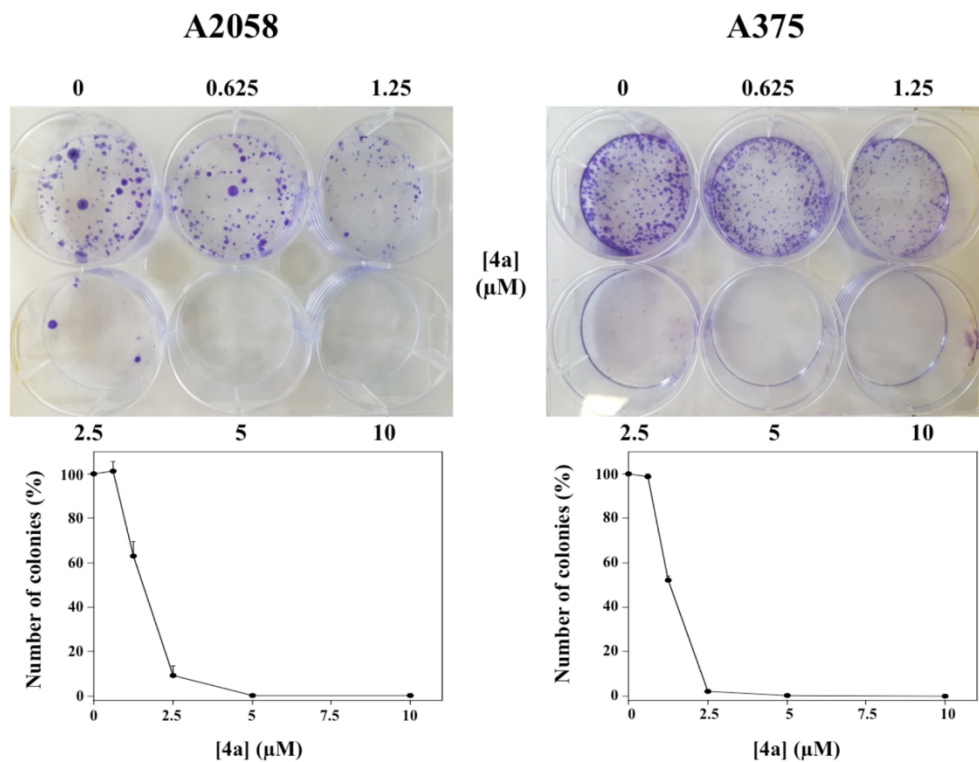


Figure 6. Cell toxicity of NPA derivatives. Panels A and B. A2058 cells were incubated for 48 or 72 h with 0.5 % (v/v) DMSO (open bars), 2.5 μ M (gray bars) or 5.0 μ M (black bars) of compound 4 (panel A) or 4a (panel B). Panel C. BJ-5ta cells were incubated for 24, 48 or 72 h with 0.5 % (v/v) DMSO (open bars), 2.5 μ M (light gray bars), 5.0 μ M (dark gray bars) or 10 μ M (black bars) of compound 4a. Data of cell viability were obtained from at least three independent experiments and expressed in arbitrary units (AU), as the mean \pm SE. **, $p < 0.01$; ***, $p < 0.001$ compared to control cells. Other details are in the Experimental Section.



32 Figure 7. Effect of 4a on the colony formation of melanoma cells. A2058 and A375 cells were treated with
33 vehicle alone or 0.625, 1.25, 2.5, 5.0, or 10 μM 4a. After 10-days treatment, plates were photographed and
34 images of representative experiments are shown. The bottom plots report the number of colonies counted
35 as indicated in the Experimental Section; values are expressed in percentages and reported as the mean \pm
36 SE from at least three different experiments.

37
38
39
40
41
42
43
44
45
46
47
48
49
50
51
52
53
54
55
56
57
58
59
60

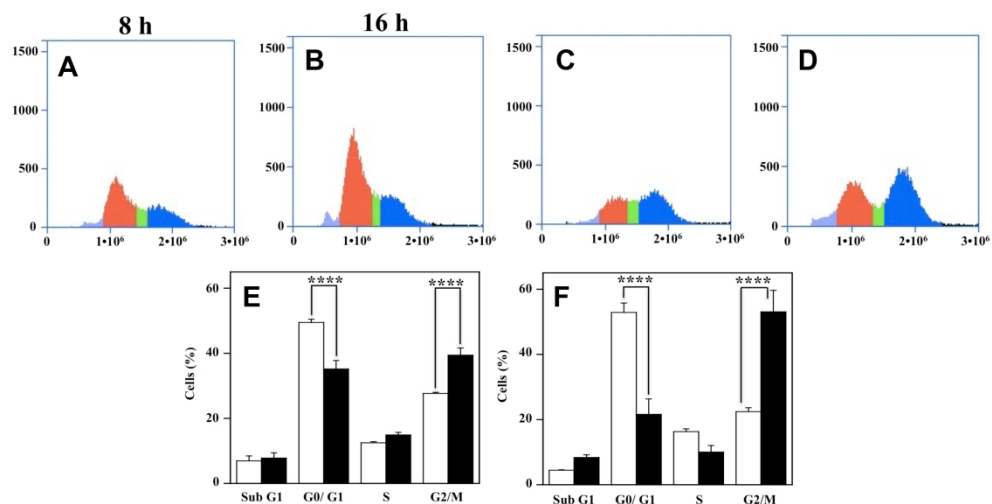


Figure 8. Effect of 4a on the distribution of cell cycle phases of A2058 cells. The distribution of cells in the different phases was evaluated after 8 h (panels A and C) or 16 h (panels B and D) from treatment with 0.5% DMSO (Panels A and B) or 10 μ M 4a (Panels C and D) as described in the Experimental Section. Cell cycle phases colours: sub G1, light blue; G0/G1, red; S, green; G2/M, dark blue. Histograms show the cell percentage distribution among the various phases after 8 h (Panel E) or 16 h (Panel F). Data obtained from triplicate experiments in the presence of DMSO (open bars) or 4a (black bars) are reported as the mean \pm SE. ****, $p < 0.0001$ compared to control cells.

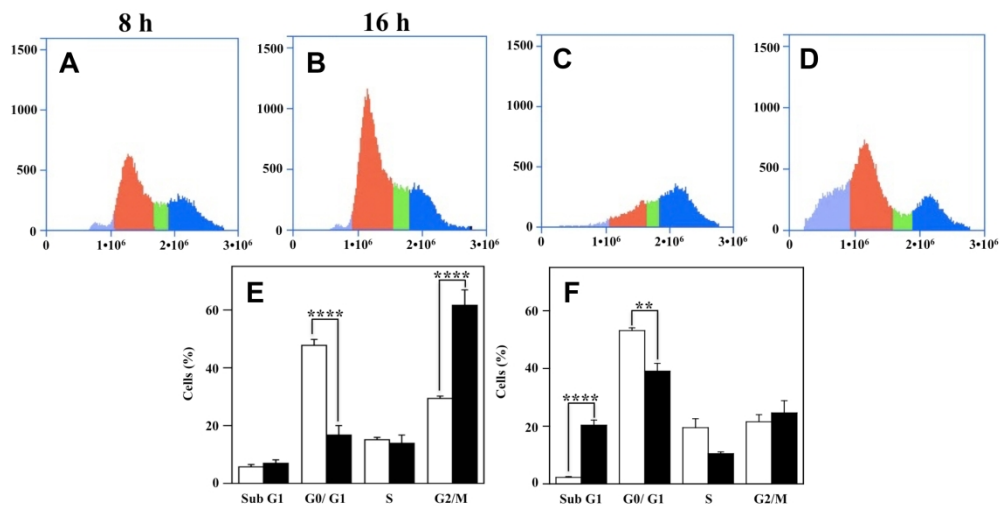


Figure 9. Effect of 4a on the distribution of cell cycle phases of A375 cells. The same protocol described in the legend to Fig. 8 was followed for analyzing the cell phases distribution of A375 cells. **, $p < 0.01$; ****, $p < 0.0001$ compared to control cells.

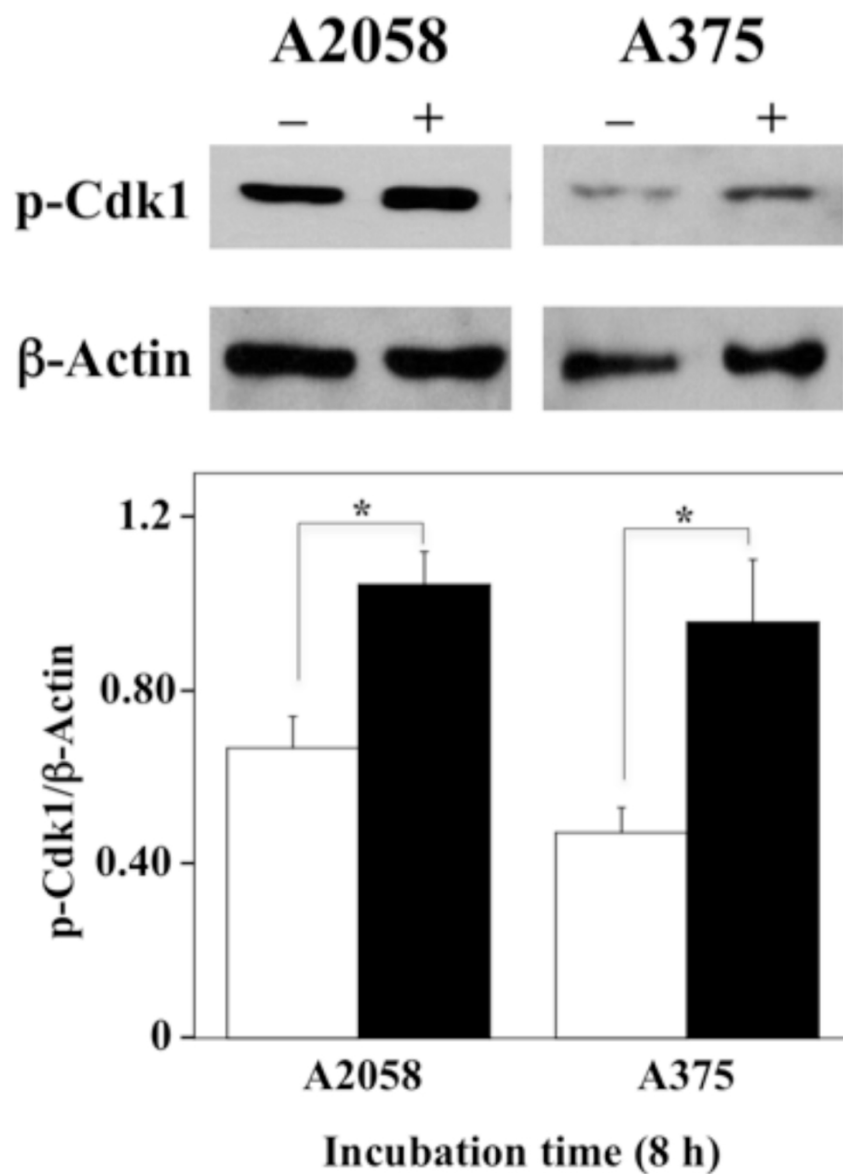


Figure 10. Effect of 4a on p-Cdk1 protein levels. A2058 and A375 cells were incubated in the absence or in the presence of 10 μ M 4a for 8 h and total protein extracts were used to detect p-Cdk1 levels through Western blot. β -actin was used as an internal loading control. *, $p < 0.05$ compared to control cells.